

**CZECH TECHNICAL UNIVERSITY  
IN PRAGUE**

**FACULTY OF ELECTRICAL  
ENGINEERING**



**DOCTORAL  
THESIS**

**2024**

**ANTONÍN  
KRPENSKÝ**



Dissertation Thesis



Czech  
Technical  
University  
in Prague

**F3**

Faculty of Electrical Engineering  
Department of Physics

## Control and analysis of acoustic and elastic wave fields based on selected inhomogeneous structures

**Ing. Antonín Krpenský**

Supervisor: prof. Dr. Ing. Michal Bednařík  
Doctoral study programme: P0788D110001 Akustika/Acoustics  
February 2024



## Acknowledgements

I would like to thank my supervisor Michal Bednařík for his guidance, support and patience during my studies. Also, I would like to express my gratitudes to Jean-Philippe Groby who supervised me during my stay in LAUM. Last but not least, I would like to thank my family, friends, and Markéta for their loving support.

This work was supported by the Grant Agency of the Czech Republic (GACR) grants No.

- 18-24954S ,
- 22-33896S ,

and by the Grant Agency of the Czech Technical University in Prague grants No.

- SGS21/115/OHK3/2T/13 ,
- SGS23/057/OHK3/1T/13 .

## Declaration

I hereby declare I have written this doctoral thesis independently and I quoted all the sources of information used in accordance with methodological instructions on ethical principles for writing an academic thesis. Moreover, I state that this thesis has neither been submitted nor accepted for any other degree.

In Prague, 29. February 2024

Ing. Antonín Krpenský

## Abstract

The topic of this dissertation thesis is the control and analysis of acoustic and elastic wave fields based on selected inhomogeneous structures. The work is conceived as a set of six author publications, each of which is directly related to the topic of this work. The introductory theoretical part is devoted to a brief overview of mathematical methods that are often used in the attached publications. In the next section, the mentioned publications are attached, each of which is provided with a summary comment. The first two publications relate to the description of the propagation of Love-type elastic surface waves in an inhomogeneous isotropic layer, the further one then to the propagation of acoustic waves in a waveguide with a non-uniform mean flow. The fourth publication discusses a new type of elastic inhomogeneous structure that allows manipulation of elastic P-waves, such as focusing and deflecting. This is followed by a publication devoted to finding exact analytical solutions of the model equation describing the propagation of elastic SH-waves in locally periodic functionally graded materials. The last attached publication deals with finding the Willis model for an acoustic waveguide with a continuously varying cross-sectional area. The conclusion of the work contains an overall summary and further potential research opportunities.

**Keywords:** elastic waves, acoustic waves, inhomogeneous structures, Heun functions, triconfluent Heun functions, functionally graded materials, locally periodic structures, Webster-type equation, Floquet-Bloch method

## Abstrakt

Tématem této disertační práce je řízení a analýza akustických a elastických vlnových polí na základě vybraných nehomogenních struktur. Práce je koncipována jako soubor šesti autorových publikací, přičemž každá z nich přímo souvisí s tématem této práce. Úvodní teoretická část je věnována stručnému přehledu matematických metod, které se v přiložených publikacích často využívají. V další části jsou poté přiloženy zmíněné publikace, přičemž každá z nich je opatřena shrnujícím komentářem. První dvě publikace se týkají popisu šíření elastických povrchových vln Loveho typu v nehomogenní izotropní vrstvě, další pak šíření akustických vln ve vlnovodu s neuniformním středním prouděním. Čtvrtá publikace pojednává o novém typu elastické nehomogenní struktury, která umožňuje manipulaci elastických P-vln, jako například fokusace a deflexe. Následuje publikace věnující se nalezení přesných analytických řešení modelové rovnice popisující šíření elastických SH-vln v lokálně periodických funkčně gradovaných materiálech. Poslední přiložená publikace se zabývá nalezením Willisova modelu pro akustický vlnovod se spojitě proměnným průřezem. Závěr práce obsahuje celkové shrnutí a další potenciální možnosti výzkumu.

**Klíčová slova:** elastické vlny, akustické vlny, nehomogenní struktury, Heunovy funkce, trikonfluentní Heunovy funkce, funkčně gradované materiály, lokálně periodické struktury, rovnice Websterova typu, Floquetova-Blochova metoda

# Contents

<b>1 Introduction</b>	<b>1</b>	<b>3 Collection of publications</b>	<b>21</b>
<b>2 Mathematical methods</b>	<b>3</b>	3.1 Paper I . . . . .	24
2.1 Heun equations . . . . .	4	3.2 Paper II . . . . .	39
2.1.1 Singular points of differential equations . . . . .	4	3.3 Paper III . . . . .	48
2.1.2 Frobenius solution around regular singular point . . . . .	4	3.4 Paper IV . . . . .	60
2.1.3 Heun equation . . . . .	6	3.5 Paper V . . . . .	75
2.1.4 Triconfluent Heun equation . . . . .	9	3.6 Paper VI: . . . . .	88
2.2 Webster-type equation . . . . .	10	<b>4 Conclusions and future work</b>	<b>99</b>
2.3 WKB approximation . . . . .	11	<b>Bibliography</b>	<b>103</b>
2.4 Floquet-Bloch theory . . . . .	12	<b>A List of author's publications</b>	<b>105</b>
2.4.1 Equation with periodic coefficients . . . . .	13	A.1 Related to the thesis . . . . .	105
2.4.2 Liouville's formula . . . . .	13	A.1.1 Publications indexed in Web of Science . . . . .	105
2.4.3 Floquet theory . . . . .	14	A.1.2 Publications indexed in Scopus . . . . .	106
2.4.4 Bloch waves . . . . .	16	A.2 Not related to the thesis . . . . .	106
2.5 Functionally graded materials . . . . .	17	A.2.1 Publications indexed in Web of Science . . . . .	106
		A.2.2 Other . . . . .	106







# Chapter 1

## Introduction

This dissertation thesis deals with the control and analysis of acoustic and elastic wave fields based on selected inhomogeneous structures as its title suggests. The possibility of controlling acoustic and elastic wave fields is an issue of great scientific potential from both a theoretical and a practical perspective. Even though many types of inhomogeneous structures are intensively studied, the majority of research in this area is devoted to either numerical simulations or practical experiments. Therefore, this thesis focuses primarily on employing various types of exact or approximate analytical methods to express the closed form analytical solutions to the selected problems in acoustics and elastoacoustics (elastodynamics) in order to determine how does the specific inhomogeneous structure affect the propagation of the respective type of waves and how can this be potentially used for a specific type of wave manipulation. We mean by inhomogeneous structure that one or more parameters that characterise the structure are spatially dependent, whereas in this thesis the dependence is assumed only along one of the chosen coordinate axes, typically in the same direction as the waves propagate or perpendicular to it. The further requirement is that all of the studied wave related issues are in the linear regime. The main advantages of using the exact/approximate analytical solutions is that they enable a much simpler and more elegant way for any further mathematical manipulations compared to the numerical methods. Additionally, they typically offer a much deeper insight into the behavior of waves within the respective inhomogeneous structure. Moreover, they can serve as a benchmark solution for any other type of approximate analytical or numerical method.

The thesis is conceived as a collection of six author publications and is organised as follows: First, in Chap. 2 a brief overview of the mathematical

methods which are often used in the presented papers is provided in order to make reading easier for anyone not familiar with them. Next, in Chap. 3 the author publications are presented together with an introductory text describing an analytical approach used for solving the specific problems in each one of the publications and highlighting the advantages of analytical solutions in more detail. Also, each publication is provided with a short author commentary for the sake of readability. Finally, in Chap. 4 a summary of the work is presented together with possibilities for a further research.

This dissertation thesis does not include a separate chapter devoted to the state of the art, as this is present in the introduction of each of the presented publications, which would lead to an unnecessary duplication.



## Chapter 2

### Mathematical methods

Since this thesis is realized as a collection of selected papers published by the author, the most appropriate way to start the thesis is to provide the reader with a brief overview of some of the mathematical methods used in the papers that are usually discussed only very superficially in the appendices (of the mentioned papers) and therefore the reading experience can sometimes feel a bit cumbersome for someone not familiar with those.

The text in this chapter is organised as follows: First, the Heun differential equation and its triconfluent form are discussed in Sec. 2.1 together with a brief classification of the singular points of differential equations and derivation of the corresponding exact analytical solutions. Then, the Webster-type equation representing the model equation for the majority of the presented papers is defined in Sec. 2.2. Next, the Wentzel–Kramers–Brillouin approximation method is presented in Sec. 2.3. Sec. 2.4 is then devoted to the Floquet-Bloch theory - a very powerful tool to solve problems regarding wave propagation in (locally) periodic structures. Lastly, Sec. 2.5 deals with the mathematical description of the so called functionally graded materials, which are materials whose parameters vary continuously along one or more spatial directions according to some material function.

## 2.1 Heun equations

This section starts with a brief classification of singular points of linear second order differential equations. Next, the Frobenius solution is presented for a general linear second order differential equation around its regular singular point followed by the direct application to the Heun differential equation to obtain the so called Heun functions. Finally, the triconfluent Heun equation is presented together with the corresponding series solutions - the triconfluent Heun functions.

### 2.1.1 Singular points of differential equations

To begin this part, assume the most general form of a second order linear differential equation with non-constant coefficients  $p(z)$ ,  $q(z)$  in the following form

$$\frac{d^2 f(z)}{dz^2} + p(z) \frac{df(z)}{dz} + q(z)f(z) = 0. \quad (2.1)$$

Now we pick an arbitrary point  $z = z_0$ . If at this point the functions  $p(z)$ ,  $q(z)$  can be expressed by a Taylor series as

$$p(z) = \sum_{n=0}^{\infty} p_n (z - z_0)^n, \quad q(z) = \sum_{n=0}^{\infty} q_n (z - z_0)^n, \quad (2.2)$$

then we say that both the functions are analytic at  $z = z_0$  and the point itself is called an ordinary point, see e.g., [1]. On the contrary, if  $p(z)$  or  $q(z)$  (or both) diverge at  $z = z_0$  then this point is called a singular point. However, the differential equation can still possess a finite solution at a singular point  $z = z_0$  if  $(z - z_0)p(z)$  and  $(z - z_0)^2 q(z)$  are both analytic at  $z = z_0$ . In this case we call  $z = z_0$  the regular singular point of the corresponding differential equation. Otherwise, we call it an irregular singular point (see e.g., [1]).

### 2.1.2 Frobenius solution around regular singular point

Now, let's focus on finding the analytical expression for the solution of a differential equation in the vicinity of its regular singular point  $z = z_0$ , hereinafter referred to as the Frobenius solution, see e.g., [1, 2]. First, let's rewrite Eq. (2.1) into the more convenient form:

$$\frac{d^2 f(z)}{dz^2} + \frac{P(z)}{z - z_0} \frac{df(z)}{dz} + \frac{Q(z)}{(z - z_0)^2} f(z) = 0, \quad (2.3)$$

where we now assume both  $P(z), Q(z)$  to be analytic at  $z = z_0$ , i.e.,

$$P(z) = \sum_{n=0}^{\infty} P_n(z - z_0)^n, \quad Q(z) = \sum_{n=0}^{\infty} Q_n(z - z_0)^n. \quad (2.4)$$

Therefore (according to the definition provided in the previous subsection),  $z = z_0$  is a regular singular point of Eq. (2.3). For the sake of the text to follow, the expressions for the coefficients  $P_0, Q_0$  which play a significant role (as will be shown further in the text) for the currently presented method should be written down in terms of the functions  $p(z), q(z)$  (the derivation follows simply by comparing Eqs. (2.1) and (2.3)) as

$$P_0 = \lim_{z \rightarrow z_0} (z - z_0)p(z), \quad Q_0 = \lim_{z \rightarrow z_0} (z - z_0)^2 q(z). \quad (2.5)$$

Let's now focus on finding a solution to Eq. (2.3) in the following form

$$f(z) = (z - z_0)^\sigma \sum_{n=0}^{\infty} c_n (z - z_0)^n, \quad (2.6)$$

which is usually referred to as the Frobenius solution, see e.g., [1, 2]. The first and second derivative of the Frobenius solution (2.6) can then be expressed as

$$\begin{aligned} f'(z) &= \sum_{n=0}^{\infty} (\sigma + n)c_n (z - z_0)^{\sigma+n-1}, \\ f''(z) &= \sum_{n=0}^{\infty} (\sigma + n)(\sigma + n - 1)c_n (z - z_0)^{\sigma+n-2}. \end{aligned} \quad (2.7)$$

For convenience, we rewrite Eq. (2.3) as

$$(z - z_0)^2 \frac{d^2 f(z)}{dz^2} + (z - z_0)P(z) \frac{df(z)}{dz} + Q(z)f(z) = 0. \quad (2.8)$$

In order to ensure that the assumed Frobenius solution (2.6) solves Eq. (2.3) we insert the expressions (2.4), (2.6) and (2.7) into Eq. (2.8) and set the term before each of the (linearly independent) respective power of  $(z - z_0)$  equal to 0, resulting in (after some algebra) the following system of equations (see e.g., [2])

$$\begin{aligned} c_0 I(\sigma) &= 0, \\ c_1 I(\sigma + 1) + c_0 [P_1 \sigma + Q_1] &= 0, \\ c_2 I(\sigma + 2) + c_1 [P_1(\sigma + 1) + Q_1] + c_0 [P_2 \sigma + Q_2], \\ &\vdots \\ c_n I(\sigma + n) + \sum_{m=1}^n c_{n-m} [P_m(\sigma + n - m) + Q_m] &= 0, \end{aligned} \quad (2.9)$$

where  $I(\sigma)$  is defined as

$$I(\sigma) \equiv \sigma^2 + (P_0 - 1)\sigma + Q_0. \quad (2.10)$$

The first observation we make from the system of Eqs. (2.9) is that the value of  $c_0$  can be chosen arbitrarily, whereas the standard choice is (without the loss of generality)

$$c_0 = 1. \quad (2.11)$$

The first of Eqs. (2.9) that can now be expressed as

$$\sigma^2 + (P_0 - 1)\sigma + Q_0 = 0 \quad (2.12)$$

is usually called the indicial equation of Eq. (2.3) and since it represents a quadratic equation in  $\sigma$  it determines the two possible values of  $\sigma$ , each corresponding to the one of the linearly independent Frobenius solution to Eq. (2.3).

In general, by solving the system of Eqs. (2.9) we can determine the coefficients  $c_n$  of the Frobenius solution (2.6) for each respective root of the indicial equation (2.12)  $\sigma_1, \sigma_2$  and by that the solution is complete. However, to solve this system one needs to know the coefficients  $P_n, Q_n$  of the Taylor series of the functions  $P(z), Q(z)$  (2.4) which are typically unknown and their computation can be unnecessarily complicated. Therefore, in the following subsection another method to obtain the coefficients of the Frobenius solution specifically for the so called Heun equation is presented that is much more practical particularly for the numerical evaluation of its respective solution at a given point.

It should also be noted that in order that both the Frobenius solutions of Eq. (2.3) corresponding to the two roots of the indicial equation (2.12)  $\sigma_1, \sigma_2$  are guaranteed linearly independent then the following condition must hold (proof can be found in e.g., [2]):

$$\sigma_1 - \sigma_2 \notin \mathbb{Z}. \quad (2.13)$$

### ■ 2.1.3 Heun equation

In this part the previously derived indicial equation (2.12) is employed to express the Frobenius solution to the Heun equation, which is the most general second order linear differential equation with four regular singularities, meaning that every second order linear differential equation with four regular singular points can be transformed to the Heun equation, see e.g., [3–5].

The canonical form of the Heun equation can be written in the following form (see e.g., [2–4, 6]):

$$\frac{d^2 f(z)}{dz^2} + \left( \frac{\gamma}{z} + \frac{\delta}{z-1} + \frac{\varepsilon}{z-a} \right) \frac{df(z)}{dz} + \frac{\alpha\beta z - q}{z(z-1)(z-a)} f(z) = 0, \quad (2.14)$$

with the regular singular points located at  $z = 0, 1, a, \infty$ , where  $a \in \mathbb{C}$  and (for simplicity)  $|a| > 1$ . The generally complex parameters  $\alpha, \beta, \gamma, \delta, \varepsilon$  must satisfy the condition (see e.g., [2, 3, 6])

$$\alpha + \beta + 1 = \gamma + \delta + \varepsilon. \quad (2.15)$$

Furthermore, the choice of the parameter  $q \in \mathbb{C}$  is arbitrary. In order to express the Frobenius solution (see the subsection above) to Eq. (2.14) around one of its regular singular points we start by calculating the two roots of the indicial equation (2.12) by employing the expressions (2.5). The results for all of the four singularities are given in Tab. 2.1, see e.g., [2]. Please note that in the case of the singular point  $z_0 = \infty$  the first step is to perform a coordinate transformation  $z = 1/w$  on Eq. (2.14) and then to solve the indicial equation for the transformed singularity  $w_0 = 1/z_0 = 0$ .

Point	Roots $\sigma$
$z = 0$	$0, 1 - \gamma$
$z = 1$	$0, 1 - \delta$
$z = a$	$0, 1 - \varepsilon$
$z = \infty$	$\alpha, \beta$

**Table 2.1:** Roots of the indicial equation for all of the regular singular points of the Heun equation.

Assume now the regular singular point  $z_0 = 0$ . The Frobenius solution corresponding to the first root of the indicial equation  $\sigma_1 = 0$  can therefore be written in the form of the following Maclaurin series (see Eq. (2.6))

$$f(z) = \sum_{n=0}^{\infty} c_n z^n. \quad (2.16)$$

By substituting the expression (2.16) into Eq. (2.14), multiplying both sides with the term  $z(z-1)(z-a)$  and after some algebra we get

$$\begin{aligned} \sum_{n=0}^{\infty} (n + \alpha)(n + \beta) c_n z^{n+1} - \sum_{n=0}^{\infty} \{n[(n-1 + \gamma)(1+a) + a\delta + \varepsilon] + q\} c_n z^n \\ + \sum_{n=0}^{\infty} a n(n-1 + \gamma) c_n z^{n-1} = 0, \end{aligned} \quad (2.17)$$

where we have also used the condition (2.15). If we set the term before each of the respective powers of  $z^n$  equal to zero we get the recurrence relation for the coefficients  $c_n$  (see e.g., [6])

$$T_n c_{n+1} - (S_n + q) c_n + R_n c_{n-1} = 0, \quad (2.18)$$

where

$$\begin{aligned} R_n &= (n-1 + \alpha)(n-1 + \beta), \\ S_n &= n[(n-1 + \gamma)(1+a) + a\delta + \varepsilon], \\ T_n &= a(n+1)(n + \gamma). \end{aligned} \quad (2.19)$$

Since the recurrence equation (2.18) is of a second order, we need to specify the first two coefficients of the Frobenius solution (2.16)  $c_0, c_1$ . The first one is given (according to the previous subsection) by Eq. (2.11). The second one can be obtained either from the second of Eqs. (2.9) or directly by Eq. (2.18) by setting  $c_{-1} = 0$ , which is consistent with the Maclaurin series (2.16). Hence, the following values for the first two coefficients can be expressed as

$$c_0 = 1, \quad c_1 = \frac{q}{a\gamma} \quad (2.20)$$

The recurrence equation (2.18) together with the initial conditions (2.20) then define the first Frobenius solution to the Heun equation (for  $z_0 = 0, \sigma_1 = 0$ ) - the (local) Heun function (see e.g., [3, 6])

$$H\ell(a, q; \alpha, \beta, \gamma, \delta; z) \equiv \sum_{n=0}^{\infty} c_n z^n. \quad (2.21)$$

The second linearly independent solution corresponding to the second root of the indicial equation  $\sigma_2 = 1 - \gamma$  can then be found by the same procedure, resulting in

$$z^{1-\gamma} H\ell(a, (a\delta + \varepsilon)(1 - \gamma) + q; \alpha + 1 - \gamma, \beta + 1 - \gamma, 2 - \gamma, \delta; z). \quad (2.22)$$

It should be noted that both of those solutions converge for (see e.g., [2, 6])

$$|z| < 1. \quad (2.23)$$

Since the approach is the same for all the other (regular) singular points (see Tab. 2.1), the expressions for the corresponding local solutions to the Heun equation (2.14) will be just stated here without repeating the whole procedure described above (see e.g., [6]):

- $z_0 = 1, \sigma_1 = 0$ :

$$H\ell(1 - a, \alpha\beta - q; \alpha, \beta, \delta, \gamma; 1 - z), \quad (2.24)$$

- $z_0 = 1, \sigma_2 = 1 - \delta$ :

$$(1 - z)^{1-\delta} H\ell(1 - a, ((1 - a)\gamma + \varepsilon)(1 - \delta) + \alpha\beta - q; \alpha + 1 - \delta, \beta + 1 - \delta, 2 - \delta, \gamma; 1 - z), \quad (2.25)$$

- $z_0 = a, \sigma_1 = 0$ :

$$H\ell\left(\frac{a}{a-1}, \frac{\alpha\beta a - q}{a-1}; \alpha, \beta, \varepsilon, \delta; \frac{a-z}{a-1}\right), \quad (2.26)$$



- $z_0 = a, \sigma_1 = 1 - \varepsilon$ :

$$\left(\frac{a-z}{a-1}\right)^{1-\varepsilon} \text{H}\ell\left(\frac{a}{a-1}, \frac{(a(\delta+\gamma)-\gamma)(1-\varepsilon)}{a-1} + \frac{\alpha\beta a - q}{a-1}; \alpha+1-\varepsilon, \beta+1-\varepsilon, 2-\varepsilon, \delta; \frac{a-z}{a-1}\right), \quad (2.27)$$

- $z_0 = \infty, \sigma_1 = \alpha$ :

$$z^{-\alpha} \text{H}\ell\left(\frac{1}{a}, \alpha(\beta-\varepsilon) + \frac{\alpha}{a}(\beta-\delta) - \frac{q}{a}; \alpha, \alpha-\gamma+1, \alpha-\beta+1, \delta; \frac{1}{z}\right), \quad (2.28)$$

- $z_0 = \infty, \sigma_1 = \beta$ :

$$z^{-\beta} \text{H}\ell\left(\frac{1}{a}, \beta(\alpha-\varepsilon) + \frac{\beta}{a}(\alpha-\delta) - \frac{q}{a}; \beta, \beta-\gamma+1, \beta-\alpha+1, \delta; \frac{1}{z}\right). \quad (2.29)$$

Note the functional dependence  $1/z$  in the last two Eqs. (2.28) and (2.29) which corresponds to the coordinate transformation  $w = 1/z$  as mentioned above. The respective regions of convergences can then be determined by the radius of convergence of the Heun function (2.23) for each of the cases individually. Moreover, for all of the expressions above an additional condition on one (or more) of the parameters should be ensured according to Eq. (2.13), e.g.,  $\gamma \notin \mathbb{Z}$  in the case  $z_0 = 0$ . But this situation is not relevant for the papers presented in Chapt. 3.

### 2.1.4 Triconfluent Heun equation

The triconfluent Heun equation (THE) can be derived by the coalescence of all of the regular singular points of the Heun equation (2.14) at  $\infty$  (see e.g., [3, 5]), resulting in the following canonical form

$$\frac{d^2 f(z)}{dz^2} - (3z^2 + \gamma) \frac{df(z)}{dz} + [\alpha + (\beta - 3)z]f(z) = 0, \quad (2.30)$$

where the parameters  $\alpha, \beta, \gamma$  are generally complex. Therefore, the THE (2.30) has only one singular point at  $z = \infty$  that is now an irregular singular point. The solution around the ordinary point  $z_0 = 0$  can now be express simply in the form of the Maclaurin series

$$f(z) = \sum_{n=0}^{\infty} c_n z^n. \quad (2.31)$$

The procedure is now exactly the same as presented in the previous subsection. We substitute the series solution (2.31) into Eq. (2.30) and by setting the terms before each respective power of  $z$  equal to 0 we get the following recurrence equation for the coefficients  $c_n$ :

$$n(n-1)c_n - (n-1)\gamma c_{n-1} + \alpha c_{n-2} + (\beta + 6 - 3n)c_{n-3} = 0. \quad (2.32)$$

Together with the following set of initial conditions (see e.g., [3])

$$c_0 = 1, \quad c_1 = 0, \quad c_2 = -\frac{\alpha}{2} \quad (2.33)$$

the recurrence equation (2.32) defines the triconfluent Heun function (THF):

$$\text{THF}(\alpha, \beta, \gamma; z) \equiv \sum_{n=0}^{\infty} c_n z^n. \quad (2.34)$$

The second linearly independent solution to the triconfluent Heun equation can then be written as (see e.g., [3])

$$f(z) = \exp(z^3 + \gamma z) \text{THF}(\alpha, -\beta, \gamma; -z), \quad (2.35)$$

where the following condition must hold

$$\gamma \neq 0, \quad (2.36)$$

and the radius of convergence for both the solutions is (again)

$$|z| < 1. \quad (2.37)$$

To close this section it is convenient to point out that both the Heun functions and the triconfluent Heun functions are implemented in some of the most widely used computer algebraic systems such as Maple (version 17 or higher) and Mathematica (version 12.1 and higher). Therefore, it is very straightforward and simple to evaluate those functions for any combination of the input parameters at any point.

## 2.2 Webster-type equation

For the purpose of this thesis and especially for the papers presented in Chapter 3 it is convenient to introduce a general form of the Webster-like equation which is a second order linear differential equation that can be used to describe various physical problems regarding the propagation of linear waves in a media that is inhomogeneous in one direction (in this case along

the  $z$  coordinate). The name comes from the similarity with the so-called Webster horn equation, which is an equation describing the propagation of linear acoustic waves inside of a duct of slowly varying cross-sectional area, see e.g., [7]. The general form of this equation for can be written as

$$\frac{d^2 f(z)}{dz^2} + \frac{1}{\eta(z)} \frac{d\eta(z)}{dz} \frac{df(z)}{dz} + k^2 \zeta^2(z) f(z) = 0, \quad (2.38)$$

where the function  $\eta(z)$  describes the profile of the inhomogeneity of various parameters of the inhomogeneous media (density, Young modulus, shear modulus, flow velocity distribution, waveguide cross-sectional area, etc.) and  $k$  stands for the wavenumber, which is a monotonically increasing function of the frequency. The function  $\zeta(z)$  has no general physical interpretation and in some cases is equal to 1 (e.g., in the original Webster horn equation). Note that in the case of inhomogeneous elastic materials the function  $\eta(s)$  is usually referred to as the material function, see Sec. 2.5.

## 2.3 WKB approximation

Wentzel–Kramers–Brillouin (WKB) approximation method is a powerful tool to express a closed form approximate analytical solution to linear differential equation with non-constant coefficients. In this section this technique is applied specifically to the Webster-type equation, as defined in Sec. 2.2. The procedure to follow is inspired by the book [8].

For convenience we assume all the components of the equation  $f(z)$ ,  $\eta(z)$ ,  $\zeta(z)$ ,  $k$ ,  $z$  to be dimensionless. By expressing the solution in the following form (see e.g., [8])

$$f(z) = \exp\left(i \int \kappa(z) dz\right), \quad (2.39)$$

where  $i$  denotes the imaginary unit, and substituting into Eq. (2.38) we obtain

$$i\kappa'(z) - \kappa^2(z) + i \frac{\eta'(z)}{\eta(z)} \kappa(z) + k^2 \zeta^2(z) = 0, \quad (2.40)$$

where the notation  $' \equiv d/dz$  is used hereinafter for the sake of readability. The following series expansion is now assumed for the function  $\kappa(z)$  (see e.g., [8]):

$$\kappa(z) = k\kappa_1(z) + \kappa_2(z) + \frac{\kappa_3(z)}{k} + \frac{\kappa_4}{k^2} + \dots \quad (2.41)$$

We now substitute the expression (2.41) into Eq. (2.40), resulting in the following system of equations corresponding to the coefficients of the respective

powers of  $k$ :

$$\begin{aligned}\zeta^2 - \kappa_1^2(z) &= 0, \\ i\frac{\eta'(z)}{\eta(z)}\kappa_1(z) + i\kappa_1'(z) - 2\kappa_1(z)\kappa_2(z) &= 0, \\ &\vdots\end{aligned}\tag{2.42}$$

The solution to the system of Eqs. (2.42) is then

$$\kappa_1(z) = \pm\zeta(z), \quad \kappa_2(z) = \frac{i}{2} \left( \frac{\eta'(z)}{\eta(z)} + \frac{\zeta'(z)}{\zeta(z)} \right), \quad \dots\tag{2.43}$$

Since the dimensionless wavenumber  $k$  is a monotonically increasing function of the frequency, the high frequency approximation can be written as

$$k \gg 1.\tag{2.44}$$

The function  $\kappa(z)$  can now be approximated by keeping only the first two terms of the expansion (2.41):

$$\kappa(z) \approx k\kappa_1(z) + \kappa_2(z) = \pm k\zeta(z) + \frac{i}{2} \left( \frac{\eta'(z)}{\eta(z)} + \frac{\zeta'(z)}{\zeta(z)} \right).\tag{2.45}$$

By returning back to the expression (2.39) the WBK solution to the Webster-like equation (2.38) can be expressed as a linear combination of the two linearly independent functions

$$f(z) \approx \frac{\mathcal{A}}{\sqrt{\eta(z)\zeta(z)}} \exp\left( ik \int_{z_0}^z \zeta(\tilde{z}) d\tilde{z} \right) + \frac{\mathcal{B}}{\sqrt{\eta(z)\zeta(z)}} \exp\left( -ik \int_{z_0}^z \zeta(\tilde{z}) d\tilde{z} \right),\tag{2.46}$$

where  $\mathcal{A}, \mathcal{B}$  stand for the integration constants. Finally, it is important to emphasise that this solution can be considered as a truly analytical solution if and only if the integral  $\int \zeta(z) dz$  can be evaluated analytically, otherwise a numerical method would need to be employed and we can no longer consider such solution as an analytical one.

## 2.4 Floquet-Bloch theory

This section focuses on one of the most widely used method for obtaining solution to the differential equation with periodic non-constant coefficients - the Floquet-Bloch theory. A very good and comprehensive review of this theory with applications to the Schrödinger's equation can be found in the book [9].

### 2.4.1 Equation with periodic coefficients

First, let's start with writing down the most general form of a second order linear differential equation with periodic coefficients as

$$f''(z) + p(z)f'(z) + q(z)f(z) = 0, \quad (2.47)$$

where (once again) the notation  $' \equiv d/dz$  for the derivative is used in this section for the sake of readability and the functions  $p(z), q(z)$  are both periodic with the period  $d$ , which can be expressed as

$$p(z + d) = p(z), \quad q(z + d) = q(z). \quad (2.48)$$

### 2.4.2 Liouville's formula

It is now convenient to derive the Liouville's formula for the Wronskian of Eq. (2.47) that is defined as (see e.g., [1])

$$W[f_1, f_2](z) = \det \begin{pmatrix} f_1(z) & f_2(z) \\ f_1'(z) & f_2'(z) \end{pmatrix} = f_1(z)f_2'(z) - f_1'(z)f_2(z), \quad (2.49)$$

where  $f_1(z), f_2(z)$  are the two linearly independent solutions of the equation. Therefore, we can write

$$\begin{aligned} f_1''(z) + p(z)f_1'(z) + q(z)f_1(z) &= 0, \\ f_2''(z) + p(z)f_2'(z) + q(z)f_2(z) &= 0. \end{aligned} \quad (2.50)$$

By multiplying the second of Eqs. (2.50) by  $f_1(z)$  and subtracting the first equation multiplied by  $f_2(z)$  we get

$$f_1(z)f_2''(z) - f_1''(z)f_2(z) + p(z)[f_1(z)f_2'(z) - f_1'(z)f_2(z)] = 0, \quad (2.51)$$

which can be rewritten by using the expression (2.49) as

$$W'(z) + p(z)W(z) = 0, \quad (2.52)$$

where for simplicity we denote  $W[f_1, f_2](z)$  as only  $W(z)$  hereinafter. By rearranging Eq. (2.52) into

$$\frac{W'(z)}{W(z)} = -p(z), \quad (2.53)$$

and further integrating we arrive at the Liouville's formula for the Wronskian (see e.g., [9])

$$W(z) = W(z_0) \exp \left( - \int_{z_0}^z p(\tilde{z}) d\tilde{z} \right). \quad (2.54)$$

### 2.4.3 Floquet theory

Assume a normalised solution of Eq. (2.47) satisfying the following initial conditions

$$\begin{aligned} u(0) &= 1, & v(0) &= 0, \\ u'(0) &= 0, & v'(0) &= 1. \end{aligned} \quad (2.55)$$

Any solution of Eq. (2.47) can now be written as a linear combination of the normalised solution  $u(z), v(z)$  as

$$f(z) = f(0)u(z) + f'(0)v(z). \quad (2.56)$$

We are now looking for a solution satisfying the so-called Floquet condition that can be written as (see e.g., [9])

$$F(z + d) = \lambda F(z), \quad (2.57)$$

where  $\lambda$  is called the Floquet multiplier and the function  $F(z)$  is then called the Bloch wave. Due to the periodicity of the functions  $p(z), q(z)$  if  $f(z)$  is a solution to Eq. (2.47) then  $f(z + d)$  is also a solution (see e.g., [9]). Therefore, by employing the expression (2.56) we can write

$$\begin{aligned} u(z + d) &= u(d)u(z) + u'(d)v(z), \\ v(z + d) &= v(d)u(z) + v'(d)v(z). \end{aligned} \quad (2.58)$$

Now, let's express the Bloch wave  $F(z)$  as

$$F(z) = \mathcal{C}_1 u(z) + \mathcal{C}_2 v(z), \quad (2.59)$$

where  $\mathcal{C}_1, \mathcal{C}_2$  stand for the integration constants. By combining Eqs. (2.57), (2.58) and (2.59) we get the following equation

$$\mathcal{C}_1 [u(d)u(z) + u'(d)v(z)] + \mathcal{C}_2 [v(d)u(z) + v'(d)v(z)] = \lambda [\mathcal{C}_1 u(z) + \mathcal{C}_2 v(z)], \quad (2.60)$$

which can be further rearranged as

$$[(u(d) - \lambda)\mathcal{C}_1 + v(d)\mathcal{C}_2]u(z) + [u'(d)\mathcal{C}_1 + (v'(d) - \lambda)\mathcal{C}_2]v(z). \quad (2.61)$$

But since the functions  $u(z), v(z)$  are linearly independent the following must apply

$$\begin{aligned} (u(d) - \lambda)\mathcal{C}_1 + v(d)\mathcal{C}_2 &= 0, \\ u'(d)\mathcal{C}_1 + (v'(d) - \lambda)\mathcal{C}_2 &= 0. \end{aligned} \quad (2.62)$$

The system of equations (2.62) represents an eigenvalue problem

$$\mathbf{A}\mathbf{c} = \lambda\mathbf{c}, \quad (2.63)$$

where

$$\mathbf{A} = \begin{pmatrix} u(d) & v(d) \\ u'(d) & v'(d) \end{pmatrix}, \quad \mathbf{c} = \begin{pmatrix} \mathcal{C}_1 \\ \mathcal{C}_2 \end{pmatrix}. \quad (2.64)$$

To ensure that Eq. (2.63) possesses a nontrivial solution it is required that

$$\det(\mathbf{A} - \lambda \mathbf{I}) = 0, \quad (2.65)$$

where  $\mathbf{I}$  denotes the identity matrix, resulting in the following characteristic equation

$$\lambda^2 - [u(d) + v'(d)]\lambda + \det(\mathbf{A}) = 0, \quad (2.66)$$

which can be rewritten by employing Eq. (2.49) as

$$\lambda^2 - [u(d) + v'(d)]\lambda + W[u, v](d) = 0. \quad (2.67)$$

According to Eq. (2.67) the following must apply for its roots  $\lambda_1, \lambda_2$  (the respective Floquet multipliers):

$$\begin{aligned} \lambda_1 + \lambda_2 &= u(d) + v'(d), \\ \lambda_1 \lambda_2 &= W[u, v](d). \end{aligned} \quad (2.68)$$

By employing the Liouville's formula for the Wronskian (2.54) and focusing on the Webster-type equation (2.38) for which

$$p(z) = \frac{\eta'(z)}{\eta(z)}, \quad (2.69)$$

we get

$$W[u, v](d) = W[u, v](0) \exp\left(-\int_0^d \frac{\eta'(z)}{\eta(z)} dz\right) = \frac{\eta(0)}{\eta(d)}, \quad (2.70)$$

but since  $\eta(z)$  is now a periodic function with the period  $d$ , i.e.,

$$\eta(z + d) = \eta(z), \quad (2.71)$$

then according to Eq. (2.70)

$$W[u, v](d) = 1 \quad (2.72)$$

and the whole problem simplifies to

$$\lambda^2 - [u(d) + v'(d)]\lambda + 1 = 0, \quad (2.73)$$

where the Floquet multipliers  $\lambda_1, \lambda_2$  satisfy

$$\begin{aligned} \lambda_1 + \lambda_2 &= u(d) + v'(d), \\ \lambda_1 \lambda_2 &= 1. \end{aligned} \quad (2.74)$$

### 2.4.4 Bloch waves

In order to find the Bloch waves for the Webster-type equation (2.38) we first express the roots of the characteristic equation (2.73) as

$$\lambda_{1,2} = \frac{h \pm \sqrt{h^2 - 4}}{2}, \quad (2.75)$$

where

$$h \equiv u(d) + v'(d). \quad (2.76)$$

Eqs. (2.75) now become linearly dependent, so without the loss of generality we substitute the expression (2.76) into one of them (in this case the first one), resulting in the following expression for the integration constants  $\mathcal{C}_1, \mathcal{C}_2$

$$\mathcal{C}_1 = 1, \quad \mathcal{C}_2 = \frac{\lambda_{1,2} - u(d)}{v(d)}, \quad (2.77)$$

(the choice  $\mathcal{C}_1 = 1$  is arbitrary). Therefore, according to Eq. (2.59) the two linearly independent Bloch waves in the first period can be written as

$$F_{1,2}(z) = u(z) + \frac{\lambda_{1,2} - u(d)}{v(d)}v(z). \quad (2.78)$$

Now comes the principal part of the Floquet-Bloch theory. Up to this point, we have expressed the Bloch waves based on the normalised solution (2.55). The question now follows - how do we find the normalised solution to Eq. (2.47) in the whole domain? The answer is simple - we don't! On the contrary, we only need to specify the normalised solution in the first period of the respective domain, i.e.,  $z \in \langle 0, d \rangle$ . All that is required now is to extend the corresponding Bloch waves to the rest of the domain by simply employing the Floquet condition (2.57) as follows:

$$F_{1,2}^{(\text{ext})}(z) = \lambda_{1,2}^{\lfloor z/d \rfloor} F_{1,2}(z - \lfloor z/d \rfloor d), \quad (2.79)$$

where  $F_{1,2}^{(\text{ext})}(z)$  denotes the Bloch wave extended to the whole domain and the function  $\lfloor x \rfloor$  returns the nearest integer less than or equal to  $x$ .

To sum up, in order to find the general solution to Eq. (2.47) in terms of the Bloch waves we only need to find the normalised solution in the first period, use it to express the Bloch waves (again in the first period) according to Eq. (2.77) and finally extend the Bloch waves to the rest of the domain by simply employing the formula (2.79).

The Floquet-Bloch theory provides us with an extremely effective and elegant method of how to express the solutions to the Webster-type equation with periodic non-constant coefficients ( $\eta(z)$  and  $\zeta(z)$ ) in contrast to e.g., the transfer matrix method (TMM, see e.g., [10]) which also provides an effective method for solving wave related problems in (locally) periodic structures, but to express the solutions in the whole domain can feel a bit cumbersome.



## 2.5 Functionally graded materials

As the title suggests, the topic of this thesis is related to all sort of elastic and acoustic inhomogeneous structures. Regarding the acoustic part it is usually pretty straightforward to realize e.g., an acoustic waveguide (duct) of continuously varying cross-sectional area or an uniform waveguide but now with a nonuniform distribution of the mean flow velocity profile. But it might not be immediately obvious how to realize an elastic material of continuously varying density, Young modulus, shear modulus etc. On one hand, most solids that can be find in nature (except for crystals, but those are usually strongly anisotropic, which is beyond the scope of this work) are typically inhomogeneous, the most obvious example can be the composition of the Earth itself. But this type of inhomogeneity is a priori given by the nature. Therefore, this section is devoted to the Functionally Graded Materials (hereinafter referred to as FGM) which are artificial elastic materials whose physical properties can be controlled by the manufacturing process.

First, since all of the papers included in Chapt. 3 deal with structures that are inhomogeneous in only one spatial direction, we will make the same assumption here. Hence, let's start by assuming a FGM whose one or more properties vary along (without the loss of generality) the  $z$  coordinate. The mathematical way of how to describe such an inhomogeneity is by introducing the corresponding material function  $\eta(z)$  (see Sec. 2.2) with the following expression for the material property  $P$ :

$$P(z) = P_0\eta(z), \quad (2.80)$$

where  $P(z)$  designates the value of the respective material property at point  $z$ . The conventional choice it that  $P_0$  represents the value at  $z = 0$  implying  $\eta(0) = 1$ . The situation is depicted in Fig. 2.1 for a FGM of the length  $\ell$ .

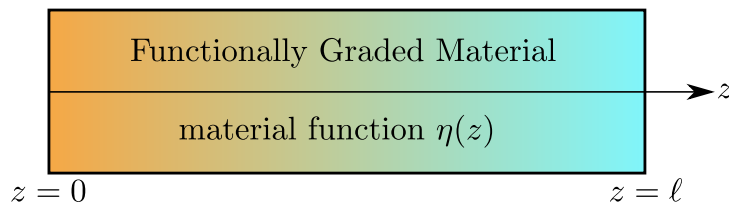


**Figure 2.1:** Material function.

Now, let's focus on the concept of how to design such a material (at least in theory). We start with two distinct materials denoted as  $M_I$  and  $M_{II}$  with the corresponding material properties  $P_I \neq P_{II}$ . Assume now that the FGM is composed by discrete layers of thickness  $\delta z$  and each of those layers consists

of two sublayers, one made of material  $M_I$  with the respective thickness  $\delta z_1$  and the second one of  $M_{II}$  with the respective thickness  $\delta z_2$ . The two thicknesses then satisfy the following condition

$$\delta z_1 + \delta z_2 = \delta z. \quad (2.81)$$

The  $n$ -th such layer corresponding to the point  $z_n = n\delta z$  is depicted in Fig. 2.2 (the function  $V(z_n)$  will be explained further in the text).

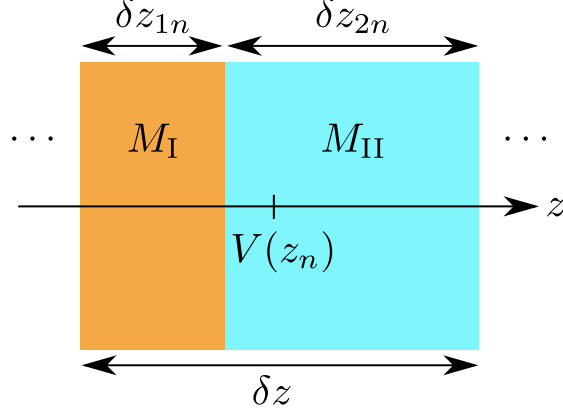


**Figure 2.2:**  $n$ -th layer of the FGM.

Now assume that we want to analyse the propagation of elastic waves (at this point it is not necessary to specify the type of the waves) along the  $z$  direction inside of such FGM material. If the thickness of the layer  $\delta z$  is substantially smaller than the corresponding wavelength  $\lambda$  of the elastic wave

$$\delta z \ll \lambda, \quad (2.82)$$

we can approximate the material property of the  $n$ -th layer by the so called rule of mixtures (see e.g., [11])

$$P(z_n) \approx \frac{\delta z_{1n} P_I + \delta z_{2n} P_{II}}{\delta z}. \quad (2.83)$$

It is now useful to define the volume fraction function (see e.g., [11])  $V(z_n)$  for each layer as

$$V(z_n) \equiv \frac{\delta z_{2n}}{\delta z}, \quad (2.84)$$

which gives a percentage of the material  $M_{II}$  inside of the  $n$ -th layer. Hence, the following condition must hold

$$0 \leq V(z_n) \leq 1. \quad (2.85)$$

Eq. (2.83) can now be rewritten as

$$P(z_n) \approx P_I[1 - V(z_n)] + P_{II}V(z_n), \quad (2.86)$$

where we used the condition (2.81). If we now assume that the thickness of each layer is also substantially smaller than the overall length of the FGM

$$\delta z \ll \ell, \quad (2.87)$$

we can treat the discrete position of each layer as an continuous variable

$$z_n \rightarrow z \quad (2.88)$$

and therefore rewrite Eq. (2.86) as

$$P(z) = P_I[1 - V(z)] + P_{II}V(z), \quad (2.89)$$

where the approximation symbol is omitted hereinafter. Eq. (2.89) now describes any material property  $P$  as a continuously varying function of  $z$ .

At this point we might want to return to the definition of the material function given by Eq. (2.80). For that purpose, we rearrange Eq. (2.89) to the following form

$$P(z) = P_I[1 + \mathcal{P}V(z)], \quad (2.90)$$

where  $\mathcal{P} \equiv (P_{II}/P_I - 1)$ . By the comparison of Eqs. (2.80) and (2.90) we get the following relation between the material function and the volume fraction function

$$\eta(z) = 1 + \mathcal{P}V(z). \quad (2.91)$$

Please note that as mentioned at the beginning of this section the typical choice is that  $\eta(0) = 1$ . According to Eq. (2.91) this implies  $V(0) = 0$  meaning that the beginning of the FGM is composed purely of the material  $M_I$ . But of course in general this does not have to be true and one can start the FGM with any fractional composition of the two materials.

FGMs are a topic of a great scientific importance and this section covers only a very simplified one-dimensional mathematical model for the purposes of this thesis. For further information regarding the properties, fabrication, analysis, application etc. of the FGMs the reader is referred to e.g., [12, 13].





## Chapter 3

### Collection of publications

This is the main chapter of the thesis where six papers published by the author are presented. Five of the mentioned papers are published in peer reviewed journals indexed in Web of Science and one of them is a conference paper. All the papers have one specific topic in common - they all deal with the propagation of acoustic or elastic waves in inhomogeneous media of some kind (in line with the topic of this dissertation thesis), whereas the primary approach is always to employ some analytical or approximate analytical method. The purpose of the following text is to summarize the typical steps involved in each one of the papers.

The first step is to formulate the problem with an appropriate model equation (or equations) that describe the propagation of the specific wave type in the corresponding inhomogeneous structure. Note that this equation is usually of the Webster-type, see Sec. 2.2, Eq. (2.38). The spatial inhomogeneity of the structure is then typically described by the corresponding function  $\eta(s)$ . The second step is to employ a convenient mathematical method in order to find a closed form exact or approximate analytical solution to the respective equation. In the majority of the presented papers (4 out of 6) the approach is to transform the model equation into the form of the canonical Heun equation (2.14) or the triconfluent Heun equation (2.30) for which we can write the exact analytical solution according to Sec. 2.1. This step can be done either in special cases where the functions  $\eta(z), \zeta(z)$  (see Sec. 2.2) are given by a specific spatial dependence allowing the transformation or some form of an approximation technique can be employed to realize the transformation. Another possibility is to use the WKB method (see Sec. 2.3), which can also serve as a benchmark solution to the solutions expressed by the (triconfluent) Heun functions in the case where the condition (2.44) is met.

In the last presented paper a special technique involving the second order approximation of the transfer matrix is used. Once the analytical solutions (or other analytical expressions for the specific quantities of interest) are formulated, the next steps then follows from the specific issue that is being solved. Sometimes, the solutions themselves constitute the desired outcome, while in other cases, certain boundary conditions are applied, leading to the corresponding dispersion relation. Alternatively, a specific form of a wave manipulation structure (such as a lens) may be constructed based on the properties of the (approximate) analytical solution. Furthermore, the transmission and reflection coefficients can be calculated, etc. Since all of those papers are mostly theoretical, the typical last step involves some form of a numerical solution/simulation in order to validate the correctness of the proposed analytical approach.

A typical question for someone dealing with an exact/approximate analytical approach in order to solve the specific wave related problems can be: Why do we need the analytical solutions when they are often given by complicated expressions (except for the simplest textbook examples) and the numerical methods nowadays provide the solution much more easily? To this it is possible to propose the following answer: The analytical approach can sometimes be a bit more laborious to derive than using numerical methods, but the closed form analytical expression of the desired solution can be extremely useful in many scenarios. Let's sum up some of the major advantages here. First, an analytical solution provides us with much more information than the numerical one and therefore enables deeper understanding of how do the waves behave inside of the respective (inhomogeneous) structure. Second, with the analytical solution, it is possible to perform various further mathematical manipulations and thereby obtain additional quantities characterizing the behavior of the investigated waves. The exact analytical solutions can also serve as benchmark solutions for the numerical schemes. Moreover, in specific situations, the analytical solutions can be more advantageous for several types of optimization procedures.

Let's demonstrate this with the following example. Assume that we want to analyze the wave propagation inside of an inhomogeneous structure described by the corresponding function  $\eta$  controlled by the parameter  $p$ . That means the material function depends simultaneously on the coordinate  $z$  and also on  $p$ , which we can write as

$$\eta = \eta(p; z). \quad (3.1)$$

Now, we want to assess how we can control the wave propagation inside of such inhomogeneous structure by varying this parameter. The typical numerical approach will then be to solve the model equation again and again for various values of the parameter  $p$ . In contrast, once the exact/approximate analytical solution is expressed including the dependence on the parameter  $p$

as

$$f = f(p; z) \quad (3.2)$$

there is no need to solve the model equation again. On the contrary, we can now perform various types of further analytical manipulations, such as employing different types of boundary conditions in order to determine the corresponding dispersion relation or to express the analytical formulas for the transmission and reflection coefficient for the corresponding structure. Further, in case we can assume a locally periodic structure by repeating the original inhomogeneous one several times, we can directly extend the solution to the whole system by simply employing the Floquet-Bloch theory (see Sec. 2.4, Eq. (2.79)). The next possibility could be to separate the analytical solution by using the wave-splitting method to the two parts travelling in the opposing directions to understand what happens inside of the respective inhomogeneous structure, etc. Of course that all of this could potentially somehow be achieved numerically. But it is much easier, convenient and elegant to work with analytical expressions that most types of computer algebraic systems (CAS) such as Maple and Mathematica can easily process and evaluate. Furthermore, it should be emphasised that when working with the numerical solutions there is always a risk that the solution is incorrect even though at first glance it might seem physically reasonable. Or that the numerics diverges with e.g., just a slight deviation of the initial settings that originally provided a correct solution. Basically, the numerical solutions cannot be blindly trusted and should always be treated carefully.

In conclusion, there is certainly no intention to belittle the importance of numerical methods. On the contrary, the aim is solely to emphasize the advantages of having the analytical solutions, as they can potentially offer overall better insight into the studied problems and are typically much more convenient and enjoyable to work with.

### 3.1 Paper I

**Title:** *Surface Love-type waves propagating through viscoelastic functionally graded media*

The first paper published in The Journal of the Acoustical Society of America deals with the propagation of the so called Love-type waves, which are surface shear horizontal (SH) elastic waves propagating inside of a generally inhomogeneous elastic surface layer of finite thickness laid over a homogeneous substrate extended up to infinity. The term SH means that the particles oscillate perpendicularly to the direction of propagation and in the plane parallel to the surface. The Love-type waves are often characterised as a form of guided waves, whereas the surface layer then represents the corresponding waveguide structure. The energy is then concentrated at the surface (therefore the term surface wave) and decreasing exponentially inside of the substrate towards the infinite depth. In this paper we assume a surface layer consisting of a FGM (see Sec. 2.5) that is inhomogeneous along the thickness direction, whereas the continuously varying parameters whose profile is given by the respective material function (2.80) are the density and the shear modulus. First, the model equation in the form of the Webster-type equation (2.38) is derived including the viscoelastic losses. It is then shown that this equation can be transformed into the form of the triconfluent Heun equation (see Sec. 2.1) in the special case where the material function itself is expressed as a combination of the triconfluent Heun functions that can be controlled by up to eight distribution parameters. Therefore, we are able to express the general closed form exact analytical solution to the model equation also as a combination of the triconfluent Heun functions for a completely new class of material function profiles, which greatly extends the set of other material function profiles for which the exact analytical solutions are known. Based on the specific boundary conditions and by using the found analytical solution the corresponding dispersion equation is then expressed.

In the next part of the paper we demonstrate the applicability of the theory presented above onto the specific examples. First, we show that the viscoelastic losses of the substrate have a negligible effect on the real part of the dispersion curves (in the case of the homogeneous surface layer) and therefore we neglect them in the further calculations. Next, the dispersion curves (in this case the dependence of the phase velocity of the Love-type waves on the dimensionless wavenumber) corresponding to the first three modes of the solution (Love modes) are plotted for the two selected profiles of the material function realized by the two specific sets of the distribution parameters defined above. Then, for selected values of the dimensionless wavenumber the corresponding solutions of the model equation are plotted together with the results obtained via the standardly used numerical method



Runge-Kutta-Fehlberg 45 (RKF45) in order to validate their correctness. For comparison, the approximate analytical WKB solutions (see Sec. 2.3) are also displayed, showing that (as expected) the WKB solution does not provide correct results in the case of relatively low values of the dimensionless wavenumber where the condition (2.44) is not met.

Finally, a case study is conducted for the gaussian-like profile of the material function where we assess the effect of the height of the gaussian on the corresponding dispersion curves with the following result - the bigger the height of the gaussian the wider the gap between the two dispersion curves corresponding to the first and the second Love mode. This effect is very interesting and can be possibly utilized in various types of practical applications where we require only the first Love mode to propagate. One of the possible continuation of this research could be the study of how does the boundary condition at the surface (which is assumed traction free in this paper) affects the corresponding dispersion curves for various profiles of the material function. In practice, this means that we assume a presence of another material at the top of the layer (e.g., some type of liquid). The other possibility is to extend the found analytical solution to a locally periodic structure consisting of  $N$  such inhomogeneous layers laid over each other, whereas this is the topic of the Paper II.

NOVEMBER 03 2021

## Surface Love-type waves propagating through viscoelastic functionally graded media

A. Krpensky; M. Bednarik



*J. Acoust. Soc. Am.* 150, 3302–3313 (2021)

<https://doi.org/10.1121/10.0006964>



View  
Online



Export  
Citation

CrossMark



LEARN MORE

Advance your science and career as a member of the  
**Acoustical Society of America**

# Surface Love-type waves propagating through viscoelastic functionally graded media

A. Krpensky<sup>a)</sup> and M. Bednarik

Faculty of Electrical Engineering, Czech Technical University in Prague, Technicka 2, Prague 6, 166 27, Czech Republic

## ABSTRACT:

This paper deals with the solution of the model equations, which describes the propagation of the surface Love-type waves in a waveguide structure consisting of a lossy isotropic inhomogeneous layer placed on a viscoelastic homogeneous substrate. The paper points to the possibility of using the triconfluent Heun differential equation to solve the model equation. The exact analytical solution within the inhomogeneous layer is expressed by the triconfluent Heun functions. The exact solutions are general in the sense that only the internal parameters of the triconfluent Heun functions can change the spatial dependencies of the material parameters in the inhomogeneous layer's thickness direction. Based on the comparison, the limits of the WKB method applicability are discussed. It is further demonstrated that substrate losses affect the dispersion characteristics only to a small extent. Using examples in which the surface layer is represented by functionally graded materials, it was shown that the distance between the modes can be influenced through those materials. © 2021 Acoustical Society of America. <https://doi.org/10.1121/10.0006964>

(Received 17 May 2021; revised 5 October 2021; accepted 7 October 2021; published online 3 November 2021)

[Editor: Lixi Huang]

Pages: 3302–3313

## I. INTRODUCTION

The propagation of the shear surface elastic waves of Love type (hereinafter only referred to as Love waves) in functionally graded materials is an issue of considerable scientific and practical interest. We can encounter the use of Love waves in many areas, especially in sensor technology, seismology, geophysics, nondestructive testing of materials, seismic engineering, and geotechnical engineering. A very well-organized overview devoted to Love waves and their use is published in Ref. 1 (Chap. 2). To understand the behavior of Love waves, which propagate through an inhomogeneous layer, it is important to have the exact analytical solutions of the corresponding model equations at our disposal. The model equation describing the propagation of the time-harmonic SH (shear horizontal) Love waves in an inhomogeneous layer can be reduced to an ordinary second-order differential equation with variable coefficients representing a general Sturm-Liouville equation. Thus, finding a solution to the model equation for the given boundary conditions leads to a Sturm-Liouville problem. Although the Sturm-Liouville theory is well developed for a general Sturm-Liouville equation with variable coefficients, the practical solutions of the problems (see, e.g., Ref. 2) are only studied on equations with constant coefficients (constant material parameters) in layered media (see, e.g., Ref. 3) or only for variable coefficients given by elementary mathematical functions (linear, exponential, sinusoidal function, etc.). This is the reason why the model equations' exact analytical solutions have, so far, been published only for

simple material functions expressing the spatial dependencies of the material parameters in the thickness direction; see, e.g., Refs. 4–7) However, if it is necessary to consider the more complex profiles of the material functions, then, usually, the solution of the Sturm-Liouville problem relies on an appropriate numerical method (e.g., the transfer matrix method, the finite difference method), the use of some approximate analytical method, such as the Wentzel-Kramers-Brillouin (WKB) method (see, e.g., Refs. 8 and 9), the series expansion method (see, e.g., Ref. 10), or the Green's function approach method (see, e.g., Refs. 11–13).

It is, therefore, desirable to seek a solution to the Sturm-Liouville problem for other material function profiles that come into consideration. The exact solution of the model equation for the functionally graded and lossy materials allows us to assess the influence of the losses and selected profiles of the material functions on the Love waves' propagation characteristics. So far, comparably very few published works have addressed the issue of propagating surface elastic waves through lossy media, and it is possible to refer to some of them, e.g., Refs. 14–22.

Specifically, in this paper, we focus on the description of the propagation of elastic Love waves in an inhomogeneous isotropic surface layer in which the spatial dependence of the density and shear modulus in the thickness direction is considered. Our main motivation is to present a method to solve the corresponding model equations for the inhomogeneous viscoelastic surface layer exactly, where the spatial dependence of the material parameters involved can be designed over a relatively wide range. Using a suitable transformation, we can convert the model equation into the form of the triconfluent Heun differential equation (THE) for which the exact analytical solutions, called the

<sup>a)</sup>Electronic mail: antonin.krpensky@fel.cvut.cz, ORCID: 0000-0003-3150-6592.

triconfluent Heun functions, are known (see, e.g., Refs. 23 and 24). The evaluation of the triconfluent Heun functions is already a standard part of the mathematical software such as Maple (Maplesoft, Waterloo, Canada) or Mathematica (Wolfram, Witney, United Kingdom). The material function itself can be expressed as a linear combination of the triconfluent Heun functions. Employing this approach, it is then possible to find the exact analytical solution of the model equation for various material function profiles. The exact solutions may involve losses that occur in both the inhomogeneous layer and the substrate. Although in this paper we only deal with isotropic materials, there are some works dedicated to ortotropic and anisotropic materials; see, e.g., Refs. 25–28.

This paper is organized as follows. An outline of the model equation’s derivation describing the propagation of Love waves in a viscoelastic surface layer is given in Sec. II. Section III is devoted to finding the exact analytical solution of the model equation for the inhomogeneous viscoelastic layer. The expression of the material function using the triconfluent Heun functions is shown in Sec. IV. The possibility to describe the material functions, using the finite polynomials, is presented in Sec. V. The determination of the dispersion equation is shown in Sec. VI. The presented analytical solutions’ applicability is demonstrated on the two specifically chosen examples of the inhomogeneous surface layer in Sec. VII, and the results based on the exact, approximate, and numerical solutions are discussed and compared. Finally, Sec. VIII provides our conclusions and discussion. To make this paper sufficiently self-contained, some features concerning the THE and its polynomial solution are outlined in Appendixes A and B.

## II. MODEL EQUATIONS

The geometry of the waveguide structure and corresponding coordinate system are illustrated in Fig. 1. The materials used for the waveguide are considered to be isotropic, and the surface layer (coating) with a thickness  $H$  is inhomogeneous in the thickness direction and has an infinite extent in the  $xy$ -plane. The half-space (substrate) is homogeneous. Without

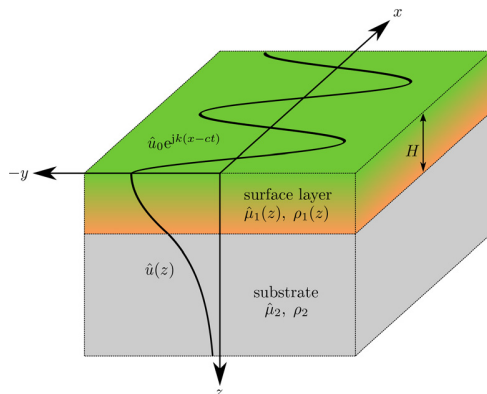


FIG. 1. (Color online) The geometry of the Love waveguide structure (an isotropic inhomogeneous surface layer over an isotropic homogeneous half-space).

loss of generality, we assume a time-harmonic elastic SH surface Love wave propagating along the  $x$  direction. Assuming the mechanical displacement vector  $[0, u_1(x, z, t), 0]$ , we can write the stress equation of motion for the inhomogeneous layer (see, e.g., Refs. 4 and 7) as

$$\frac{\partial \sigma_{y,x}^{(1)}}{\partial x} + \frac{\partial \sigma_{y,z}^{(1)}}{\partial z} = \rho(z) \frac{\partial^2 u_1}{\partial t^2}, \tag{1}$$

where  $\rho(z)$  is the mass density function, and the shear stress components are given as

$$\sigma_{y,x}^{(1)} = \hat{\mu}(z) \frac{\partial u_1(x, z, t)}{\partial x}, \quad \sigma_{y,z}^{(1)} = \hat{\mu}(z) \frac{\partial u_1(x, z, t)}{\partial z}. \tag{2}$$

Considering the Kelvin-Voigt model of the viscoelastic medium, we can express the position-dependent shear modulus  $\hat{\mu}(z)$  (see, e.g., Refs. 4, 14, and 29) as

$$\hat{\mu}(z) = \mu(z) + \mu'(z) \frac{\partial}{\partial t}, \tag{3}$$

where  $\mu(z)$  is the position-dependent storage shear modulus and  $\mu'(z)$  represents the viscosity.

If we consider the spatial distribution of the material parameters (see, e.g., Refs. 7, 29, and 30),

$$\hat{\mu}(z) = \hat{\mu}_1 \eta(z), \quad \rho(z) = \rho_1 \eta(z), \tag{4}$$

where  $\eta(z)$  denotes the material function, then after substitution of the shear-viscosity stress components [Eq. (2)] into Eq. (1), we arrive at the following form of the governing elastodynamic equation:

$$\frac{\partial^2 u_1(x, z, t)}{\partial x^2} + \frac{\partial^2 u_1(x, z, t)}{\partial z^2} + \frac{1}{\hat{\mu}(z)} \frac{d\hat{\mu}(z)}{dz} \frac{\partial u_1(x, z, t)}{\partial z} = \frac{1}{\hat{c}_1^2} \frac{\partial^2 u_1(x, z, t)}{\partial t^2}, \tag{5}$$

where  $\hat{c}_1 = \sqrt{\hat{\mu}_1 / \rho_1}$ .

For the homogeneous substrate, we obtain the governing equation in a similar way with the difference that both the shear modulus and mass density are constant, thus,

$$\frac{\partial^2 u_2(x, z, t)}{\partial x^2} + \frac{\partial^2 u_2(x, z, t)}{\partial z^2} = \frac{1}{\hat{c}_2^2} \frac{\partial^2 u_2(x, z, t)}{\partial t^2}, \tag{6}$$

where  $\hat{c}_2 = \sqrt{\hat{\mu}_2 / \rho_2}$ .

The solutions of Eqs. (5) and (6) can be assumed to possess, respectively, the following forms:

$$\tilde{u}_1(x, z, t) = \hat{u}_1(z) \exp [ik(x - \hat{c}t)], \tag{7}$$

$$\tilde{u}_2(x, z, t) = \hat{u}_2(z) \exp [ik(x - \hat{c}t)], \tag{8}$$

where  $k$  is the wavenumber,  $\hat{c}$  is the complex phase velocity, and  $i = \sqrt{-1}$  is the imaginary unit. By introducing the dimensionless variables,

$$s = \frac{z}{\ell}, \quad \hat{U}_{1,2} = \frac{\hat{u}_{1,2}}{\ell}, \quad K = k\ell, \quad \hat{K}_{1,2} = \frac{\omega\ell}{\hat{c}_{1,2}}, \quad (9)$$

where  $\ell$  is a characteristic length and  $\omega$  is the angular frequency, and substituting Eqs. (7) and (8) into the corresponding Eqs. (5) and (6), we obtain the equations in their dimensionless forms,

$$\frac{d}{ds} \left( \eta(s) \frac{d\hat{U}_1(s)}{ds} \right) + \eta(s) (\hat{K}_1^2 - K^2) \hat{U}_1(s) = 0, \quad (10)$$

$$\frac{d^2 \hat{U}_2(s)}{ds^2} + (\hat{K}_2^2 - K^2) \hat{U}_2(s) = 0, \quad (11)$$

where Eq. (10) is expressed in the Sturm-Liouville form.

The complex shear modulus  $\hat{\mu}_{1,2}$ , which is vertically distributed according to the material function  $\eta(s)$ , can then be expressed as

$$\hat{\mu}_{1,2} = \mu_{1,2} - i \frac{K \hat{c} \mu'_{1,2}}{\ell}. \quad (12)$$

### III. EXACT ANALYTICAL SOLUTION OF THE GOVERNING EQUATIONS

The exact analytical general solution of Eq. (11) is

$$\hat{U}_2(s) = \mathcal{A}_2 \exp \left( -i \sqrt{\hat{K}_2^2 - K^2} s \right) + \mathcal{B}_2 \exp \left( i \sqrt{\hat{K}_2^2 - K^2} s \right), \quad (13)$$

where  $\mathcal{A}_2$  and  $\mathcal{B}_2$  represent the integration constants.

To solve the equation for the inhomogeneous layer [Eq. (10)], the method published in Ref. 31 can be used. The solution of Eq. (10) can be reduced to a time-independent Schrödinger-like differential equation,

$$\frac{d^2 \psi(s)}{ds^2} + [\mathcal{G}(s) + \hat{\kappa}^2] \psi(s) = 0, \quad (14)$$

where the function  $\mathcal{G}(s)$  is defined below and

$$\hat{\kappa}^2 = \hat{K}_1^2 - K^2. \quad (15)$$

Using the following transformation,

$$\psi(s) = \phi(s) \hat{U}_1(s), \quad (16)$$

it is possible to map Eq. (14) into Eq. (10).

Substituting the transformation relation (16) into Eq. (14), we obtain

$$\frac{d^2 \hat{U}_1}{ds^2} + \frac{2}{\phi} \frac{d\phi}{ds} \frac{d\hat{U}_1}{ds} + \frac{\hat{U}_1}{\phi} \frac{d^2 \phi}{ds^2} + [\mathcal{G}(s) + \hat{\kappa}^2] \hat{U}_1 = 0. \quad (17)$$

By identifying this equation with Eq. (10), we get the following conditions on the transformation:

$$\phi(s) = \sqrt{\eta(s)}, \quad (18)$$

$$\frac{d^2 \phi}{ds^2} + \mathcal{G}(s) \phi(s) = 0. \quad (19)$$

Thus, searching for the general solution of Eq. (10) is reduced to finding the general solution of the time-independent Schrödinger-like differential equation (14). We can see from Eqs. (18) and (19) that the function  $\mathcal{G}(s)$  determines the material function  $\eta(s)$ . If we were able to solve Eq. (14) for a given function  $\mathcal{G}(s)$ , then using the transformation relation (16), we could solve Eq. (10).

In this work, we assume that the function  $\mathcal{G}(s)$  is a quartic polynomial, which enables us to solve Eq. (19) exactly and, in addition, this function contains a sufficient number of coefficients that allow us to determine an appropriate material function profile. Hence, the function can be expressed as

$$\mathcal{G}(s) = a_0 + a_1(s - s_0) + 2a_2(s - s_0)^2 + a_3(s - s_0)^3 - a_4(s - s_0)^4, \quad a_4 \neq 0. \quad (20)$$

Substituting this expression into Eq. (14), we obtain the following equation:

$$\frac{d^2 \psi(s)}{ds^2} + \left[ \hat{\kappa}^2 + a_0 + a_1(s - s_0) + 2a_2(s - s_0)^2 + a_3(s - s_0)^3 - a_4(s - s_0)^4 \right] \psi(s) = 0, \quad (21)$$

which represents the THE. Using the change of variable  $s \rightarrow \xi$  as

$$s - s_0 = q\xi + \frac{a_3}{4a_4}, \quad \text{where } q = \left( \frac{3}{2\sqrt{a_4}} \right)^{1/3}, \quad (22)$$

it is possible to normalize Eq. (21) to the representative form of the THE [see Eq. (A2)],

$$\frac{d^2 \psi(\xi)}{d\xi^2} + \left( A_0(\hat{\kappa}) + A_1 \xi + A_2 \xi^2 - \frac{9}{4} \xi^4 \right) \psi(\xi) = 0. \quad (23)$$

Here,

$$A_0(\hat{\kappa}) = \frac{q^2 [3a_3^4 + 32a_2a_3^2a_4 + 64a_1a_3a_4^2 + 256(a_0 + \hat{\kappa}^2)a_4^3]}{256a_4^3},$$

$$A_1 = \frac{q^3(a_3^3 + 8a_2a_3a_4 + 8a_1a_4^2)}{8a_4^2}, \quad A_2 = \frac{q^4(3a_3^2 + 16a_2a_4)}{8a_4}. \quad (24)$$

Based on the transformation,

$$\psi(\xi) = \exp \left( -\frac{\xi^3}{2} + \frac{A_2}{3} \xi \right) \varphi(\xi), \quad (25)$$

we obtain the THE in its canonical form,

$$\frac{d^2 \varphi}{d\xi^2} - (3\xi^2 + \gamma) \frac{d\varphi}{d\xi} + [\alpha(\hat{\kappa}) + (\beta - 3)\xi] \varphi(\xi) = 0, \quad (26)$$

where

$$\alpha(\hat{\lambda}) = A_0(\hat{\lambda}) + \frac{A_2^2}{9}, \quad \beta = A_1, \quad \gamma = -\frac{2}{3}A_2. \quad (27)$$

Employing Eq. (A12), we can write the general solution of Eq. (26) as

$$\begin{aligned} \varphi(\xi) = & \mathcal{A}_1 \text{THF}(\alpha(\hat{\lambda}), \beta, \gamma; \xi) \\ & + \mathcal{B}_1 \exp(\xi^3 + \gamma\xi) \text{THF}(\alpha(\hat{\lambda}), -\beta, \gamma; -\xi), \end{aligned} \quad (28)$$

where  $\mathcal{A}_1$  and  $\mathcal{B}_1$  are integration constants and THF stands for the triconfluent Heun function.

Using Eqs. (22), (25), and (28), we can write the general solution of Eq. (21) in the following form:

$$\begin{aligned} \psi(s) = & \mathcal{A}_1 \exp \left[ -\frac{Q^3 \left( s - \frac{a_3}{4a_4} - s_0 \right)^3 + \gamma Q \left( s - \frac{a_3}{4a_4} - s_0 \right)}{2} \right] \text{THF} \left[ \alpha(\hat{\lambda}), \beta, \gamma; Q \left( s - \frac{a_3}{4a_4} - s_0 \right) \right] \\ & + \mathcal{B}_1 \exp \left[ \frac{Q^3 \left( s - \frac{a_3}{4a_4} - s_0 \right)^3 + \gamma Q \left( s - \frac{a_3}{4a_4} - s_0 \right)}{2} \right] \text{THF} \left[ \alpha(\hat{\lambda}), -\beta, \gamma; -Q \left( s - \frac{a_3}{4a_4} - s_0 \right) \right], \end{aligned} \quad (29)$$

where  $Q = 1/q$ .

Employing the transformation relation [Eq. (16)] and the solution [Eq. (29)], it is possible to write the general closed-form solution of Eq. (10) as

$$\begin{aligned} \hat{U}_1(s) = & \mathcal{A}_1 \frac{\exp \left[ -\frac{Q^3 \left( s - \frac{a_3}{4a_4} - s_0 \right)^3 - \gamma \frac{Q}{2} \left( s - \frac{a_3}{4a_4} - s_0 \right)}{\sqrt{\eta(s)}} \right]}{\sqrt{\eta(s)}} \text{THF} \left[ \alpha(\hat{\lambda}), \beta, \gamma; Q \left( s - \frac{a_3}{4a_4} - s_0 \right) \right] \\ & + \mathcal{B}_1 \frac{\exp \left[ \frac{Q^3 \left( s - \frac{a_3}{4a_4} - s_0 \right)^3 + \gamma \frac{Q}{2} \left( s - \frac{a_3}{4a_4} - s_0 \right)}{\sqrt{\eta(s)}} \right]}{\sqrt{\eta(s)}} \text{THF} \left[ \alpha(\hat{\lambda}), -\beta, \gamma; -Q \left( s - \frac{a_3}{4a_4} - s_0 \right) \right] \\ = & \frac{\mathcal{A}_1}{\sqrt{\eta(s)}} \Phi_1[\alpha(\hat{\lambda}), \beta, \gamma; s] + \frac{\mathcal{B}_1}{\sqrt{\eta(s)}} \Phi_2[\alpha(\hat{\lambda}), \beta, \gamma; s]. \end{aligned} \quad (30)$$

#### IV. MATERIAL FUNCTIONS BASED ON THE THFS

It is clear from Eqs. (18) and (19) that the function  $\mathcal{G}(s)$ , represented by a quartic polynomial [Eq. (20)] determines the profile of the material function  $\eta(s)$ . For this reason, we refer to the function  $\mathcal{G}(s)$  as the generating function. Because Eq. (19) has the same form as Eq. (14), its general solution is given by Eq. (30), where  $\hat{\lambda} = 0$ . As the parameters  $\alpha(0)$ ,  $\beta$ , and  $\gamma$  depend on the constants of the quartic polynomial  $a_0, a_1, a_2, a_3, a_4, s_0$ , we can write the material function according to Eq. (18) as

$$\begin{aligned} \eta(s) = & [\mathcal{C}_1 \Phi_1(a_0, a_1, a_2, a_3, a_4, s_0; s) \\ & + \mathcal{C}_2 \Phi_2(a_0, a_1, a_2, a_3, a_4, s_0; s)]^2, \end{aligned} \quad (31)$$

and the integration constants  $\mathcal{C}_1$  and  $\mathcal{C}_2$  are optional.

Thus, we have eight optional distribution parameters  $\{a_0, a_1, a_2, a_3, a_4, s_0, \mathcal{C}_1, \mathcal{C}_2\}$ , and the combination of which the material function can be adjusted. This fact enables us to find a wide class of material functions of various profiles for

which we have one general solution of Eq. (10) by substituting Eq. (31) for  $\eta(s)$  into the general solution [Eq. (30)].

To ensure that the shear modulus at the point  $s = 0$  corresponds to the value  $\hat{\mu}_1$ , we choose values of the integration constants  $\mathcal{C}_{1,2}$  in such a way that the material function  $\eta(0) = 1$ . In the case when the specific value of the material function  $\eta(s)$  at another point  $s_i \in (0, s_H]$  is required, where  $s_H = H/\ell$  is a dimensionless thickness of the inhomogeneous layer, we can change one of the optional distribution parameters and fix the remaining distribution parameters until the material function reaches the required value at the given point  $s_i$ .

It is worth noting that if the argument of the THFs is equal to zero, then these functions equal unity for any values of the parameters  $\alpha, \beta$ , and  $\gamma$ . Additionally, the first derivative of the THFs are always equal to zero if their arguments are zero.

Examples of the material function profiles for various optional distribution parameters are shown in Fig. 2 (the THFs are evaluated with the mathematical software Maple, version 17).

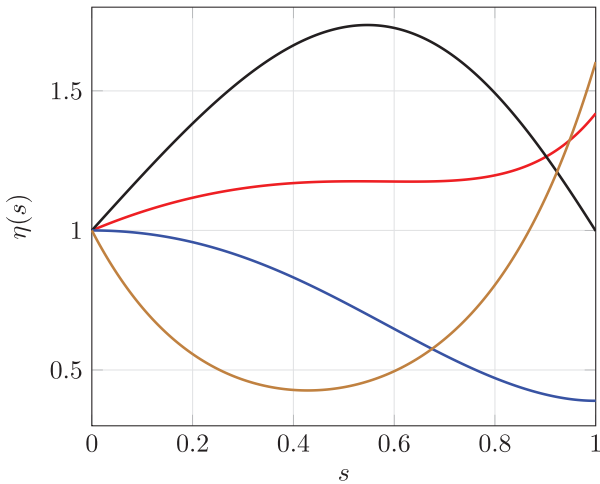


FIG. 2. (Color online) Examples of the material function profiles  $\eta(s)$  for a given sequence of optional parameters  $\{C_1, C_2, a_0, a_1, a_2, a_3, a_4, s_0\}$ .  $\{1,0,1,-1.5,1,0,7,0\}$ , red line;  $\{1,0,1.04,1,1,0,1,0\}$ , black line;  $\{1,0,1,1,0,0,9,0\}$ , blue line; and  $\{0,1,-5,-3,3,0,3,0\}$ , brown line are shown.

**V. MATERIAL FUNCTIONS BASED ON POLYNOMIAL SOLUTIONS**

As it is relatively difficult to estimate the profiles of the THFs based on their parameters, it is convenient to express a solution of Eq. (19) using finite polynomials if certain conditions are satisfied.

Based on the theorem presented in Appendix B, where the meaning of the used symbols below is also given, it is possible to write the first three polynomials:

- (1) For  $N=0$  ( $\beta=3$ ), we can directly find that  $D_1 \equiv \alpha = 0$  and  $P_0 = p_0$  and the confluent function is equal to unity, i.e.,

$$\text{THF}(0, 3, \gamma; \xi) = 1; \tag{32}$$

- (2) For  $N=1$  ( $\beta=6$ ),  $D_2 \equiv \alpha^2 + 3\gamma = 0$ ,

$$P_1(\xi) = \xi - \frac{\alpha}{3};$$

- (3) For  $N=2$  ( $\beta=9$ ),  $D_3 \equiv \alpha^3 + 12\alpha\gamma + 36 = 0$ ,

$$P_2(\xi) = \xi^2 - \frac{\alpha}{3}\xi + \frac{\alpha^2}{36} - \frac{1}{\alpha}.$$

It should be noted that the polynomial solutions for  $N \geq 1$  do not represent the THFs according to the commonly used definition because they do not satisfy the condition  $b_1 = 0$ , as it is supposed in Eq. (A9). The polynomial solutions of Eq. (19) for  $N \geq 1$  may be expressed as linear combinations of the two standard solutions [Eq. (31)]. For  $N > 3$ , we can continue in finding the couples  $(\alpha, \gamma)$  that enable us to express the THFs in their polynomial form as higher order polynomials are no longer suitable in the sense of the estimation of their profiles.

Using the first two polynomial solutions above, we obtain the following expressions for the material function  $\eta(s)$ :

- (1)  $N=0$ ,

$$\eta(s) = C_1 \exp \left[ -\frac{3}{2} Q^3 s \left( \frac{s^2}{3} - s_0 s + s_0^2 - \frac{a_2}{a_4} \right) \right]. \tag{33}$$

- (2)  $N=1$ ,

$$\eta(s) = C_1 \exp \left[ -\frac{3}{2} Q^3 s \left( \frac{s^2}{3} - s_0 s + s_0^2 - \frac{a_2}{a_4} \right) \right] \times \left[ Q(s - s_0) - \frac{\alpha}{3} \right]^2. \tag{34}$$

It is necessary to note that it is not possible to express the second independent solution in the polynomial form for the same optional parameters ( $C_2 = 0$ ).<sup>32</sup> The material functions based on the first two polynomial solutions enable us to calculate the corresponding optional parameters analytically; some results are shown in Fig. 3.

**VI. DETERMINATION OF INTEGRATION CONSTANTS AND DISPERSION RELATIONS**

To demonstrate the applicability of the general results presented in Secs. III–V, we use the following boundary conditions:

- (1) The surface of the structure is traction-free, i.e., the transverse shear stress is equal to zero, resulting in the following condition:

$$\frac{d\hat{U}_1}{ds} \Big|_{s=0} = 0. \tag{35}$$

- (2) The displacement vector and its first derivative must be continuous throughout the interval  $[0, \infty)$ , therefore, the following equations must hold:

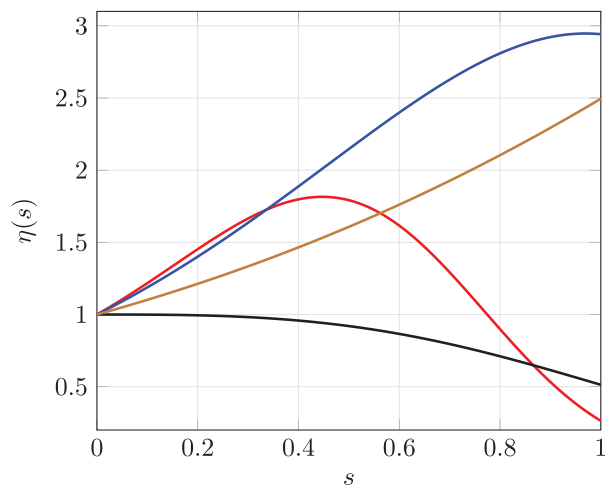


FIG. 3. (Color online) Examples of the material function profiles for the polynomial solutions for a given sequence of parameters  $\{C_1, N, a_0, a_1, a_2, a_3, a_4, s_0\}$ .  $\{1,0,-1,10,5,0,25,0\}$ , red line;  $\{1,0,0,20,0,1,0\}$ , black line;  $\{0.68,1,-0.5,1.5,0.52,0,0,14,0\}$ , blue line; and  $\{0.56,1,-0.2,0,1,0,02,0,0.001,0\}$ , brown line are shown.

$$\hat{U}_1(s_H) = \hat{U}_2(s_H), \tag{36}$$

$$\hat{\mu}(s_H) \frac{d\hat{U}_1}{ds} \Big|_{s=s_H} = \hat{\mu}_2 \frac{d\hat{U}_2}{ds} \Big|_{s=s_H}, \tag{37}$$

where  $s_H = H/\ell$ .

(3) The regularity condition at infinity,

$$\lim_{s \rightarrow \infty} \hat{U}_2(s) = 0. \tag{38}$$

From the last condition [Eq. (38)], we immediately get that  $\mathcal{B}_2 = 0$  and, therefore, we are left with three remaining equations for the three integration constants  $\mathcal{A}_1$ ,  $\mathcal{B}_1$ , and  $\mathcal{A}_2$ . These equations form a linear system that has a nontrivial solution if the corresponding determinant is zero, which

results in the following implicit form of the complex dispersion relation:

$$F(\hat{z}) = -\frac{\hat{\mu}_2}{\eta(s_H)\hat{\mu}_1} \sqrt{\hat{K}_1^2 - \hat{K}_2^2 - \hat{z}^2}, \tag{39}$$

where

$$F(\hat{z}) \equiv \frac{\Psi'_1(\hat{z}; 0)\Psi'_2(\hat{z}; s_H) - \Psi'_1(\hat{z}; s_H)\Psi'_2(\hat{z}; 0)}{\Psi'_1(\hat{z}; 0)\Psi_2(\hat{z}; s_H) - \Psi_1(\hat{z}; s_H)\Psi'_2(\hat{z}; 0)}. \tag{40}$$

Here,

$$\Psi_i(\hat{z}; s) \equiv \frac{\Phi_i[\alpha(\hat{z}), \beta, \gamma; s]}{\sqrt{\eta(s)}}. \tag{41}$$

By solving Eq. (39), we obtain the resulting dispersion relation in the form

$$\hat{c}(K) = \frac{c_1}{2} \frac{\sqrt{4\mu_1^2 H^2 [K^2 + \hat{z}^2(K)] - c_1^2 \mu_1'^2 [K^2 + \hat{z}^2(K)]^2 - ic_1 \mu_1' [K^2 + \hat{z}^2(K)]}}{\mu_1 K H}, \tag{42}$$

where  $c_1 = \sqrt{\mu_1/\rho_1}$ . The dependence  $\hat{z}(K)$  can then be calculated from Eqs. (15) and (39). As will be seen in Sec. VII, for a given dimensionless wavenumber  $K$ , there could exist more solutions of Eq. (42), which define the various Love modes. Using the dispersion relation and boundary conditions [Eqs. (35)–(38)], we can determine the resulting wave solutions of Eq. (10), called the THF solutions, which describe the Love waves.

Using the standard WKB method (see, e.g., Refs. 8 and 33), we can obtain the approximate analytical solution of Eq. (10),

$$\hat{U}_1^{(WKB)}(s) = \frac{\mathcal{A}_1}{\sqrt{\eta(s)}} e^{i\hat{z}s} + \frac{\mathcal{B}_1}{\sqrt{\eta(s)}} e^{-i\hat{z}s}, \tag{43}$$

where  $\mathcal{A}_1$  and  $\mathcal{B}_1$  are the integration constants.

Based on the WKB solution, we can calculate the dispersion relation from the same formula as in the case of the THF solution, i.e., Eqs. (39)–(42), where we use the following substitutions:  $\hat{U}_1(s) \rightarrow \hat{U}_1^{(WKB)}(s)$ ,  $\Phi_1(s) \rightarrow \exp(j\hat{z}s)$ , and  $\Phi_2(s) \rightarrow \exp(-j\hat{z}s)$ .

It can be seen that if we set the material function  $\eta = 1$ , then the WKB solution takes on the form of the standard solution for a homogeneous surface layer.

### VII. RESULTS AND DISCUSSION

For the purpose of the numerical simulations, we borrow the following material parameters from Ref. 14.

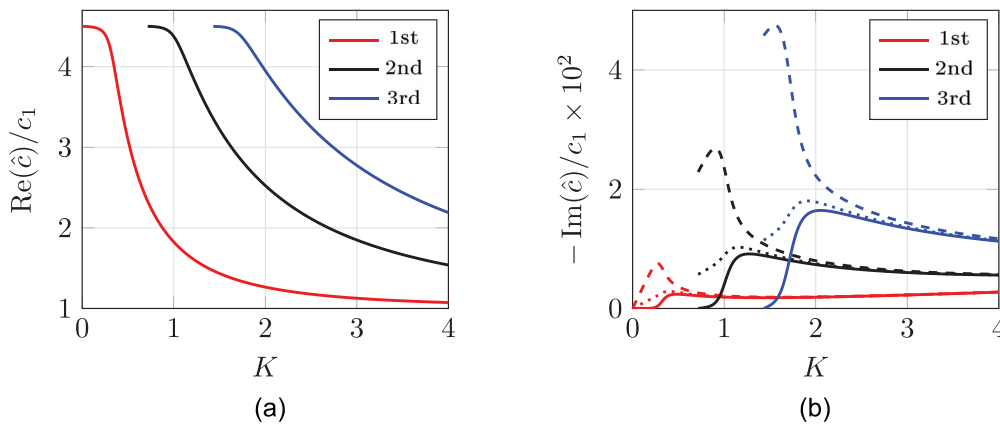


FIG. 4. (Color online) The dispersion curves for various values of  $\mu_2$ .  $\mu_2 = 0$ , solid line;  $\mu_2 = 25\mu_1'$ , dotted line; and  $\mu_2 = 100\mu_1'$ , dashed line are shown. (Left) The real part of the dimensionless complex phase velocity and (right) imaginary part of the dimensionless complex phase velocity are shown.



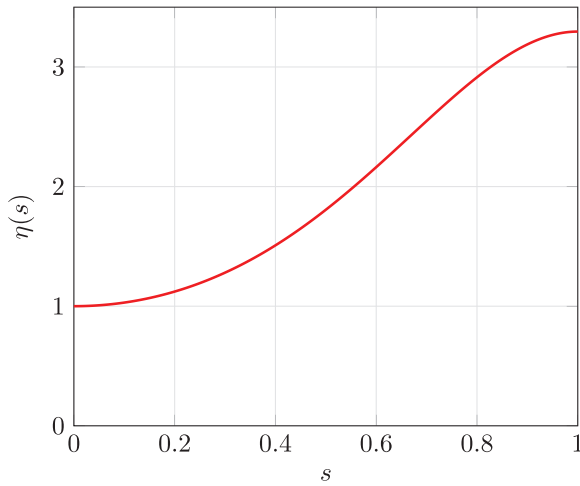


FIG. 5. (Color online) The transient profile of the material function.

The viscoelastic inhomogeneous layer,

$$\begin{aligned} \mu_1 &= 1.43 \times 10^9 \text{ N m}^{-2}; & \rho_1 &= 1180 \text{ kg m}^{-3}; \\ \mu'_1 &= 0.37 \text{ Pa s}; & H &= 239 \text{ }\mu\text{m}. \end{aligned} \quad (44)$$

The homogeneous substrate,

$$\mu_2 = 5.4 \times 10^{10} \text{ N m}^{-2}; \quad \rho_2 = 2200 \text{ kg m}^{-3}. \quad (45)$$

The validity of the exact analytical solution [Eq. (30)] is verified using the numerical method RKF 45 (Runge-Kutta-Fehlberg; see, e.g., Ref. 34).

Assuming that both the surface layer and substrate are homogeneous, the dispersion curves' dependencies are plotted for the first three Love modes for various substrate viscosity parameter values  $\mu'_2$ ; see Fig. 4.

It turns out that the substrate viscosity parameters from the assumed range  $\mu'_2 \in [0, 100\mu'_1]$  have an only negligible effect on the dispersion curves of the real part of the dispersion relation (graphically indistinguishable for the given range of parameters  $\mu'_2$ ) and, therefore, the curves only for  $\mu'_2 = 0$  are plotted; see Fig. 4(a). As for the imaginary part, the substrate

attenuation's effect decreases with increasing values of the dimensionless wavenumber  $K$ ; see Fig. 4(b). We can observe here that for increasing values of the dimensionless wavenumber, the curves of the individual modes for different values of the substrate viscosity parameter gradually approach each other. This finding means that it is reasonable for the WKB method to ignore the substrate's viscoelastic character because the accuracy of this method increases with increasing  $K$ . Hereafter, we will not consider the effect of the substrate attenuation ( $\mu'_2 = 0$ ) for all of the subsequent calculations. A similar case was investigated in Ref. 17, where a lossless homogeneous substrate and lossy homogeneous layer were assumed.

Based on the following values of the distribution parameters,

$$\begin{aligned} s_0 &= 0; & a_0 &= -3.00; & a_1 &= -0.07; & a_2 &= 4.81; \\ a_3 &= 0; & a_4 &= 3.00; & \mathcal{C}_1 &= \mathcal{C}_2 &= 0.5, \end{aligned} \quad (46)$$

we obtain the transient profile of the material function shown in Fig. 5. The real and imaginary parts of the dispersion curves for the first three Love modes are plotted in Figs. 6(a) and 6(b).

Figures 7–9 show the first three Love modes calculated based on the exact solution. These modes are compared with the results obtained using the WKB method and numerical solutions for three different values of a dimensionless wave-number  $K$ .

We can see that with increasing values of the dimensionless wave number  $K$ , the accuracy of the WKB method solutions improves, which is consistent with the assumptions of the WKB approximation. We can also observe that the WKB solutions are refined in the case of the higher modes. The corresponding numerical solutions clearly show that the THF solutions are correct in all of the cases.

The following considered barrier-type material function is expressed using the polynomial solution of the THE [see Eq. (34)] to which these distribution parameters correspond,

$$\begin{aligned} s_0 &= 0; & a_0 &= -1.29; & a_1 &= 6.00; & a_2 &= 3.33; \\ a_3 &= 0; & a_4 &= 2.25; & \mathcal{C}_1 &= 0.67. \end{aligned} \quad (47)$$

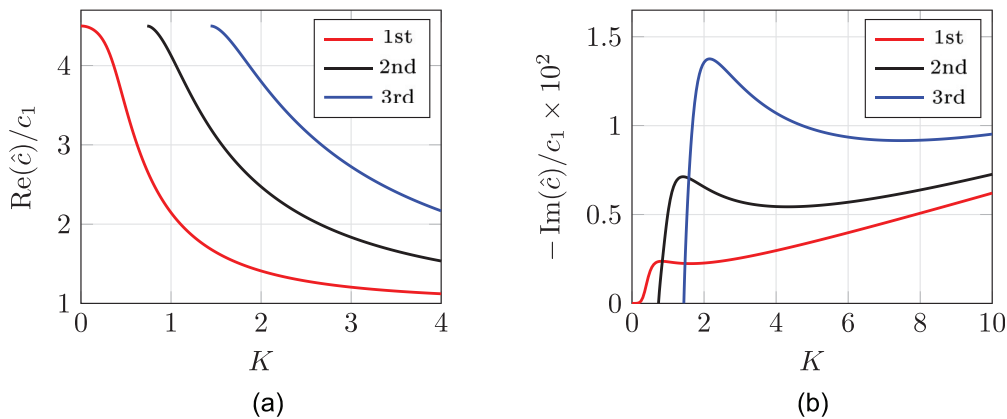


FIG. 6. (Color online) The dispersion curves for the first three Love modes. (Left) The real part of the dimensionless complex phase velocity and (right) imaginary part of the dimensionless complex phase velocity are shown.

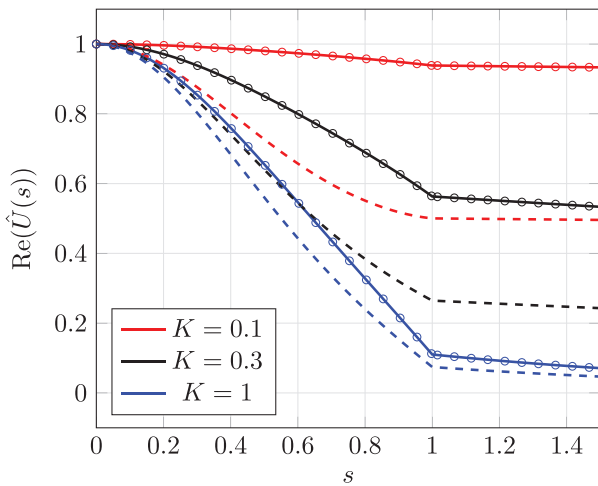


FIG. 7. (Color online) A comparison of the first Love mode obtained by means of the THF solution, WKB solution, and numerical solution for various values of the dimensionless wavenumber  $K$ . The THF solutions, solid lines; WKB solutions, dashed lines; and numerical solutions, circles, are shown.

The resulting material function profile is shown in Fig. 10. The real and imaginary parts of the dispersion curves belonging to this profile can be seen in Figs. 11(a) and 11(b).

The first three Love modes calculated via the exact analytical solution are plotted in Figs. 12–14, where they are compared with the modes calculated on the basis of the WKB and numerical solutions. Again, we can see that with increasing values of the dimensionless wavenumber  $K$ , the accuracy of the approximate WKB solutions increases.

By comparing Figs. 6(a) and 11(a), it can be seen that in the case of the barrier-type material function profile, the cut-on wavenumber of the second mode (here, represents the wave number from which the second mode begins to propagate) is larger than that of the transient profile. Figure 15(b) compares the dependencies of the phase velocities corresponding to the first three modes on the dimensionless

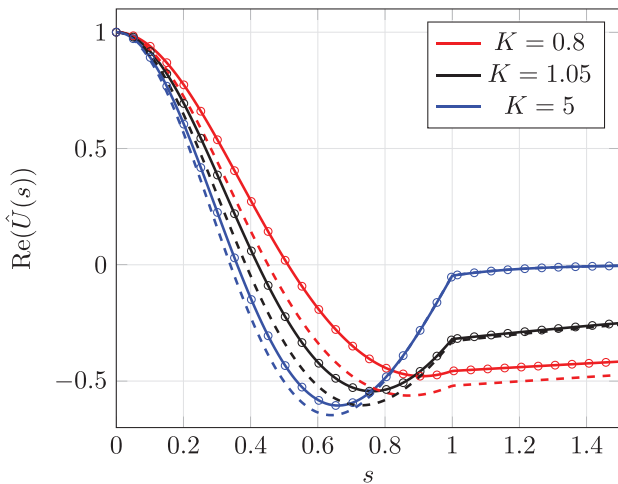


FIG. 8. (Color online) A comparison of the second Love mode obtained by means of the THF solution, WKB solution, and numerical solution for various values of the dimensionless wavenumber  $K$ . The THF solutions, solid lines; WKB solutions, dashed lines; and numerical solutions, circles, are shown.

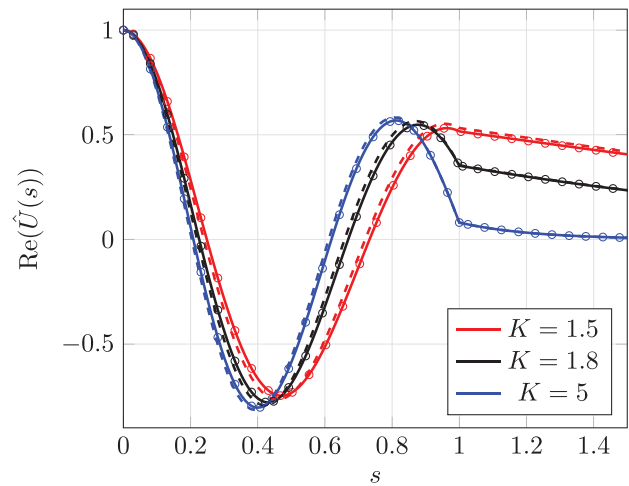


FIG. 9. (Color online) A comparison of the third Love mode obtained by means of the THF solution, WKB solution, and numerical solution for various values of the dimensionless wavenumber  $K$ . The THF solutions, solid lines; WKB solutions, dashed lines; and numerical solutions, circles, are shown.

wavenumber for the case of the constant material function and the material function having the barrier character that is shown in Fig. 15(a), which is given by the following distribution parameters (in this case, we assumed the surface layer to be lossless):

$$\begin{aligned}
 s_0 &= 0; & a_0 &= -29.61; & a_1 &= 263.32; \\
 a_2 &= -362.21; & a_3 &= 922.22; & a_4 &= 461.11; \\
 C_1 &= C_2 = 1.07.
 \end{aligned}
 \tag{48}$$

It can be seen from Fig. 15(b) that the dispersion relation can be influenced by a suitable choice of the material function profile  $\eta(s)$ . The cut-on wavenumber of the second mode was increased by  $\Delta_1 \approx 37\%$  for the lower barrier-like profile (dashed line) and  $\Delta_2 \approx 53\%$  for the higher barrier-like profile (solid line). For the higher modes, we can observe this phenomenon to a lesser extent. We can observe that the height of the barrier profile shifts the position of the cut-on

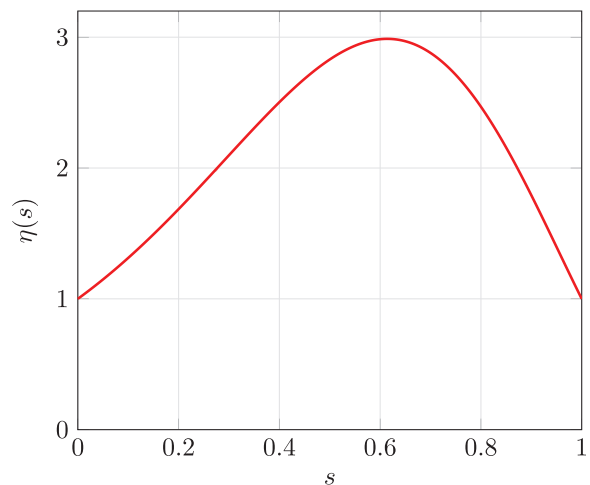


FIG. 10. (Color online) The barrier-type profile of the material function.

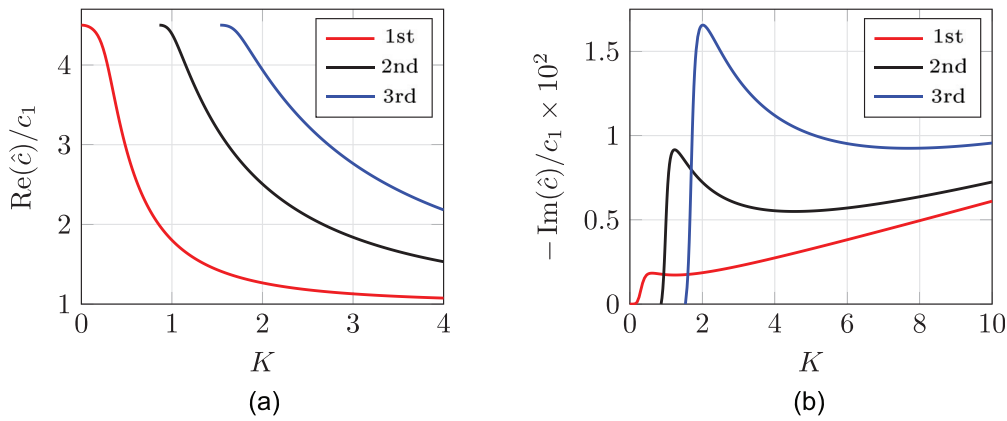


FIG. 11. (Color online) The dispersion curves for the first three Love modes. (Left) The real part of the dimensionless complex phase velocity and (right) imaginary part of the dimensionless complex phase velocity are shown.

wavenumbers of the higher modes. This means that by choosing a suitable material function profile, the frequency range for which only the first mode can be excited may be varied, which is particularly applicable in sensor technology using Love waves. The exact solutions we have found allow us to vary the profile of the material functions in a wide range and, thus, to investigate the influence of the profile shape for this purpose, preferably using some suitable optimization method, but this research is already beyond the scope of this paper.

**VIII. CONCLUSIONS**

In this work, we focused on finding the exact analytical solution of the model equation describing the propagation of Love waves in a viscoelastic inhomogeneous isotropic layer of constant width determined by the position-dependent complex shear modulus and material density. The spatial distribution of these material parameters is described using the same material function. We have shown that the model equation's solution can be reduced to the issue of solving

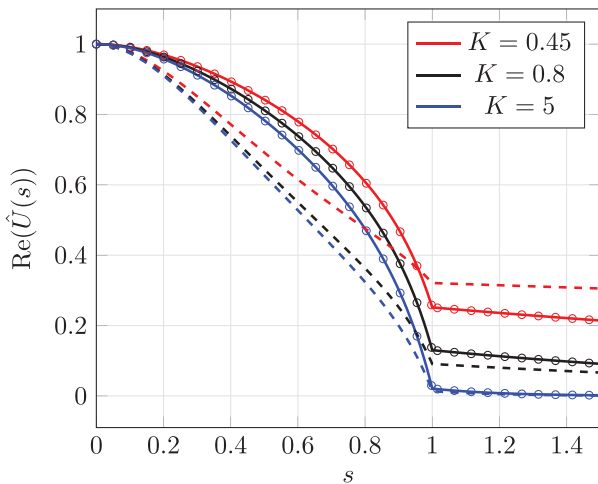


FIG. 12. (Color online) A comparison of the first Love mode obtained by means of the THF solution, WKB solution, and numerical solution for various values of the dimensionless wavenumber  $K$ . The THF solutions, solid lines; WKB solutions, dashed lines; and numerical solutions, circles, are shown.

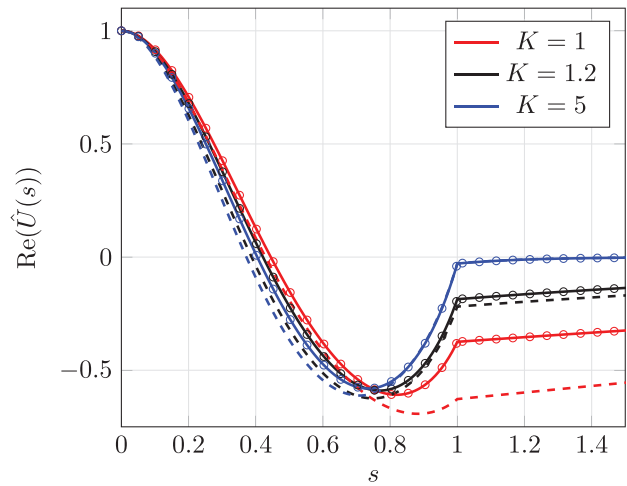


FIG. 13. (Color online) A comparison of the second Love mode obtained by means of the THF solution, WKB solution, and numerical solution for various values of the dimensionless wavenumber  $K$ . The THF solutions, solid lines; WKB solutions, dashed lines; and numerical solutions, circles, are shown.

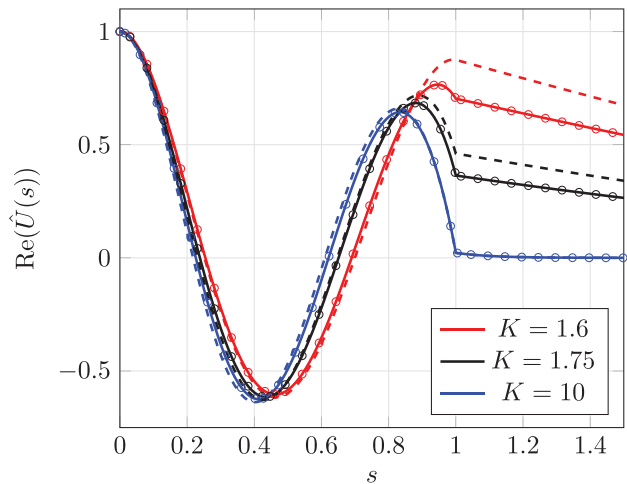


FIG. 14. (Color online) A comparison of the third Love mode obtained by means of the THF solution, WKB solution, and numerical solution for various values of the dimensionless wavenumber  $K$ . The THF solutions, solid lines; WKB solutions, dashed lines; and numerical solutions, circles, are shown.

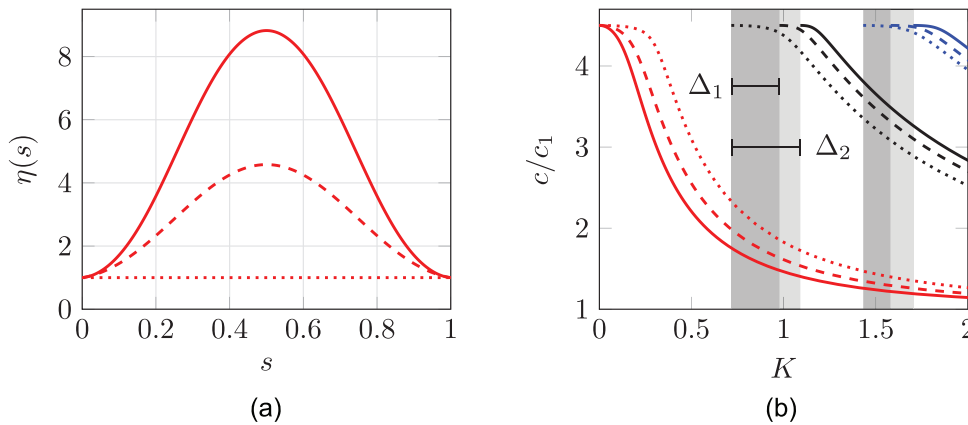


FIG. 15. (Color online) A comparison of the dispersion curves (right) belonging to the barrier-type profiles (solid and dashed lines) and the constant profile (dotted line) of the material functions (left). The first mode, red line; second mode, black line; and third mode, blue line, are shown.

the time-independent Schrödinger-like differential equation, which can be transformed under certain conditions into the THE, whose solution can be expressed by the linear combination of the two THFs. By meeting these conditions, it has defined a wide class of material functions for which the exact solution can be found. The material functions of this class are determined by eight distribution parameters, which allow changing their profiles to a large extent. The expression of material functions using the THFs has been supplemented by the possibility of their description using polynomial solutions when certain conditions are met.

To demonstrate the applicability and benefits of the presented exact solutions, we have compared the presented exact analytical solutions with the solutions based on the numerical method RKF 45 and the WKB method, which is usually used in cases where the exact analytical solution is not known. We have employed two illustrative profiles of the material functions to calculate both mode solutions and dispersion curves of the first three modes. The numerical solutions verified the correctness of all of the results based on the presented exact solutions. As expected, it turned out that in the case of the relatively lower values of the wavenumbers, the presented exact solutions differ significantly from the WKB approximation, and with increasing values of the wavenumber, the WKB solution became more accurate.

Based on the performed calculations, it was found that the substrate viscosity parameter  $\mu'_2$  significantly affects the imaginary part of the dispersion relation. In contrast, its influence on its real part is negligible when considering the same range of its values. However, the effect of the viscosity parameter decreases with increasing values of the dimensionless wave number  $K$ , therefore, it seems justified to ignore the substrate viscosity when using the WKB method because its accuracy is based on larger wavenumber values.

The presented exact analytical solutions allow us to study the influence of functionally graded materials on the dispersion behavior of Love waves. Furthermore, these solutions can also be used to study the effects of various boundary conditions (e.g., imperfect interfaces), the effect of the initial stress, and locally periodic structures of the surface layer on the Love waves.

We have demonstrated that in the case of the barrier-type profile of the material function, the cut-on wavenumber of the higher modes can be shifted based on its height, indicating that the dispersion character of the Love waves can be controlled by a suitable choice of the material function profile. This fact could be the subject of further research, especially when using an appropriate optimization method.

#### ACKNOWLEDGMENTS

This work was supported by the Grant Agency of the Czech Republic (GACR) Grant No. 18-24954S and the Grant Agency of the Czech Technical University in Prague No. SGS21/115/OHK3/2T/13.

#### APPENDIX A: GENERAL SOLUTION OF THE TRICONFLUENT HEUN EQUATION

The triconfluent Heun equation is derived from the Heun equation by the coalescence of the three finite regular singular points with infinity.<sup>23</sup> The canonical triconfluent Heun equation has the form (see, e.g., Refs. 23 and 24)

$$\frac{d^2\varphi(\xi)}{d\xi^2} - (3\xi^2 + \gamma)\frac{d\varphi(\xi)}{d\xi} + [\alpha + (\beta - 3)\xi]\varphi(\xi) = 0, \quad (A1)$$

and its symmetric (self-adjoint) used form is

$$\frac{d^2\Phi(\xi)}{d\xi^2} + \left(\alpha - \frac{\gamma^2}{4} + \beta\xi - \frac{3}{2}\gamma\xi^2 - \frac{9}{4}\xi^4\right)\Phi(\xi) = 0, \quad (A2)$$

where

$$\Phi(\xi) = \exp\left(-\frac{\xi^3 + \gamma\xi}{2}\right)\varphi(\xi). \quad (A3)$$

The quartic polynomial in Eq. (A2) does not contain the  $\xi^3$  term, and the coefficient of  $\xi^4$  is set equal to 9/4. This normalization can be arranged by subjecting the independent variable  $\xi$  to an innocuous transformation of the form  $\xi' = d_1\xi + d_0$  ( $d_0$  and  $d_1$  are constants) but other

normalizations could equally well be used. The normalization herein is commonly used; see, e.g., Ref. 23.

An analytical solution  $\varphi(\xi)$  of Eq. (A1) can be expressed using a power series of the form

$$\varphi(\xi) = \sum_{n=0}^{\infty} b_n \xi^n, \quad |\xi| < 1. \quad (\text{A4})$$

The derivatives of  $\varphi$  with respect to  $\xi$  are

$$\frac{d\varphi(\xi)}{d\xi} = \sum_{n=0}^{\infty} n b_n \xi^{n-1} = \sum_{n=0}^{\infty} (n+1) b_{n+1} \xi^n, \quad (\text{A5})$$

$$\frac{d^2\varphi(\xi)}{d\xi^2} = \sum_{n=0}^{\infty} n(n-1) b_n \xi^{n-2} = \sum_{n=0}^{\infty} (n+2)(n+1) b_{n+2} \xi^n. \quad (\text{A6})$$

By substituting the power series, Eqs. (A4)–(A6), into Eq. (A1), we obtain the recurrence relation

$$n(n-1)b_n - (n-1)\gamma b_{n-1} + \alpha b_{n-2} + (\beta + 6 - 3n)b_{n-3} = 0. \quad (\text{A7})$$

From the recurrence relation [Eq. (A7)], we can write

$$b_n = \frac{\gamma(n-1)b_{n-1} - \alpha b_{n-2} - (\beta + 6 - 3n)b_{n-3}}{n(n-1)}, \quad n \geq 3, \quad (\text{A8})$$

where

$$b_0 = 1, \quad b_1 = 0, \quad b_2 = -\frac{\alpha}{2}. \quad (\text{A9})$$

For  $(\alpha, \beta, \gamma) \in \mathbb{C}$ , the THF represents a solution of the triconfluent Heun equation (A1) and can be written as

$$\text{THF}(\alpha, \beta, \gamma; \xi) = \sum_{n=0}^{\infty} b_n \xi^n; \quad |\xi| < 1, \quad (\text{A10})$$

where  $b_n$  are given by Eqs. (A9) and (A8). The derivative of the THF (the prime THF) can be expressed as

$$\begin{aligned} \frac{d}{d\xi} \text{THF}(\alpha, \beta, \gamma; \xi) &\equiv \text{THF}'(\alpha, \beta, \gamma; \xi) \\ &= \sum_{n=0}^{\infty} n b_n \xi^{n-1}; \quad |\xi| < 1. \end{aligned} \quad (\text{A11})$$

The general solution of the triconfluent Heun equation (A1) is (see, e.g., Ref. 23)

$$\begin{aligned} \varphi(\xi) &= \mathcal{C}_1 \text{THF}(\alpha, \beta, \gamma; \xi) \\ &\quad + \mathcal{C}_2 \exp(\xi^3 + \gamma\xi) \text{THF}(\alpha, -\beta, \gamma; -\xi), \end{aligned} \quad (\text{A12})$$

where  $\mathcal{C}_1$  and  $\mathcal{C}_2$  are the integration constants.

There is the following identity:

$$\text{THF}(\alpha, \beta, 0; \xi) = \exp(\xi^3) \text{THF}(\alpha, -\beta, 0; -\xi), \quad (\text{A13})$$

which means that if  $\gamma=0$ , then the presented solutions in Eq. (A12) are not linearly independent.

We can obtain the general solution of the symmetric form of the triconfluent equation (A2) using the solution (A12) and the transformation relation (A3),

$$\begin{aligned} \Phi(\xi) &= \mathcal{C}_1 \exp\left(-\frac{\xi^3 + \gamma\xi}{2}\right) \text{THF}(\alpha, \beta, \gamma; \xi) \\ &\quad + \mathcal{C}_2 \exp\left(\frac{\xi^3 + \gamma\xi}{2}\right) \text{THF}(\alpha, -\beta, \gamma; -\xi). \end{aligned} \quad (\text{A14})$$

## APPENDIX B: POLYNOMIAL SOLUTION OF THE TRICONFLUENT HEUN EQUATION

We can see that the evaluation of successive terms of a series solution [Eq. (A4) or (A10)] to the triconfluent Heun equation (A1) is performed by means of a recurrence relation (A8), where the coefficient  $b_n$  depends on  $n$ , the previous values of  $b_r$  ( $r < n$ ), and the three parameters  $(\alpha, \beta, \gamma)$ . Based on this recursive relation, it is possible to express a solution of the triconfluent equation by a finite polynomial if certain conditions are met. The conditions for the existence of polynomial solutions can be formulated by the following theorem (see, e.g., Refs. 23 and 35).

**Theorem 1.** Suppose that in the triconfluent Heun equation (A1), the parameters  $\alpha$ ,  $\beta$ , and  $\gamma$  satisfy the following two conditions:

- (a)  $\beta = 3(N + 1)$ ,  $N = 0, 1, 2, \dots$ ;
- (b) the determinant  $D_{N+1}(\alpha, \gamma) = 0$  of the matrix

$$\mathbf{M}_{N+1} = \begin{pmatrix} \alpha & -\gamma & 2 \cdot 1 & 0 & 0 & \dots & 0 \\ 3N & \alpha & -2\gamma & 2 \cdot 3 & 0 & \dots & 0 \\ 0 & 3(N-1) & \alpha & -3\gamma & 3 \cdot 4 & \dots & 0 \\ 0 & 0 & 3(N-2) & \alpha & -4\gamma & \dots & 0 \\ \vdots & \vdots & \vdots & \vdots & \vdots & \ddots & \vdots \\ & & & & & & & 3 \cdot 3 & \alpha & -(N-1)\gamma & N(N-1) \\ & & & & & & & 0 & 3 \cdot 2 & \alpha & -N\gamma \\ 0 & & & \dots & 0 & 0 & 3 \cdot 1 & \alpha & & & \end{pmatrix}. \quad (\text{B1})$$

Then the triconfluent Heun equation (A1) has a polynomial (Liouvillian) solution

$$\varphi(\xi) = P_{\beta/3-1}(\xi),$$

where  $P_{\beta/3-1}(\xi)$  denotes a polynomial of degree  $\beta/3 - 1$ , whose coefficients  $p_n$  ( $n = 0, 1, \dots, \beta/3 - 1$ ) are the solutions of the following linear system of equations:

$$\mathbf{M}_{\beta/3} \cdot (p_0, p_1, \dots, p_{\beta/3-1}) = 0. \quad (\text{B2})$$

- <sup>1</sup>P. Kielczyński, "Properties and applications of love surface waves in seismology and biosensors," in *Surface Waves—New Trends and Developments*, edited by F. Ebrahimi (InTech, London, 2018).
- <sup>2</sup>V. V. Kravchenko, *Direct and Inverse Sturm-Liouville Problems* (Springer International Publishing, Cham, Switzerland, 2020).
- <sup>3</sup>P. Kumar, A. Chattopadhyay, M. Mahanty, and A. K. Singh, "Analysis on propagation characteristics of the shear wave in a triple layered concentric infinite long cylindrical structure: An analytical approach," *Eur. Phys. J. Plus* **134**(1), 35 (2019).
- <sup>4</sup>S. A. Sahu, P. K. Saroj, and N. Dewangan, "SH-waves in viscoelastic heterogeneous layer over half-space with self-weight," *Arch. Appl. Mech.* **84**(2), 235–245 (2014).
- <sup>5</sup>P. Kielczyński, M. Szalewski, A. Balcerzak, and K. Wieja, "Group and phase velocity of love waves propagating in elastic functionally graded materials," *Arch. Acoust.* **40**(2), 273–281 (2015).
- <sup>6</sup>R. Kakar, "Rheological model of Love wave propagation in viscoelastic layered media under gravity," *Multidiscip. Model. Mater. Struct.* **11**(3), 424–436 (2015).
- <sup>7</sup>S. Kowalczyk, S. Matysiak, and D. M. Perkowski, "On some problems of SH wave propagation in inhomogeneous elastic bodies," *J. Theor. Appl. Mech.* **54**, 1125–1135 (2016).
- <sup>8</sup>Z.-H. Qian, F. Jin, K. Kishimoto, and T. Lu, "Propagation behavior of love waves in a functionally graded half-space with initial stress," *Int. J. Solids Struct.* **46**(6), 1354–1361 (2009).
- <sup>9</sup>L. G. Zhang, H. Zhu, H. B. Xie, and J. Wang, "Love wave in an isotropic half-space with a graded layer," *Appl. Mech. Mater.* **325-326**, 252–255 (2013).
- <sup>10</sup>H. Zhu, L. Zhang, J. Han, and Y. Zhang, "Love wave in an isotropic homogeneous elastic half-space with a functionally graded cap layer," *Appl. Math. Comput.* **231**, 93–99 (2014).
- <sup>11</sup>P. Kumar, A. K. Singh, and A. Chattopadhyay, "Influence of an impulsive source on shear wave propagation in a mounted porous layer over a foundation with dry sandy elastic stratum and functionally graded substrate under initial stress," *Soil Dyn. Earthquake Eng.* **142**, 106536 (2021).
- <sup>12</sup>P. Kumar, M. Mahanty, A. Chattopadhyay, and A. K. Singh, "Green's function technique to study the influence of heterogeneity on horizontally polarised shear-wave propagation due to a line source in composite layered structure," *J. Vib. Control* **26**(9-10), 701–712 (2020).
- <sup>13</sup>R. Kumhar, S. Kundu, D. K. Pandit, and S. Gupta, "Green's function and surface waves in a viscoelastic orthotropic FGM enforced by an impulsive point source," *Appl. Math. Comput.* **382**, 125325 (2020).
- <sup>14</sup>P. Kielczyński, "Attenuation of love waves in low-loss media," *J. Appl. Phys.* **82**(12), 5932–5937 (1997).
- <sup>15</sup>Y. Jiangong, "Viscoelastic shear horizontal wave in graded and layered plates," *Int. J. Solids Struct.* **48**(16-17), 2361–2372 (2011).
- <sup>16</sup>R. Kakar, "Love waves in Voigt-type viscoelastic inhomogeneous layer overlying a gravitational half-space," *Int. J. Geomech.* **16**(3), 04015068 (2016).
- <sup>17</sup>P. Kielczyński, "Direct Sturm–Liouville problem for surface Love waves propagating in layered viscoelastic waveguides," *Appl. Math. Modell.* **53**, 419–432 (2018).
- <sup>18</sup>S. Kundu, R. Kumhar, M. Maity, and S. Gupta, "Influence of point source on Love-type waves in anisotropic layer overlying viscoelastic FGM half-space: Green's function approach," *Int. J. Geomech.* **20**(1), 04019141 (2020).
- <sup>19</sup>P. Kumar, A. Chattopadhyay, M. Mahanty, and A. K. Singh, "Stresses induced by a moving load in a composite structure with an incompressible poroviscoelastic layer," *J. Eng. Mech.* **145**(9), 04019062 (2019).
- <sup>20</sup>P. Kumar, A. Chattopadhyay, and A. K. Singh, "Propagation of edge wave in homogeneous viscoelastic sandy media," in *Lecture Notes in Mechanical Engineering*, edited by S. Dutta, E. Inan, and S. K. Dwivedy (Springer, Singapore, 2020), pp. 481–494.
- <sup>21</sup>R. Kumhar, S. Kundu, and S. Gupta, "Modelling of Love waves in fluid saturated porous viscoelastic medium resting over an exponentially graded inhomogeneous half-space influenced by gravity," *J. Appl. Comput. Mech.* **6**, 517–530 (2020).
- <sup>22</sup>D. Kumar, S. Kundu, R. Kumhar, and S. Gupta, "Vibrational analysis of Love waves in a viscoelastic composite multilayered structure," *Acta Mech.* **231**(10), 4199–4215 (2020).
- <sup>23</sup>A. Ronveaux, *Heun's Differential Equations* (Oxford University Press, Oxford, 1995).
- <sup>24</sup>F. W. Olver, D. W. Lozier, R. F. Boisvert, and C. W. Clark, *NIST Handbook of Mathematical Functions*, 1st ed. (Cambridge University Press, Cambridge, UK, 2010).
- <sup>25</sup>M. K. Pal and A. K. Singh, "On the characteristics of reflected waves in rotating functionally graded initially stressed piezoelectric-orthotropic half-space," *Waves Random Complex Media* **2021**, 1–15.
- <sup>26</sup>M. K. Pal and A. K. Singh, "Analysis of reflection and transmission phenomenon at distinct bonding interfaces in a rotating pre-stressed functionally graded piezoelectric-orthotropic structure," *Appl. Math. Comput.* **409**, 126398 (2021).
- <sup>27</sup>M. Mahanty, A. Chattopadhyay, P. Kumar, and A. K. Singh, "Effect of initial stress, heterogeneity and anisotropy on the propagation of seismic surface waves," *Mech. Adv. Mater. Struct.* **27**(3), 177–188 (2020).
- <sup>28</sup>M. Mahanty, P. Kumar, A. K. Singh, and A. Chattopadhyay, "Dynamic response of an irregular heterogeneous anisotropic poroelastic composite structure due to normal moving load," *Acta Mech.* **231**(6), 2303–2321 (2020).
- <sup>29</sup>R. Kakar, "Dispersion of love wave in an isotropic layer sandwiched between orthotropic and prestressed inhomogeneous half-spaces," *Latin Am. J. Solids Struct.* **12**(10), 1934–1949 (2015).
- <sup>30</sup>N. Dewangan and S. A. Sahu, "On phase velocity of Love type waves in heterogeneous visco-elastic medium," *Procedia Eng.* **173**, 1034–1041 (2017).
- <sup>31</sup>M. Bednarik and M. Cervenka, "A wide class of analytical solutions of the Webster equation," *J. Sound Vib.* **469**, 115169 (2020).
- <sup>32</sup>For the second independent solution, one would need to use the THF.
- <sup>33</sup>P. Kumar, M. Mahanty, A. Chattopadhyay, and A. K. Singh, "Effect of interfacial imperfection on shear wave propagation in a piezoelectric composite structure: Wentzel–Kramers–Brillouin asymptotic approach," *J. Intell. Mater. Syst. Struct.* **30**(18-19), 2789–2807 (2019).
- <sup>34</sup>J. Mathews, *Numerical Methods Using MATLAB* (Prentice Hall, Upper Saddle River, N.J., 1999).
- <sup>35</sup>D. Batic, D. Mills-Howell, and M. Nowakowski, "Potentials of the Heun class: The triconfluent case," *J. Math. Phys.* **56**(5), 052106 (2015).

## ■ 3.2 Paper II

**Title:** *Surface love-type waves propagating through locally periodic inhomogeneous media*

The second paper is a conference paper presented at The 29th International Congress on Sound and Vibration and is a direct follow-up to the previously presented Paper I with the following extension - the FGM surface layer is now repeated periodically  $N$ -times, resulting in a locally periodic inhomogeneous elastic surface layer laid over a homogeneous substrate. In order to simplify the whole calculation, the viscoelastic losses are neglected for both the surface layer and the substrate. The solution is first obtained for the first spatial period of the layer in exactly the same way as in Paper I, therefore as a combination of the triconfluent Heun functions, and is then extended to the whole domain by employing the Floquet-Bloch theory (see Sec. 2.4), resulting in a very elegant analytical expression for the total solution inside of the locally periodic FGM layer. The dispersion equation is then formulated based on the same boundary conditions as presented in Paper I. The case study follows for a gaussian-like profile of the material function and the corresponding dispersion curves are plotted for various values of  $N$  with the following observation: the original dispersion curves (corresponding to  $N = 1$ ) tend to split into  $N$  curves positioned closely together which then form more widely separated groups in the overall dispersion graph. Since this was only a short conference paper, no other profiles of the material function were studied. Therefore, there are still a lot of further research possibilities in this area. Then (similarly as mentioned above regarding Paper I.), the effect of different boundary conditions at the top of the layer can also be studied in the presence of the locally periodic surface layer.



# SURFACE LOVE-TYPE WAVES PROPAGATING THROUGH LOCALLY PERIODIC INHOMOGENEOUS MEDIA

Antonín Krpenský, Michal Bednařík

*Czech Technical University in Prague, Faculty of Electrical Engineering, Prague, Czech Republic*

*e-mail: antonin.krpensky@fel.cvut.cz*

In this paper, we introduce a novel exact analytical solution for the model equation governing the propagation of Love-type waves in a locally periodic surface layer with continuous density and shear modulus variations along the thickness direction, represented by a material function. Specifically, we utilize the triconfluent Heun functions to obtain the solution for the base spatial period of the layer and extend it to the entire layer through the Floquet-Bloch theory. Our approach allows for the derivation of the dispersion equation and plotting the corresponding dispersion curves by applying appropriate boundary conditions. The significance of this work lies in the extension of the class of material function profiles for which exact analytical solutions can be obtained, demonstrating the potential for broader applicability of our solution in diverse research fields.

Keywords: LOVE-TYPE WAVES, FUNCTIONALLY GRADED MATERIAL, FLOQUET-BLOCH THEORY, TRICONFLUENT HEUN FUNCTIONS

---

## 1. Introduction

The propagation of Love-type shear surface elastic waves in functionally graded materials (FGMs) is a subject of significant scientific and practical interest. Love waves find applications in various fields, including seismology, geophysics, nondestructive testing of materials, seismic engineering, geotechnical engineering and sensor technology. A comprehensive and well-structured review of Love waves and their uses is available in chapter two of the book by Ebrahimi (2018) [1].

To fully understand the behavior of Love waves that propagate through an inhomogeneous layer, it is essential to have access to exact analytical solutions of the corresponding model equations. These solutions are crucial for predicting the response of the system under various conditions and for designing efficient and effective wave-based technologies.

A significant advancement in exact analytical solutions of the model equation describing Love waves in inhomogeneous media is presented in articles [2], [3]. Our intention is to utilize these published exact solutions, which are based on the triconfluent Heun functions, to study the behavior of Love waves propagating through a locally periodic structure consisting of inhomogeneous layers realized using FGMs. Our approach is based on the utilization of the Floquet-Bloch theory (see e.g., [4]), which enables this task to be solved effectively.

## 2. Exact analytical solution of the governing equations

In this paper, we investigate the propagation of Love-type waves in an inhomogeneous isotropic elastic surface layer of thickness  $\ell$ , where the shear modulus and density vary continuously along the



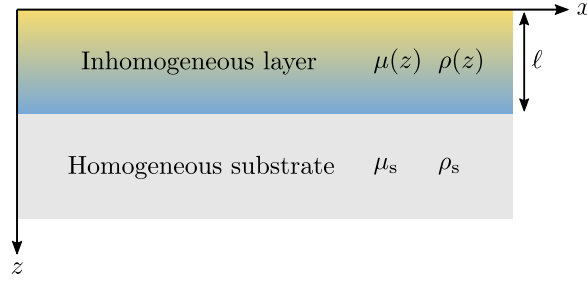


Figure 1: (Color online) Inhomogeneous layer laid on a homogeneous substrate.

thickness direction. The layer is placed on an infinite homogeneous substrate, as shown in Fig. 1.

To describe the shear modulus and density variation, we use the expressions

$$\mu(z) = \mu_0 \eta(z), \quad \rho(z) = \rho_0 \eta(z), \quad (1)$$

where  $\eta(z)$  is the material function. The model equation governing the propagation of Love-type waves in the layer along the  $x$  axis can then be expressed as

$$\frac{\partial^2 u_y(x, z, t)}{\partial x^2} + \frac{\partial^2 u_y(x, z, t)}{\partial z^2} + \frac{1}{\eta(z)} \frac{d\eta(z)}{dz} \frac{\partial u_y(x, z, t)}{\partial z} = \frac{1}{c_0^2} \frac{\partial^2 u_y(x, z, t)}{\partial t^2}, \quad (2)$$

where  $u_y(x, z, t)$  is the  $y$ -component of the displacement vector and

$$c_0 = \sqrt{\frac{\mu_0}{\rho_0}}. \quad (3)$$

By assuming a time harmonic wave of the form

$$u_y(x, z, t) = u_y(z) e^{ik(x - c_{\text{ph}} t)}, \quad (4)$$

where  $k = \omega/c_{\text{ph}}$  is the wavenumber ( $\omega$  is the angular frequency),  $c_{\text{ph}}$  stands for the phase velocity, and further introducing the following dimensionless variables:

$$s = \frac{z}{\ell}, \quad U_1 = \frac{u_y}{\ell}, \quad K = k\ell, \quad K_0 = \frac{c_{\text{ph}}}{c_0} k\ell, \quad (5)$$

we can rewrite Eq. (2) as

$$\frac{d^2 U_1(s)}{ds^2} + \frac{1}{\eta(s)} \frac{d\eta(s)}{ds} \frac{dU_1(s)}{ds} + (K_0^2 - K^2) U_1(s) = 0. \quad (6)$$

For the homogeneous substrate, the equation governing the propagation of the wave is

$$\frac{d^2 U_2(s)}{ds^2} + (K_s^2 - K^2) U_2(s) = 0. \quad (7)$$

where  $U_2(s)$  denotes the solution in the substrate,

$$K_s = \frac{c_{\text{ph}}}{c_s} k\ell, \quad (8)$$

and  $c_s = \sqrt{\mu_s/\rho_s}$  represents the phase velocity of the SH waves in the substrate.

In the following text, we will use the same procedure as in the previous works ([2],[3]) to transform Eq. (2) into a time-independent Schrödinger-like equation of the form

$$\frac{d^2\psi(s)}{ds^2} + [\mathcal{G}(s) + \varkappa^2] \psi(s) = 0, \quad (9)$$

where

$$\varkappa = K_0^2 - K^2. \quad (10)$$

By using the following transformation

$$\psi(s) = \phi(s)U_1(s), \quad (11)$$

and substituting into Eq. (9) we obtain

$$\frac{d^2U_1}{ds^2} + \frac{2}{\phi} \frac{d\phi}{ds} \frac{dU_1}{ds} + \frac{U_1}{\phi} \frac{d^2\phi}{ds^2} + [\mathcal{G}(s) + \varkappa^2] U_1 = 0. \quad (12)$$

By comparing Eqs. (2) and (12) we can write the following conditions for the transformation:

$$\phi(s) = \sqrt{\eta(s)}, \quad (13)$$

$$\frac{d^2\phi}{ds^2} + \mathcal{G}(s)\phi(s) = 0. \quad (14)$$

For the sake of this paper we assume the function  $\mathcal{G}(s)$  to be a quartic polynomial expressed as

$$\mathcal{G}(s) = a_0 + a_1(s - s_0) + 2a_2(s - s_0)^2 + a_3(s - s_0)^3 - a_4(s - s_0)^4, \quad a_4 \neq 0. \quad (15)$$

Since according to Eqs. (13) and (14)  $\mathcal{G}(s)$  determines the profile of the material function  $\eta(s)$ , we call it the generating polynomial. By further employing the transformation

$$\psi(s) = \exp\left(\frac{1}{2} \int F(s) ds\right) \varphi(s), \quad (16)$$

where

$$F(s) = -2\sqrt{a_4} \left[ (s - s_0) - \frac{a_3}{4a_4} \right]^2 + \frac{16a_2a_4 + 3a_3^2}{8a_4^{\frac{3}{2}}}, \quad (17)$$

then after some algebra Eq. (9) takes the form of the triconfluent Heun's equation

$$\frac{d^2\varphi}{d\sigma^2} - (3\sigma^2 + \gamma) \frac{d\varphi}{d\sigma} + [\alpha(\varkappa) + (\beta - 3)\sigma] \varphi(\sigma) = 0, \quad (18)$$

where

$$\sigma = Q \left[ (s - s_0) - \frac{a_3}{4a_4} \right], \quad Q = \left( \frac{2\sqrt{a_4}}{3} \right)^{\frac{1}{3}}, \quad (19)$$

and the parameters  $\alpha(\varkappa)$ ,  $\beta$ ,  $\gamma$  are expressed as

$$\alpha(\varkappa) = \frac{64(\varkappa^2 + a_0)a_4^3 + 64a_2^2a_4^2 + 32a_2a_3^3a_4 + 16a_1a_3a_4^2 + 3a_3^4}{64Q^2a_4^3},$$

$$\beta = \frac{24a_4(a_1a_4 + a_2a_3) + 3a_3^3}{16a_4^{\frac{5}{2}}}, \quad \gamma = -\frac{16a_2a_4 + 3a_3^2}{8Qa_4^{\frac{3}{2}}}. \quad (20)$$

The general solution to the triconfluent Heun's equation (Eq. (15)) is then (see e.g., [5])

$$\varphi(\sigma) = \mathcal{A}_1 \text{THF}(\alpha(\varkappa), \beta, \gamma; \sigma) + \mathcal{B}_1 \exp(\sigma^3 + \gamma\sigma) \text{THF}(\alpha(\varkappa), -\beta, \gamma; -\sigma), \quad (21)$$

where  $\mathcal{A}_1$  and  $\mathcal{B}_1$  are integration constants and THF stands for the triconfluent Heun function (see e.g., [2, 5]). By combining the relations (16), (18), (19) the general solution to the time-independent Schrödinger-like equation (Eq. (9)) can be expressed as

$$\begin{aligned} \psi(s) = & \mathcal{A}_1 \exp \left[ -\frac{Q^3 \left( s - \frac{a_3}{4a_4} - s_0 \right)^3 + \gamma Q \left( s - \frac{a_3}{4a_4} - s_0 \right)}{2} \right] \text{THF} \left[ \alpha(\varkappa), \beta, \gamma; Q \left( s - \frac{a_3}{4a_4} - s_0 \right) \right] \\ & + \mathcal{B}_1 \exp \left[ \frac{Q^3 \left( s - \frac{a_3}{4a_4} - s_0 \right)^3 + \gamma Q \left( s - \frac{a_3}{4a_4} - s_0 \right)}{2} \right] \text{THF} \left[ \alpha(\varkappa), -\beta, \gamma; -Q \left( s - \frac{a_3}{4a_4} - s_0 \right) \right] \\ & = \mathcal{A}_1 \Phi_1[\alpha(\varkappa), \beta, \gamma; s] + \mathcal{B}_1 \Phi_2[\alpha(\varkappa), \beta, \gamma; s]. \quad (22) \end{aligned}$$

It is worth noting that evaluating confluent Heun functions and their derivatives can be easily accomplished using mathematical software such as Maple (version 10 and later) and Mathematica (version 12 and later).

The exact analytical solution to Eq. (6) can then be obtained by further combining the relations (11), (13), and (22) as

$$U_1(s) = \mathcal{A}_1 \Psi_1[\alpha(\varkappa), \beta, \gamma; s] + \mathcal{B}_1 \Psi_2[\alpha(\varkappa), \beta, \gamma; s], \quad (23)$$

where  $\Psi_{1,2}(s) = \Phi_{1,2}(s)/\sqrt{\eta(s)}$ .

The exact analytical solution for the homogeneous substrate (Eq. (7)) is then simply

$$U_2(s) = \mathcal{A}_2 \exp\left(\sqrt{K^2 - K_s^2} s\right) + \mathcal{B}_2 \exp\left(-\sqrt{K^2 - K_s^2} s\right). \quad (24)$$

### 3. Material functions based on the triconfluent Heun functions

The profile of the material function is determined by the generating polynomial, as previously mentioned. By comparing equations (9) and (14), we can immediately apply the solution (22) with  $\varkappa = 0$  for the function  $\phi(s)$ . To further express the material function, we use Eq. (13), resulting in

$$\eta(s) = [\mathcal{C}_1 \Phi_1(a_0, a_1, a_2, a_3, a_4, s_0; s) + \mathcal{C}_2 \Phi_2(a_0, a_1, a_2, a_3, a_4, s_0; s)]^2, \quad (25)$$

where  $\mathcal{C}_1$  and  $\mathcal{C}_2$  are optional integration constants. Therefore, the material function is fully determined by the eight distribution parameters  $\{a_0, a_1, a_2, a_3, a_4, s_0, \mathcal{C}_1, \mathcal{C}_2\}$ . This fact enables us to determine an entire family of material functions of various profiles. Some examples of the profiles of the material function (25) are depicted in Fig. 2.

### 4. Floquet-Bloch theory

We now assume that  $N$  of the same inhomogeneous elastic layers are laid over the homogeneous substrate, resulting in a locally periodic structure for  $z \in \langle 0, N\ell \rangle$ , see Fig. 3. The locally periodic material function then reads

$$\eta_p(s) = \eta(s - \lfloor s \rfloor), \quad \text{for } s \in \langle 0, N \rangle, \quad (26)$$

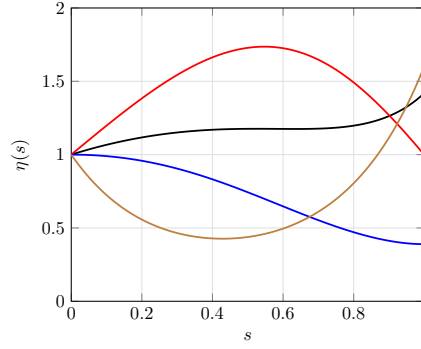


Figure 2: (Color online) Examples of the material function profiles  $\eta(s)$  for a given sequence of the distribution parameters  $\{a_0, a_1, a_2, a_3, a_4, s_0, \mathcal{C}_1, \mathcal{C}_2\}$ .  $\{1.04, 1, 1, 0, 1, 0, 1, 0\}$  – red line,  $\{1, -1.5, 1, 0, 7, 0, 1, 0\}$  – black line,  $\{1, 1, 0, 0, 9, 0, 1, 0\}$  – blue line,  $\{-5, -3, 3, 0, 3, 0, 0, 1\}$  – brown line.

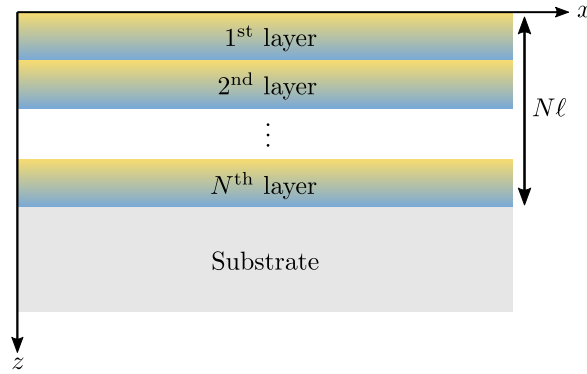


Figure 3: (Color online) Locally periodic FG material structure.

where  $\lfloor s \rfloor$  represents the greatest integer less than or equal to  $s$ . In order to obtain the solution for the whole locally periodic structure we employ the Floquet-Bloch theory, see e.g. [4]. First, we express the solution in the first layer (based on Eq. (23)) in its normalised form

$$U_1(s) = U_1(0)v(s) + U_1'(0)w(s), \quad (27)$$

where the functions  $v(s)$  and  $w(s)$  can be expressed as

$$v(s) = \frac{\Psi_2'(0)}{W[\Psi_1, \Psi_2](0)} \Psi_1(s) - \frac{\Psi_1'(0)}{W[\Psi_1, \Psi_2](0)} \Psi_2(s), \quad (28)$$

$$w(s) = \frac{-\Psi_2(0)}{W[\Psi_1, \Psi_2](0)} \Psi_1(s) + \frac{\Psi_1(0)}{W[\Psi_1, \Psi_2](0)} \Psi_2(s), \quad (29)$$

where

$$W[\Psi_1, \Psi_2](s) = \Psi_1(s)\Psi_2'(s) - \Psi_1'(s)\Psi_2(s) \quad (30)$$

is the Wronskian, meeting the conditions

$$v(0) = 1, \quad v'(0) = 0, \quad w(0) = 0, \quad w'(0) = 1. \quad (31)$$

By introducing the Floquet multipliers (see e.g., [4])

$$\lambda_{1,2} = \frac{h \pm \sqrt{h^2 - 4}}{2}, \quad (32)$$

where  $h = v(1) + w'(1)$ , we can then express the corresponding Bloch waves for the first inhomogeneous layer (unit) as

$$\tilde{F}_{1,2}(s) = v(s) + \frac{\lambda_{1,2} - v(1)}{w(1)} w(s). \quad (33)$$

The Bloch waves in the whole locally periodic structure then take on a form

$$F_{1,2}(s) = \lambda_{1,2}^{\lfloor s \rfloor} \tilde{F}_{1,2}(s - \lfloor s \rfloor). \quad (34)$$

The exact analytical solution of the model equation (6) then reads as

$$U(s) = \mathcal{A}_{\text{FB}} F_1(s) + \mathcal{B}_{\text{FB}} F_2(s), \quad s \in [0, N], \quad (35)$$

where  $\mathcal{A}_{\text{FB}}$  and  $\mathcal{B}_{\text{FB}}$  stand for the integration constants. Please note that the Bloch waves  $F_{1,2}(s)$  still depend on the parameters  $\alpha(\varkappa)$ ,  $\beta$ ,  $\gamma$ , but for the sake of readability we have omitted this explicit notation in the text above.

## 5. Dispersion relation

The dispersion relation for the locally periodic problem can be derived by introducing the specific boundary conditions as follows:

1. The surface of the first layer is assumed traction free, i.e.

$$\left. \frac{dU_1(s)}{ds} \right|_{s=0} = 0. \quad (36)$$

2. The displacement component and the respective stresses are assumed continuous on the boundary between the last layer and the substrate, i.e.

$$U_1(s = N) = U_2(s = N), \quad (37)$$

$$\mu(N) \left. \frac{dU_1(s)}{ds} \right|_{s=N} = \mu_s \left. \frac{dU_2(s)}{ds} \right|_{s=N}, \quad (38)$$

3. The regularity condition at infinity:

$$\lim_{s \rightarrow \infty} U_2(s) = 0. \quad (39)$$

From the last condition (Eq. (39)), we immediately get  $\mathcal{A}_2 = 0$ . Therefore, three integration constants ( $\mathcal{A}_{\text{FB}}$ ,  $\mathcal{B}_{\text{FB}}$ ,  $\mathcal{B}_2$ ) remain. By solving the system of Eqs. (36), (37) and (38) we obtain the respective dispersion relation in its implicit form

$$H(\varkappa) = -\frac{\mu_s}{\eta_{\text{lp}}(N)\mu_0} \sqrt{K_0^2 - K_s^2 - \varkappa^2}, \quad (40)$$

where

$$H(\varkappa) \equiv \frac{F_1'(\alpha(\varkappa), \beta, \gamma; 0)F_2'(\alpha(\varkappa), \beta, \gamma; N) - F_1'(\alpha(\varkappa), \beta, \gamma; N)F_2'(\alpha(\varkappa), \beta, \gamma; 0)}{F_1'(\alpha(\varkappa), \beta, \gamma; 0)F_2(\alpha(\varkappa), \beta, \gamma; N) - F_1(\alpha(\varkappa), \beta, \gamma; N)F_2'(\alpha(\varkappa), \beta, \gamma; 0)}. \quad (41)$$

By solving Eq. (40) we can then determine the respective dispersion characteristics  $c_{\text{ph}} = c_{\text{ph}}(K)$ .

## 6. Results and discussion

In this section we present some selected results based on the theory derived above (all the calculations were performed using Maple 17). The material parameters for the inhomogeneous layer (FG material) and the homogeneous substrate were chosen as

$$\begin{aligned} \mu_0 &= 30 \text{ GPa}, & \rho_0 &= 2700 \text{ kg m}^{-3} \quad (\text{Aluminium}); \\ \mu_s &= 150 \text{ GPa}, & \rho_s &= 3960 \text{ kg m}^{-3} \quad (\text{Alumina}). \end{aligned} \quad (42)$$

The corresponding values of  $c_0$  and  $c_s$  are then

$$c_0 = 3333 \text{ m s}^{-1}, \quad c_s = 6155 \text{ m s}^{-1}. \quad (43)$$

For the sake of this paper we use the following distribution parameters:

$$\begin{aligned} a_0 &= -69.09, & a_1 &= 668.55, & a_2 &= -1049.60, & a_3 &= 2861.29, & a_4 &= 1430.65, \\ s_0 &= 0, & C_1 &= 1.49, & C_2 &= 1.49, \end{aligned} \quad (44)$$

resulting in the Gaussian-like profile of the material function given in Fig. 4.

Based on the dispersion equation (40), the corresponding dispersion curves  $c_{\text{ph}} = c_{\text{ph}}(K)$  are plotted

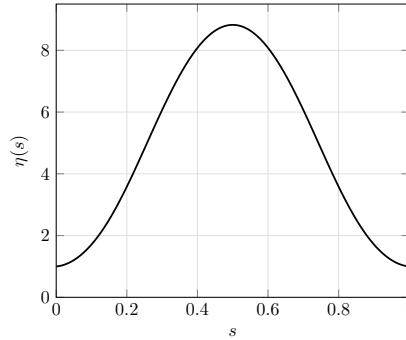


Figure 4: Gaussian-like profile of the material function.

in Fig. 5 for  $N = 1$  (a),  $N = 3$  (b) and  $N = 6$  (c) inhomogeneous layers. The figure illustrates the intriguing impact of the Gaussian-like profile of the material function on the dispersion characteristics. As evidenced by the plot, the dispersion curves that correspond to each individual Love-mode form discrete groups of  $N$ , with the separation between these groups decreasing as the mode order increases. Note that  $c_{\text{ph}} \in (c_0, c_s)$  for all the modes.

## 7. Conclusion

In this article, we present a calculation of dispersion curves for Love waves propagating through a inhomogeneous locally periodic structure comprised of layers made from functionally graded (FG) material. The material parameters of the FG material vary spatially along the  $z$ -axis according to a Gaussian-like profile of the material function. The calculations are based on the exact analytical solution for Love-type waves in an inhomogeneous layer, which is derived using the triconfluent Heun functions. To calculate the propagation of Love-type waves in a locally periodic structure, Floquet-Bloch theory is employed. The resulting dispersion curves reveal how the number  $N$  of inhomogeneous layers in the locally periodic structure influences the dispersion characteristics in a non-intuitive manner.

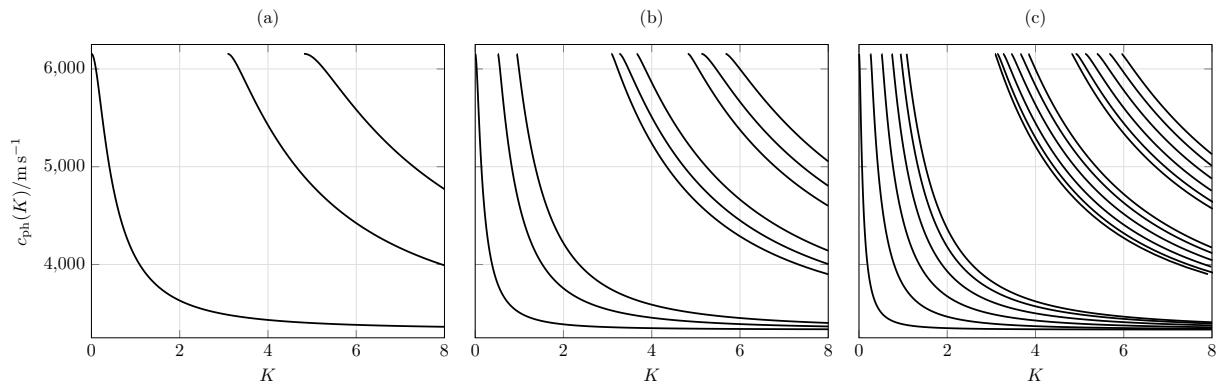


Figure 5: The dispersion curves for the gaussian-like profile of the material function. (a) First 3 modes for  $N = 1$ ; (b) First 9 modes for  $N = 3$ ; (c) First 18 modes for  $N = 6$ .

## Acknowledgments

This work was supported by the the Grant Agency of the Czech Republic (GACR) grant No. 22-33896S and by the Grant Agency of the Czech Technical University in Prague No. SGS23/057/OHK3/1T/13.

## REFERENCES

1. Kiełczyński, P., (2018), Properties and applications of love surface waves in seismology and biosensors. *Surface Waves - New Trends and Developments*, InTech.
2. Krpensky, A. and Bednarik, M. Surface love-type waves propagating through viscoelastic functionally graded media, *The Journal of the Acoustical Society of America*, **150** (5), 3302–3313, (2021).
3. Bednarik, M., Cervenka, M., Lotton, P. and Simon, L. Analytical solutions for elastic SH-waves propagating through an isotropic inhomogeneous layer, *Composite Structures*, **220**, 875–887, (2019).
4. Bednarik, M. and Cervenka, M. Propagation of electromagnetic waves through non-uniform dielectric layers, *Journal of the Optical Society of America B*, **35** (10), 2541, (2018).
5. Ronveaux, A., *Heun's Differential Equations*, Clarendon Press, Oxford, England (1995).

### 3.3 Paper III

**Title:** *A new class of approximate analytical solutions of the Pridmore-Brown equation*

The third presented paper published in the Journal of Mathematical Physics is focused on the propagation of acoustic waves through a two-dimensional acoustic waveguide (two parallel rigid walls with defined spacing) in the presence of a non-uniform (inhomogeneous) time independent parallel shear flow. That means the direction of the mean flow velocity is parallel to the waveguide walls. The spatial dependence of the mean flow velocity is then dependent only on the direction perpendicular to that one of the flow and it's profile is given by the function  $\eta$  which will be referred to as the mean flow profile hereinafter.

By assuming an acoustic wave travelling along the waveguide the corresponding model Webster-type equation describing the acoustic pressure distribution across the waveguide cross-section is derived from the more general form of the so called Pridmore-Brown equation (which generally assumes a three-dimensional waveguide) and by a similar procedure as presented in the two previous papers is transformed into the form of the triconfluent Heun equation. However, in this case the transformation can not be done exactly and therefore in the process of the transformation an approximation step is involved. The solution to the model equation (which is now only an approximate analytical) is then expressed as a combination of the triconfluent Heun functions (see Sec. 2.1). Finally, the boundary conditions at the waveguide walls are expressed, making the formulation of the problem complete. At this point, it is convenient to note that the accuracy of the approximation depends on the Mach number (defined here as the maximum of the mean flow profile divided by the speed of sound for the respective medium at rest) in a way that the higher the Mach number the worse the approximation.

The succeeding study is now divided into the two parts. First, we assume a symmetric parabolic mean flow profile for which the approximation (as mentioned above) during the process of the model equation transformation is demonstrated and the accuracy of the approximation is derived, whereas in this case the approximation error is proportional to the fourth power of the Mach number. The first four upstream and downstream modes of the solution are then plotted together with the numerical results obtained via the RKF45 method in order to assess their accuracy that is excellent for the specific case. In the second part of the study, we assume the most simple forms of the symmetric mean flow profiles expressed by an even power  $n$  of the corresponding coordinate and a comprehensive graph of the solutions







to the model equation is displayed for various values of  $n$ , providing a good assesment of the approximation method accuracy. A short discussion why in this case the high frequency limit WKB approximation (see Sec. 2.3) can not be considered as an analytical solution is also present.

The main scientific contribution of this paper is that the analytical solutions to the model equation are known only for a very limited set of functional dependencies of the mean flow profiles and our solutions, even though only approximate analytical, can be generally used to any form of the mean flow profile where the approximation is still valid.

RESEARCH ARTICLE | AUGUST 25 2022

# A new class of approximate analytical solutions of the Pridmore-Brown equation

A. Krpensky   ; V. Hruska  ; M. Bednarik 



*J. Math. Phys.* 63, 083101 (2022)

<https://doi.org/10.1063/5.0098473>

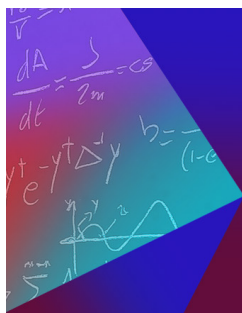


View  
Online



Export  
Citation

CrossMark



Journal of Mathematical Physics

Young Researcher Award:  
Recognizing the Outstanding Work  
of Early Career Researchers

[Learn More!](#)

# A new class of approximate analytical solutions of the Pridmore-Brown equation

Cite as: J. Math. Phys. **63**, 0831 01 (2022); doi: 10.1063/5.0098473

Submitted: 9 May 2022 • Accepted: 20 July 2022 •

Published Online: 25 August 2022



View Online



Export Citation



CrossMark

A. Krpensky,<sup>a)</sup>  V. Hruska,  and M. Bednarik 

## AFFILIATIONS

Czech Technical University in Prague, Faculty of Electrical Engineering, Technicka 2, 166 27 Prague 6, Czech Republic

<sup>a)</sup> Author to whom correspondence should be addressed: [antonin.krpensky@fel.cvut.cz](mailto:antonin.krpensky@fel.cvut.cz)

## ABSTRACT

There is only a limited amount of known analytical solutions to the Pridmore-Brown equation, mostly employing asymptotic behavior for a certain frequency limit and specifically chosen flow profiles. In this paper, we show the possibility of transformation of the Pridmore-Brown equation into the Schrödinger-like equation for the case of two-dimensional homentropic mean flow without critical layers. The corresponding potential that depends on the mean flow profile can then be approximated by a quartic polynomial, leading to a triconfluent Heun equation whose solution based on the triconfluent Heun functions is generally known. The quality of this approximation procedure is presented for the case of symmetric polynomial flow profiles for various values of polynomial order and the Mach number. A more detailed example is then shown for a quadratic mean flow profile, where the solution is accurate up to the third order of the Mach number.

Published under an exclusive license by AIP Publishing. <https://doi.org/10.1063/5.0098473>

## I. INTRODUCTION

Sound propagation in parallel shear flows presents a topic with high application relevance. Many devices, such as engine nacelles or various ventilation systems, incorporate parts in which the background flow varies across the duct but not along. Under these circumstances, the compressible Euler equations can be rearranged and linearized around the mean flow to yield a third-order wave equation for small pressure perturbations. Finding its time-harmonic solution by means of the Fourier transform in the axial direction leads to an eigenvalue problem, bearing the name of its founding author David Clifford Pridmore-Brown.<sup>1</sup> Solutions to the Pridmore-Brown equation serve not solely for the description of the sound propagation *per se*, but they also find rich opportunities in valuable auxiliary tasks, e.g., assessment of the effective liner impedance<sup>2,3</sup> or benchmarking the respective boundary conditions<sup>4</sup> or as one of the sequential steps when dealing with more advanced scenarios, e.g., the evolution of the modes along a duct with varying cross section<sup>5</sup> or estimation of fluid-dynamic loading on the structure of the pipe.<sup>6</sup>

Profound reflection of the existing literature might be found in recent articles by Rienstra.<sup>5,7</sup> From the analytical point of view, the Pridmore-Brown equation is predominantly solved by perturbation techniques (WKB, multiple-scales) when asymptotic behavior could be assumed (see, e.g., Refs. 5 and 7) or, for instance, by Frobenius expansion around a singularity occurring when the flow speed matches the phase velocity of the perturbation (see, e.g., Refs. 8–10). In addition, there are specially adapted numerical techniques for this task (see, e.g., Refs. 5, 7, and 11–14). Apart from the analytical solution by Goldstein and Rice,<sup>2</sup> there are other analytical treatments of equations similar to the Pridmore-Brown problem by means of the hypergeometric confluent functions.<sup>15–18</sup> However, these solutions relate only to the linearly sheared flow. Recently, Zhang and Oberlack employed the confluent Heun functions to solve the Pridmore-Brown equation for the exponential flow profile.<sup>19</sup> Although approximative, the solution presented below is more versatile than the relevant, yet special case discussed by Zhang and Oberlack.

Our primary goal is to present a new way of analytically solving the Pridmore-Brown equation. We are going to show that the Pridmore-Brown equation can be transformed into the Schrödinger-like equation whose potential can be approximated by a quartic polynomial leading to a closed-form analytical solution employing the triconfluent Heun functions (see, e.g., Refs. 20–23). Specifically, for the quadratic flow profile, an excellent approximation can be found for any frequency and up to the third order in the Mach number.

This paper is organized as follows. Section II is devoted to a brief derivation of the Pridmore-Brown equation and its two-dimensional form. The transformation of the employed model equation to the Schrödinger-like equation followed by the corresponding closed-form approximate analytical solution is shown in Sec. III. The solution is illustrated on a family of polynomial flow profiles given in Sec. IV. Following paragraphs are dedicated to discussion (Sec. V), and the conclusions are given in Sec. VI.

## II. PRIDMORE-BROWN EQUATION

### A. Brief derivation of the general form of the Pridmore-Brown equation

For the sake of brevity, the derivation from a general form of compressible Euler equations is omitted (see, e.g., the manipulations in the Appendix of Ref. 7). Instead, the convected wave equation in parallel inviscid shear flow is considered as the starting point. Assume a sound propagation in a duct of constant cross section oriented along  $x$ . Vectors of the mean velocity  $\mathbf{u}_0 = u_0 \mathbf{e}_x$  are parallel; their magnitudes are varying over the waveguide cross section but remain constant along the duct [ $u_0 = u_0(y, z)$ , see Fig. 1]. The latter condition is assumed for the mean density  $\rho_0(y, z)$  and speed of sound  $c_0(y, z)$  as well, while the mean pressure  $p_0$  is constant uniformly. The speed of sound  $c_0(y, z)$  is related to the mean pressure and density as  $c_0^2 = \gamma p_0 / \rho_0$ , with  $\gamma$  denoting the ratio of specific heats. Under these assumptions, the wave equation for pressure perturbations  $p'(x, y, z, t)$  reads (see, e.g., Ref. 7)

$$\frac{D_0^3 p'}{D_0 t^3} + 2c_0^2 \frac{\partial}{\partial x} (\nabla_{\perp} u_0 \cdot \nabla_{\perp} p') - \frac{D_0}{D_0 t} \nabla \cdot (c_0^2 \nabla p') = 0, \quad (1)$$

where

$$\frac{D_0}{D_0 t} = \frac{\partial}{\partial t} + u_0 \frac{\partial}{\partial x}, \quad (2)$$

$$\nabla_{\perp} = \left( \frac{\partial}{\partial y}, \frac{\partial}{\partial z} \right). \quad (3)$$

For a low Mach number flow [ $M = \max(u_0)/c_0$ ] without temperature gradient, the ambient density  $\rho_0$  and speed of sound  $c_0$  are constant, and we assume this case henceforth. The solution to Eq. (1) is sought in the form

$$p'(x, y, z, t) = P(y, z) e^{i(kx - \omega t)}, \quad (4)$$

where  $P$ ,  $\omega$ , and  $k$  denote the complex pressure amplitude, the angular frequency, and the wavenumber in the direction of the waveguide, respectively, and  $i = \sqrt{-1}$ . By inserting Eq. (4) into Eq. (1), the Pridmore-Brown equation is obtained for the pressure amplitude  $P$  after some manipulations,

$$\tilde{\Gamma}^2 \nabla_{\perp} \cdot \left( \frac{1}{\tilde{\Gamma}^2} \nabla_{\perp} P \right) + (\tilde{\Gamma}^2 - k^2) P = 0, \quad \text{where} \quad \tilde{\Gamma} = \frac{\omega - k u_0}{c_0}. \quad (5)$$

The absence of critical layers (where  $\tilde{\Gamma} \approx 0$ ) is assumed henceforth (see Ref. 10 for further commentary).

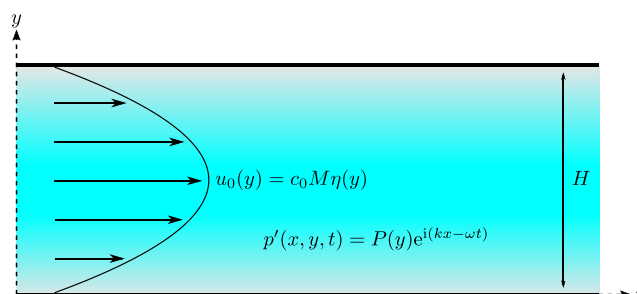


FIG. 1. Geometry of the assumed waveguide structure with parabolic mean flow.

### B. Two-dimensional case

In the following, the considerations are restricted to the  $(x, y)$  plane. For this assumption, a specific case of the Sturm–Liouville problem is obtained from Eq. (5),

$$\tilde{\Gamma}^2 \frac{d}{dy} \left( \frac{1}{\tilde{\Gamma}^2} \frac{dP}{dy} \right) + (\tilde{\Gamma}^2 - k^2)P = 0. \quad (6)$$

By expanding the first term in Eq. (6), we get

$$\frac{d^2P}{dy^2} - \frac{2}{\tilde{\Gamma}} \frac{d\tilde{\Gamma}}{dy} \frac{dP}{dy} + (\tilde{\Gamma}^2 - k^2)P = 0. \quad (7)$$

This equation stays in the focus of the paragraphs to follow. Before any further steps are taken, Eq. (7) is made dimensionless by introducing the following variables:

$$s = \frac{y}{H}, \quad \Omega = \frac{H}{c_0} \omega, \quad K = kH, \quad u_0(y) = c_0 M \eta(s), \quad (8)$$

where  $H$ ,  $s$ ,  $\Omega$ ,  $K$ , and  $M$  denote the characteristic length (such as the waveguide height), the dimensionless transversal coordinate, angular frequency, wavenumber, and the maximum Mach number through the waveguide cross section, respectively, and the normalized function  $\eta(s)$  represents the mean flow profile (see Fig. 1). Hence, the dimensionless Pridmore-Brown equation reads

$$\frac{d^2P}{ds^2} - \frac{2}{\Gamma} \frac{d\Gamma}{ds} \frac{dP}{ds} + (\Gamma^2 - K^2)P = 0, \quad \text{where } \Gamma(s) = \Omega - KM\eta(s). \quad (9)$$

Note that Eq. (9) is linear in  $P$ , and therefore, the pressure amplitude might be arbitrarily scaled.

## III. APPROXIMATE CLOSED-FORM SOLUTION AND DISPERSION RELATION

### A. Approximate analytical solution of the model equation

In this section, we are going to show that Eq. (9) can be transformed into a Schrödinger-like equation (see Refs. 24–26 for an example of a similar procedure undertaken on simpler equations and Ref. 27 for the occurrence of the Schrödinger-like equation arising from the Pridmore-Brown equation). If its potential is in the form of a quartic polynomial, it can be further transformed into the triconfluent Heun equation (see below).

By substituting

$$P = \Gamma \Psi \quad (10)$$

into Eq. (9), we arrive at its Liouville normal form

$$\frac{d^2\Psi}{ds^2} + \mathcal{G}(s)\Psi = 0, \quad \text{where } \mathcal{G}(s) = \frac{1}{\Gamma} \frac{d^2\Gamma}{ds^2} - 2 \left( \frac{1}{\Gamma} \frac{d\Gamma}{ds} \right)^2 + \Gamma^2 - K^2. \quad (11)$$

Our goal is to approximate the potential  $\mathcal{G}(s)$  by a quartic polynomial in order to be able to solve Eq. (11) analytically. First, let us rewrite  $\mathcal{G}(s)$  using the expression for  $\Gamma$  in Eq. (9). We get

$$\mathcal{G}(s) = \frac{-KM\eta''}{\Omega - KM\eta} - 2 \left( \frac{KM\eta'}{\Omega - KM\eta} \right)^2 + (\Omega - KM\eta)^2 - K^2. \quad (12)$$

One can see that for lower  $\Omega$ , the first two terms dominate. Note that these terms are generally harder to be approximated by a polynomial curve than the latter ones.

Let us now assume  $\mathcal{G}(s)$  as

$$\mathcal{G}(s) = a_0 + a_1s + 2a_2s^2 + a_3s^3 - a_4s^4, \quad a_4 \neq 0. \quad (13)$$

Using the following change of variables,

$$s = \frac{\sigma}{Q} + \frac{a_3}{4a_4}, \quad \text{where } Q = \left( \frac{2\sqrt{a_4}}{3} \right)^{\frac{1}{3}}, \quad (14)$$

Eq. (11) could be transformed into the representative form of the triconfluent Heun equation (for more details, see, e.g., Ref. 20),

$$\frac{d^2\Psi}{d\sigma^2} + \left( A_0 + A_1\sigma + A_2\sigma^2 - \frac{9}{4}\sigma^4 \right) \Psi(\sigma) = 0, \quad (15)$$

where

$$A_0 = \frac{3a_3^4 + 32a_2a_3^2a_4 + 64a_1a_3a_4^2 + 256a_0a_4^3}{256Q^2a_4^3}, \quad A_1 = \frac{a_3^3 + 8a_2a_3a_4 + 8a_1a_4^2}{8Q^3a_4^2}, \quad (16)$$

$$A_2 = \frac{3a_3^2 + 16a_2a_4}{8Q^4a_4}. \quad (17)$$

By substituting the expression

$$\Psi(\sigma) = \exp\left(-\frac{\sigma^3}{2} + \frac{A_2}{3}\sigma\right)\Phi(\sigma) \quad (18)$$

into Eq. (15), we arrive at the canonical form of the triconfluent Heun equation as (see, e.g., Ref. 20)

$$\frac{d^2\Phi}{d\sigma^2} - (3\sigma^2 + \gamma)\frac{d\Phi}{d\sigma} + [\alpha + (\beta - 3)\sigma]\Phi(\sigma) = 0. \quad (19)$$

Here,

$$\alpha = A_0 + \frac{A_2^2}{9}, \quad \beta = A_1, \quad \gamma = -\frac{2}{3}A_2. \quad (20)$$

The solution of Eq. (19) can then be expressed as (see, e.g., Ref. 20)

$$\Phi(\sigma) = \mathcal{A}_1 \text{THF}(\alpha, \beta, \gamma; \sigma) + \mathcal{B}_1 \exp(\sigma^3 + \gamma\sigma)\text{THF}(\alpha, -\beta, \gamma; -\sigma), \quad (21)$$

where  $\mathcal{A}_1$  and  $\mathcal{B}_1$  are integration constants and THF stands for the triconfluent Heun function. By substituting this back into expression (18) and further employing relations (10) and (14), we arrive at the final closed-form approximate analytical solution for the complex pressure amplitude,

$$P(s) = \mathcal{A}_1\Gamma(s)\exp\left[-\frac{Q^3}{2}\left(s - \frac{a_3}{4a_4}\right)^3 - \gamma\frac{Q}{2}\left(s - \frac{a_3}{4a_4}\right)\right]\text{THF}\left[\alpha, \beta, \gamma; Q\left(s - \frac{a_3}{4a_4}\right)\right] \\ + \mathcal{B}_1\Gamma(s)\exp\left[\frac{Q^3}{2}\left(s - \frac{a_3}{4a_4}\right)^3 + \gamma\frac{Q}{2}\left(s - \frac{a_3}{4a_4}\right)\right]\text{THF}\left[\alpha, -\beta, \gamma; -Q\left(s - \frac{a_3}{4a_4}\right)\right]. \quad (22)$$

Finally, this could be expressed in the following compact form:

$$P(s) = \mathcal{A}_1P_1(\alpha, \beta, \gamma; s) + \mathcal{B}_1P_2(\alpha, \beta, \gamma; s), \quad (23)$$

which we will use from now on.

For the purposes of practical computations, the triconfluent Heun functions might be expressed as power series (see, e.g., Refs. 20, 24, and 28) that can be easily implemented in Matlab, Python, etc. Moreover, the Heun functions are available in Maple (from Maple 10 on) and Wolfram Language (from Mathematica 12 on). The results presented below are obtained by Maple 17.

## B. Calculation of integration constants and dispersion relation

In order to determine the integration constants of the solution (23) of Eq. (11) for a chosen frequency, suitable boundary conditions must be supplemented to the problem. For a specific example, we assume that the waveguide walls are perfectly rigid, and according to Eq. (27), the mean flow is vanishing at the walls. Hence, the use of Neumann boundary conditions for perturbation pressure amplitudes is justified,

$$\frac{dP}{ds}\Big|_{s=0} = \frac{dP}{ds}\Big|_{s=1} = 0. \quad (24)$$

In order to obtain a nontrivial solution of this system of equations, the corresponding determinant must equal to zero, resulting in the equation

$$\frac{dP_1}{ds}\Big|_{s=0} \frac{dP_2}{ds}\Big|_{s=1} - \frac{dP_2}{ds}\Big|_{s=0} \frac{dP_1}{ds}\Big|_{s=1} = 0. \quad (25)$$

Equation (25) represents an implicit form of a dispersion equation  $D(\Omega, K) = 0$ , which needs to be solved by an iterative numerical method (the bisection method was sufficient for the task in our case). For every dimensionless angular frequency  $\Omega$ , there exists one or more solutions of the dispersion equation:  $K_{\Omega 0}, \dots, K_{\Omega N}$ , where  $K_{\Omega i}$  represents the dimensionless wavenumber of the individual wave mode. After solving the dispersion equation, the integration constants can be found using one of Eq. (24), and therefore, the solution is complete.

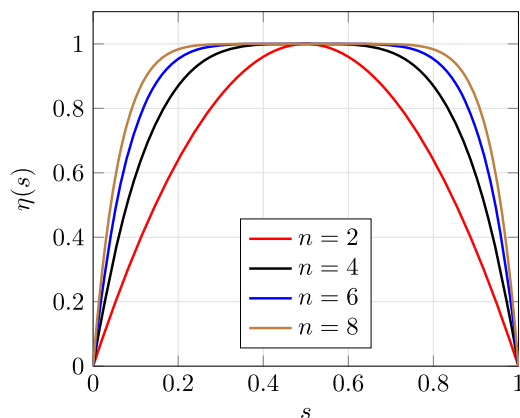


FIG. 2. First four symmetric mean flow profiles defined by Eq. (26).

### C. Set-up of numerical verification

Each solution of Eq. (9) based on the triconfluent Heun functions (THF solution) was verified by a numerical solution of the same equation. We made use of the facts that the Neumann boundary condition for the pressure is demanded by the physics of the studied case (see above), and the functions giving the eigenmode shapes can be multiplied by an arbitrary scalar. Hence, the boundary value problem was solved as the initial value one by the Runge–Kutta–Fehlberg (RK45) method (see, e.g., Ref. 29), and the wavenumber  $K$  required to satisfy the opposite boundary condition was sought by the bisection method. The above described numerical methods were implemented in Maple 17.

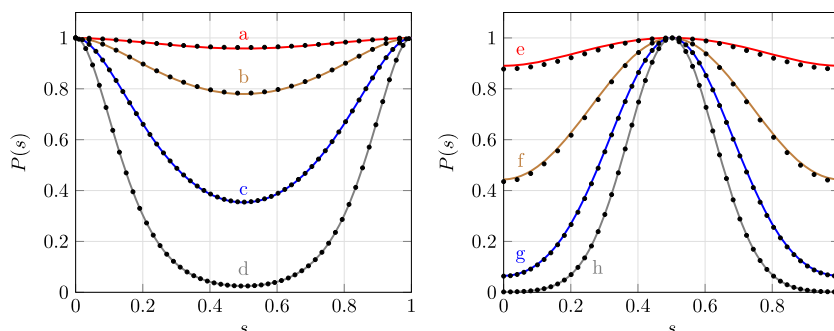


FIG. 3. Downstream [left, (a)–(d)] and upstream [right, (e)–(h)] fundamental modes for various dimensionless frequencies and the parabolic flow profile with maximum Mach number  $M = 0.4$ . (a) and (e):  $\Omega = 2$ , (b) and (f):  $\Omega = 5$ , (c) and (g):  $\Omega = 10$ , and (d) and (h):  $\Omega = 20$ . The lines and dots represent analytical and numerical solutions, respectively.

TABLE I. Values of the dimensionless wavenumber  $K$  obtained using the THF solutions and the RK45 method for various values of frequency  $\Omega$  corresponding to the fundamental downstream (left) and upstream (right) mode.

$\Omega$	$K_{\text{THF}}$	$K_{\text{RK45}}$
2	1.567	1.557
5	3.921	3.916
10	8.028	8.024
20	17.13	17.13
2	-2.719	-2.662
5	-6.937	-6.925
10	-15.02	-15.03
20	-31.75	-31.77

#### IV. APPROXIMATE CLOSED-FORM SOLUTIONS FOR SPECIFIC PROFILES

For the purpose of this paper, we use a symmetric profile  $\eta(s)$  expressed by

$$\eta(s) = 1 - 2^n \left(s - \frac{1}{2}\right)^n, \tag{26}$$

where  $n$  is even, but in general, various other profiles can be used. First four profiles defined by the expression (26) are shown in Fig. 2. The value  $M = 0.4$  is used henceforth.

Next, two specific techniques of approximation of expression (12) are introduced.

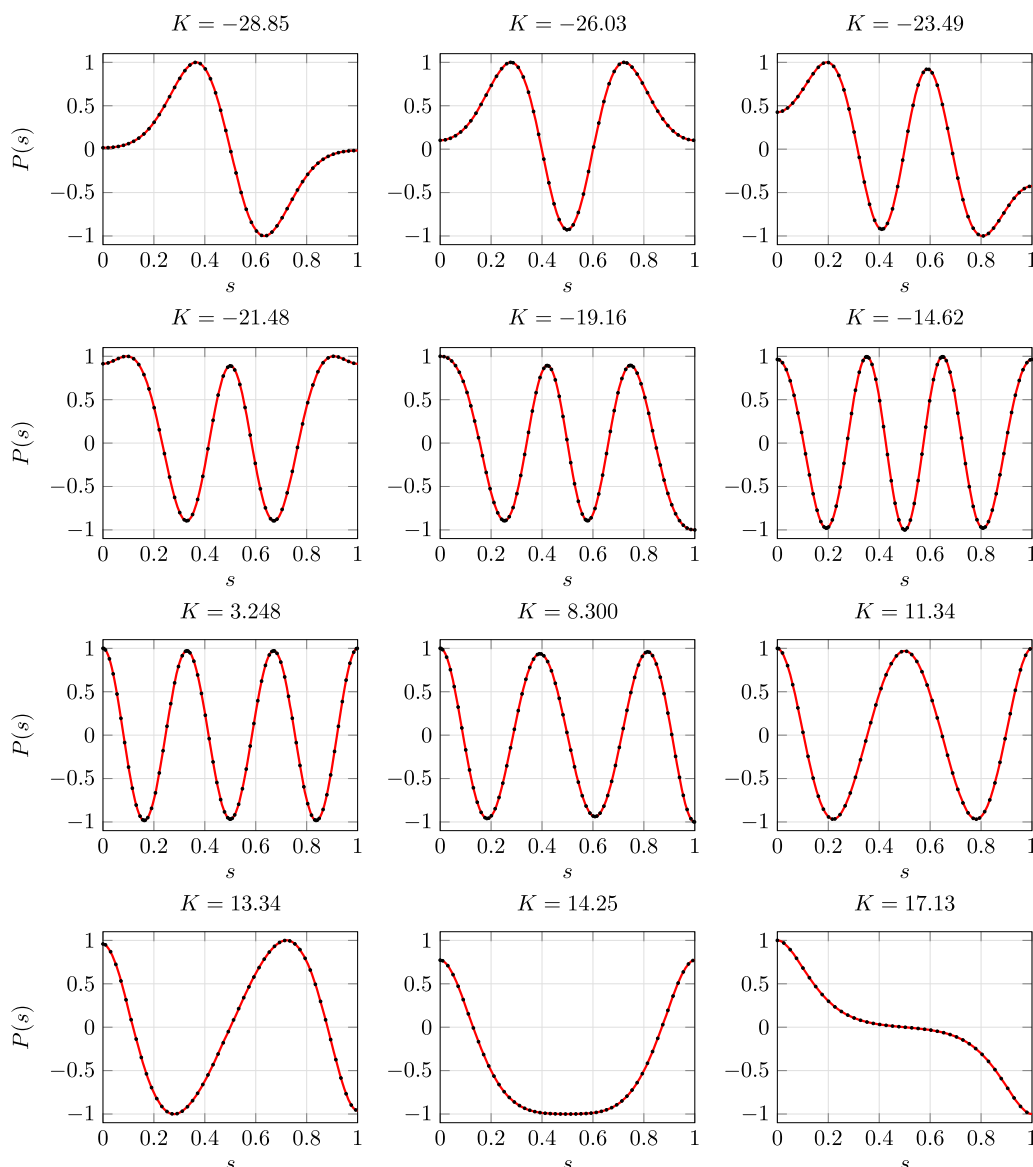


**FIG. 4.** All higher modes for dimensionless frequency  $\Omega = 20$  and the parabolic flow profile with the maximum Mach number  $M = 0.4$ . The lines and dots represent analytical and numerical solutions, respectively.



### A. Expansion for small $KM/\Omega$

In order to show a specific example of the above-given procedure, we will focus on approximating the quadratic mean flow profile expressed as

$$\eta(s) = 1 - 4\left(s - \frac{1}{2}\right)^2, \quad (27)$$

but in general, any quadratic profile can be used. After substituting expression (27) into Eq. (12) and expanding up to the third order of a small parameter  $KM/\Omega$ , we obtain the following equation:

$$\frac{d^2\Psi}{ds^2} + \mathcal{G}(s)\Psi = 0, \quad (28)$$

where

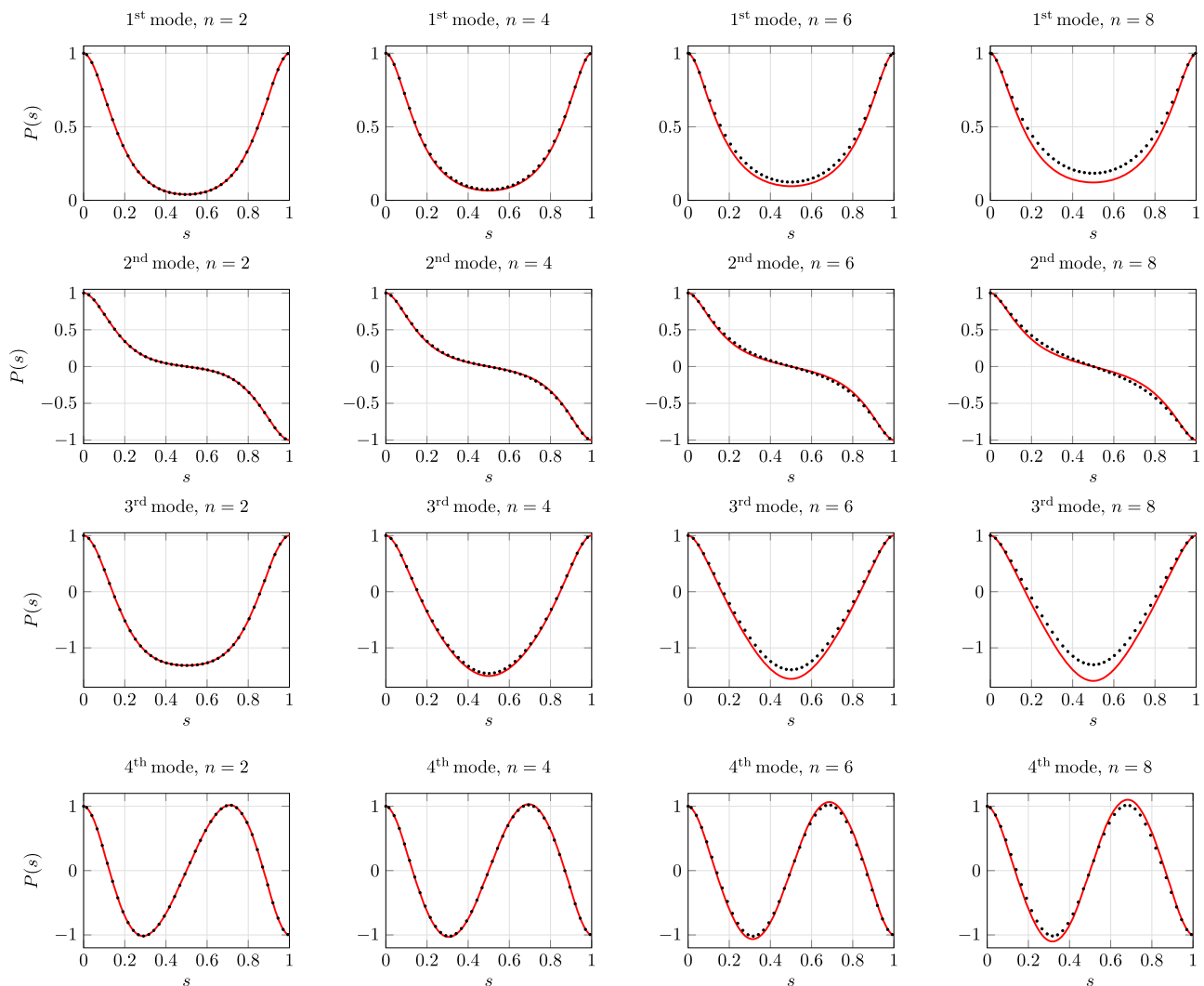


FIG. 5. The first four downstream modes for various orders of the mean flow profile and  $\Omega = 18.3$ .

$$\begin{aligned} \mathcal{G}(s) &= (\Omega - KM\eta)^2 - K^2 - \frac{d^2\eta}{ds^2} \frac{KM}{\Omega} - \left[ \eta \frac{d^2\eta}{ds^2} + 2 \left( \frac{d\eta}{ds} \right)^2 \right] \frac{K^2 M^2}{\Omega^2} \\ &\quad - \left[ \eta^2 \frac{d^2\eta}{ds^2} + 4\eta \left( \frac{d\eta}{ds} \right)^2 \right] \frac{K^3 M^3}{\Omega^3} + \mathcal{O} \left( \frac{K^4 M^4}{\Omega^4} \right) \\ &\approx a_0 + a_1 s + 2a_2 s^2 + a_3 s^3 - a_4 s^4 \end{aligned} \quad (29)$$

takes the form of a quartic polynomial. Strictly speaking, solutions  $\Psi$  of Eqs. (11) and (28) are not fully equivalent. However, we do not change the labels for the sake of readability. This solution is approximate analytical one with accuracy up to the  $\mathcal{O}(K^4 M^4 / \Omega^4)$ .

First, we demonstrate the fundamental modes in downstream and upstream directions of propagation for various dimensionless frequencies  $\Omega$  (see Fig. 3). The comparison between the wavenumber (eigenvalue) values found using the THF solution, and the numerical solution is presented in Table I. With increasing frequency, a relatively higher portion of the acoustic energy is distributed at the walls for the downstream propagation and along the centerline in the upstream one.

One can observe (e.g., from Fig. 3) that our approximation tends to slightly deviate from the numerical solution as  $\Omega \rightarrow 0$ . This is explained by considering the following: From the square bracket in Eq. (11), only the first two terms need to be approximated—the other two are already a quartic polynomial in  $s$ . Now note that for the parabolic profile, both approximated terms are inversely proportional to  $\Omega$ . Hence, with increasing  $\Omega$ , there is relatively lower importance of the approximated terms regarding the whole expression.

Next, the frequency  $\Omega = 20$  is kept constant, and various downstream and upstream mode shapes with respective wavenumbers  $K$  are calculated (see Fig. 4). Again, the disparities between the propagation directions take place in the mode shapes as well as in the distribution of the eigenvalues, similarly to the results presented by Rienstra for the linearly sheared flow profile.<sup>7</sup> Note that both fundamental modes are omitted in Fig. 4 for the sake of brevity—they have been already depicted in Fig. 3.

## B. Quartic polynomial fit

Another possibility is to fit a quartic polynomial directly to the right-hand side of Eq. (12). In this section,  $\Omega = 18.3$  was chosen (corresponding to 1 kHz at 1 m waveguide height). In order to assess and compare the quality of this approximation, the first three downstream modes are plotted in Fig. 5 for various flow profile orders  $n$ . We can see that for the case of  $n = 8$ , the approximate solutions start to deviate from the numerical ones, hence presenting a marginal case of applicability.

## V. DISCUSSION

Complexity of Eq. (12) prevents us from detailed analytical prediction regarding the family of flows that can be approximated. It is highly unlikely that there is  $\eta(s)$  leading to the quartic polynomial exactly. Our attempts have revealed that by simple means of the Taylor expansion in  $s$ , the linear [ $\eta(s) \sim s$ ] and the exponential [ $\eta(s) \sim \exp(s)$ ] flow profiles can be successfully approximated for wide ranges of subsonic Mach numbers and frequencies, as well as  $\sin^2$ -profiles and some others. However, in full generality, we must resort to the necessity of evaluating Eq. (12) case-by-case.

In the limit of high frequencies (such as  $\Omega = 20$ , which is employed in Fig. 4), the WKB method might seem to be an alternative way of the approximate solution. However, the procedure given by Rienstra for the Pridmore-Brown equation in Ref. 7 does not lead to analytically solvable expressions for the family of flows defined by Eq. (26). Note, for instance, that our solution for quadratic profiles gives good results even for  $\Omega = 2$  (see Fig. 3).

In the examples given above, the mean flow is zero at the duct wall that simplifies the matter regarding the boundary conditions. However, the use of Ingard-Myers boundary conditions<sup>30</sup> for a compliant wall with grazing flow is possible within the introduced framework. We have only chosen a less complex example for clarity and brevity.

## VI. CONCLUSIONS

It has been shown how the new class of approximate analytical solutions for the Pridmore-Brown equation are constructed utilizing the triconfluent Heun functions. The analysis is restricted to the case of two-dimensional (2D) homentropic mean flow without critical layers. The key step is reformulating the Pridmore-Brown equation as a Schrödinger-like problem and then approximating its potential by a quartic polynomial. The specific examples were given for a mean parabolic flow profile with the accuracy up to  $\mathcal{O}(K^4 M^4 / \Omega^4)$ . According to the results, the agreement with the numerical solution is excellent, and the results show the important physical features, such as Doppler compression in upstream modes or rearranging the acoustic energy distribution due to the presence of non-uniform flow (see Fig. 4).

Moreover, we have shown how our approximate solution works for the velocity profiles of higher polynomial order (see Fig. 5). Here, one can observe that  $n = 8$  at  $M = 0.4$  and  $\Omega = 18.3$  presents a marginal case of the method applicability.

It is necessary to emphasize that the approximate solution expressed by Eq. (23) is closed-form and analytical. Therefore, it allows further useful manipulations, such as assembling the dispersion relation or explicit use of boundary conditions (see Sec. III).

The presented results are useful not only for the investigation of the sound transmission in the parabolic mean flow spanning the whole cross-section of a duct, but they can serve as a basis for enhancing the description of scenarios, in which only linear or linear-then-constant profiles were employed (such as the acoustics of shear layers and their matching to the uniform flow or investigation of the singularities—see,

e.g., Refs. 8 and 10). In the future, the variation of  $\rho_0$  and  $c_0$  in the mean flow profile due to nontrivial temperature distribution might be taken into account as well by a similar procedure as presented above. Finally, let us recall once again that we have used polynomial profiles only for definiteness; however, the key condition of applicability is not the polynomial nature of the flow profile itself but the possibility of approximating the expression in Eq. (9) by a quartic polynomial, which is a more general case.

## ACKNOWLEDGMENTS

This work was supported by the Grant Agency of the Czech Republic (GACR) (Grant No. 22-33896S) and by the Grant Agency of the Czech Technical University in Prague (Grant No. SGS21/115/OHK3/2T/13).

## AUTHOR DECLARATIONS

### Conflict of Interest

The authors have no conflicts to disclose.

### Author Contributions

**A. Krpensky:** Conceptualization (equal); Formal analysis (equal); Investigation (equal); Methodology (equal); Visualization (equal); Writing – original draft (equal); Writing – review & editing (equal). **V. Hruska:** Conceptualization (equal); Investigation (equal); Methodology (equal); Resources (equal); Writing – original draft (equal); Writing – review & editing (equal). **M. Bednarik:** Supervision (equal); Validation (equal); Writing – review & editing (equal).

## DATA AVAILABILITY

The data that support the findings of this study are available within the article.

## REFERENCES

- <sup>1</sup>D. C. Pridmore-Brown, “Sound propagation in a fluid flowing through an attenuating duct,” *J. Fluid Mech.* **4**, 393 (1958).
- <sup>2</sup>M. Goldstein and E. Rice, “Effect of shear on duct wall impedance,” *J. Sound Vib.* **30**, 79–84 (1973).
- <sup>3</sup>X. Jing, S. Peng, L. Wang, and X. Sun, “Investigation of straightforward impedance eduction in the presence of shear flow,” *J. Sound Vib.* **335**, 89–104 (2015).
- <sup>4</sup>E. J. Brambley, “Well-posed boundary condition for acoustic liners in straight ducts with flow,” *AIAA J.* **49**, 1272–1282 (2011).
- <sup>5</sup>S. W. Rienstra, “Slowly varying modes in a two-dimensional duct with shear flow and lined walls,” *J. Fluid Mech.* **906**, A23 (2020).
- <sup>6</sup>J. Kutin and I. Bajsic, “Fluid-dynamic loading of pipes conveying fluid with a laminar mean-flow velocity profile,” *J. Fluids Struct.* **50**, 171–183 (2014).
- <sup>7</sup>S. W. Rienstra, “Numerical and asymptotic solutions of the pridmore-brown equation,” *AIAA J.* **58**, 3001–3018 (2020).
- <sup>8</sup>L. M. B. C. Campos, J. M. G. S. Oliveira, and M. H. Kobayashi, “On sound propagation in a linear shear flow,” *J. Sound Vib.* **219**, 739–770 (1999).
- <sup>9</sup>L. M. B. C. Campos and J. M. G. S. Oliveira, “On the acoustic modes in a duct containing a parabolic shear flow,” *J. Sound Vib.* **330**, 1166–1195 (2011).
- <sup>10</sup>E. J. Brambley, M. Darau, and S. W. Rienstra, “The critical layer in linear-shear boundary layers over acoustic linings,” *J. Fluid Mech.* **710**, 545–568 (2012).
- <sup>11</sup>M. Oppeneer, S. W. Rienstra, and P. Sijtsma, “Efficient mode matching based on closed-form integrals of pridmore-brown modes,” *AIAA J.* **54**, 266–279 (2016).
- <sup>12</sup>G. G. Vilenski and S. W. Rienstra, “Numerical study of acoustic modes in ducted shear flow,” *J. Sound Vib.* **307**, 610–626 (2007).
- <sup>13</sup>D. Casalino, “Benchmarking of different wave models for sound propagation in non-uniform flows,” *Procedia Eng.* **6**, 163–172 (2010).
- <sup>14</sup>D. Casalino, “Finite element solutions of a wave equation for sound propagation in sheared flows,” *AIAA J.* **50**, 37–45 (2012).
- <sup>15</sup>D. Jones, “The scattering of sound by a simple shear layer,” *Philos. Trans. R. Soc., A* **284**, 287–328 (1977).
- <sup>16</sup>J. Scott, “Propagation of sound waves through a linear shear layer—A closed form solution,” in *16th Aerospace Sciences Meeting* (American Institute of Aeronautics and Astronautics, 1978).
- <sup>17</sup>S. P. Koutsoyannis, “Characterization of acoustic disturbances in linearly sheared flows,” *J. Sound Vib.* **68**, 187–202 (1980).
- <sup>18</sup>S. P. Koutsoyannis, K. Karamcheti, and D. C. Galant, “Acoustic resonances and sound scattering by a shear layer,” *AIAA J.* **18**, 1446–1454 (1980).
- <sup>19</sup>Y. Zhang and M. Oberlack, “Inviscid instability of compressible exponential boundary layer flows,” *AIP Adv.* **11**, 105308 (2021).
- <sup>20</sup>P. Ronveaux, A. Ronveaux, F. M. Arscott, S. S. Yu, D. Schmidt, G. Wolf, P. Maroni, and A. Duval, *Heun’s Differential Equations*, Oxford Science Publications (Oxford University Press, 1995).
- <sup>21</sup>B. D. Sleeman and V. B. Kuznetsov, “Heun functions,” in *Nist Handbook of Mathematical Functions* (Cambridge University Press, 2010).
- <sup>22</sup>D. Batic, D. Mills-Howell, and M. Nowakowski, “Potentials of the Heun class: The triconfluent case,” *J. Math. Phys.* **56**, 052106 (2015).
- <sup>23</sup>M. Bednarik and M. Cervenka, “The exact solution of the Schrödinger equation with a polynomially spatially varying mass,” *J. Math. Phys.* **58**, 072103 (2017).
- <sup>24</sup>M. Bednarik and M. Cervenka, “A wide class of analytical solutions of the Webster equation,” *J. Sound Vib.* **469**, 115169 (2019).
- <sup>25</sup>M. Bednarik, M. Cervenka, P. Lotton, and L. Simon, “Analytical solutions for elastic SH-waves propagating through an isotropic inhomogeneous layer,” *Compos. Struct.* **220**, 875–887 (2019).
- <sup>26</sup>A. Krpensky and M. Bednarik, “Surface love-type waves propagating through viscoelastic functionally graded media,” *J. Acoust. Soc. Am.* **150**, 3302–3313 (2021).
- <sup>27</sup>G. G. Vilenski and S. W. Rienstra, “On hydrodynamic and acoustic modes in a ducted shear flow with wall lining,” *J. Fluid Mech.* **583**, 45–70 (2007).
- <sup>28</sup>A. M. Ishkhanyan, “Series solutions of confluent Heun equations in terms of incomplete Gamma-functions,” *J. Appl. Anal. Comput.* **9**, 118–139 (2019).
- <sup>29</sup>J. Mathews, *Numerical Methods Using MATLAB* (Prentice-Hall, Upper Saddle River, NJ, 1999).
- <sup>30</sup>M. K. Myers, “On the acoustic boundary condition in the presence of flow,” *J. Sound Vib.* **71**, 429–434 (1980).

## 3.4 Paper IV

**Title:** *Elastic P-wave manipulation utilizing functionally graded parallel plate gradient refractive index structures*

In the fourth paper published in Wave Motion we propose a novelty type of gradient refractive index (GRIN) structure by which the elastic P-wave (primary/pressure) field can be controlled. The designation P-waves stands for the longitudinal bulk elastic waves, meaning that the particles oscillate in the same direction as the wave propagates (they can be considered as an analogy to the classical acoustic waves in gaseous media). The main motivation of this research was the fact that not many papers deal with the manipulation of P-waves and much more typically focus on the S-waves (secondary) which are on the contrary characterised by the oscillation of the particles in the direction perpendicular to the direction of propagation.

The proposed GRIN structure consists of several inhomogeneous plates layered vertically on top of each other and separated by thin gaps. Each one of those plates is considered as a FGM (see Sec. 2.5) whose density and Young modulus vary according to the respective material function (see Eq. (2.80)). The shape of the material function is chosen as one period of the sine function squared (shifted vertically), where the height of the profile is controlled by the parameter  $q$ . Based on the model equation of the Webster-type (see Sec. 2.2) describing the propagation of longitudinal elastic waves in such inhomogeneous plates and the corresponding approximate analytical high frequency limit WKB solution (see Sec. 2.3) an approximate analytical expression of the effective phase velocity for each plate is given as a function of the parameter  $q$ . The idea is now as follows: First, we assume two homogeneous elastic half spaces on each side of the proposed GRIN structure. Now there is an incoming plane elastic P-wave incident on the GRIN structure from the left which then separates into individual partial longitudinal waves propagating inside the individual FGM plates. By a suitable choice of the parameter  $q$  for each plate we can realize a different time delay of each of the corresponding partial waves, resulting in a various possibilities of controlling the outgoing P-wave field on the right side of the GRIN structure that is then formed by the superposition of the delayed partial longitudinal waves.

Next, we have demonstrated the two specific cases of the mentioned elastic P-wave field control - focusing and deflecting. For each of those cases we derived the respective distribution of the values of the parameter  $q$  for each plate based on the simple geometric approach, resulting in a corresponding material function for each plate. Both of those distributions were then applied to the numerical simulation in COMSOL Multiphysics for specifically chosen

focusing point distance in the first case and wave deflection angle in the second one, whereas the results were compared with the theoretical calculations with excellent results. Finally, a numerical study was conducted in the focusing case to demonstrate the validity of the high frequency approximation of the WKB solution for the two previously mentioned computations.



# Elastic P-wave manipulation utilizing functionally graded parallel plate gradient refractive index structures



A. Krpensky\*, V. Hruska, M. Bednarik

Czech Technical University in Prague, Faculty of Electrical Engineering, Technická 2, 166 27 Prague 6, Czech Republic

## ARTICLE INFO

### Article history:

Received 31 October 2022  
 Received in revised form 23 June 2023  
 Accepted 4 August 2023  
 Available online 11 August 2023

### Keywords:

Functionally graded materials  
 Gradient refractive index structures  
 Elastic P-waves  
 Wave focusing  
 Wave deflecting  
 WKB approximation

## ABSTRACT

This paper presents a new Gradient Refractive Index (GRIN) structure, which utilizes a series of thin plates made of functionally graded material separated by narrow gaps, to control elastic P-wave fields. The proposed technique is demonstrated through two basic examples of wave manipulation: focusing and deflecting, but has the potential for a wide range of applications. To verify the theoretical calculations, COMSOL Multiphysics simulation software was utilized to solve the full Navier–Lamé equations. Overall, the results of this study demonstrate the effectiveness of the proposed GRIN structure in manipulating elastic P-wave fields.

© 2023 Elsevier B.V. All rights reserved.

## 1. Introduction

The control of elastic wave fields is a topic of significant scientific and practical interest. Manipulating elastic waves, including focusing, scattering, steering, reflection, and cloaking, can be achieved using various methods. One common approach involves using elastic metamaterials and phononic crystals, as demonstrated in numerous publications (e.g., [1–8]). Functionally graded materials (FGMs) are a particularly interesting means of controlling elastic waves [9]. FGMs are microscopically inhomogeneous composites made by mixing metals and ceramics, where the material properties change continuously and smoothly according to a prescribed spatial dependence. There are several advanced methods for fabricating desired FGMs (see e.g., [10]). Some spatial dependencies of the material parameters allow for exact analytical solutions to the corresponding model equations [11–13]. FGMs are especially used to control the transmission properties of phononic crystals [13–18].

Another approach to manipulating elastic waves involves using an array of plates whose dimensions are adjusted to control the waves. This technique has been demonstrated in the literature, such as in the paper by [19,20]. The mentioned passive methods enabling manipulation of elastic waves can be complemented by active methods using phase-array transducers (see, for example, [21–23]).

In this work, we present a novel approach to controlling elastic waves using an array of thin plates with an invariable geometric arrangement. Specifically, we assume that each plate is made of a different FGM composed of two distinct materials, with these materials being the same for each plate. However, the FGMs in individual plates differ in the prescribed spatial dependence of the considered material parameters, resulting in different spatial dependencies of the phase velocity of the longitudinal elastic waves. This approach of ours is inspired by the use of flat gradient-index lenses for the manipulation of electromagnetic waves in optics (see e.g., [24–26]). Our approach enables a wider frequency range

\* Corresponding author.

E-mail address: [antonin.krpensky@fel.cvut.cz](mailto:antonin.krpensky@fel.cvut.cz) (A. Krpensky).

of wave control compared to the method based on adjusting the plate dimensions and distances from one another, as demonstrated in [19,20].

In this paper, we present a detailed analysis of the properties of Functionally Graded Materials (FGMs) and their application in the design of Gradient Refractive Index (GRIN) structures for controlling elastic P-waves (primary/pressure waves). The paper is organized as follows:

Firstly, in Section 2, we briefly describe the method of representing the materials properties of FGMs. Next, in Section 3, we define an inhomogeneous plate that serves as a building block of the GRIN structure and derive an analytical expression for the effective velocity of longitudinal elastic waves propagating inside of this plate. We then proceed to define the GRIN structure itself in Section 4, providing two examples of how the P-wave field can be controlled, namely focusing and deflecting. In Section 5, we present our numerical results, which were obtained using the COMSOL Multiphysics software. Section 6 focuses on an in-depth exploration of the benefits of our GRIN structure, including the feasibility of its implementation and its potential for generating S-waves beyond the GRIN structure. Finally, we summarize our findings and conclusions in Section 7. In Appendix A, we outline the derivation of the model equation for longitudinal elastic waves in inhomogeneous thin plates. We introduce the WKB method for finding an approximate analytic solution to the model equation in Appendix B.

## 2. Properties of one-dimensional FGM constituent materials

Consider a functionally graded material (FGM) plate composed of two distinct materials, denoted as  $M_I$  and  $M_{II}$ . Any given material property  $P$  can be mathematically represented as (see e.g., [13,27–30])

$$P = P_I V_I + P_{II} V_{II}, \tag{1}$$

where  $P_I, P_{II}$  denote the properties of the corresponding materials and  $V_I, V_{II}$  represent the corresponding volume fractions while the following condition holds

$$V_I + V_{II} = 1. \tag{2}$$

Assuming now the material composition varying continuously along the  $x$  direction only and denoting  $V_{II} \equiv V(x)$  we can rewrite Eq. (1) as

$$P(x) = P_I[1 - V(x)] + P_{II}V(x). \tag{3}$$

Note that since the dimensionless function  $V(x)$  represents the volume fraction, the following condition must hold inside of the respective FG material:

$$0 \leq V(x) \leq 1. \tag{4}$$

By further rearranging we arrive at

$$P(x) = P_I[1 + \mathcal{P}V(x)], \tag{5}$$

where  $\mathcal{P} = (P_{II}/P_I) - 1$ .

With respect to Eq. (5) the effective material elastic constant  $E$  and the mass density  $\rho$  are expressed as

$$E(x) = E_{II}V(x) + E_I[1 - V(x)] = E_I[1 + aV(x)], \tag{6}$$

$$\rho(x) = \rho_{II}V(x) + \rho_I[1 - V(x)] = \rho_I[1 + bV(x)]. \tag{7}$$

Here

$$a = \frac{E_{II}}{E_I} - 1, \quad b = \frac{\rho_{II}}{\rho_I} - 1. \tag{8}$$

## 3. Effective longitudinal wave phase velocity in a FGM plate

Our research focuses on the possibility of manipulating elastic P-waves. The key element of the wave manipulation structure is a FGM plate of length  $\ell$  and thickness  $h$ , see Fig. 1.

The model equation describing the propagation of longitudinal elastic waves in such a plate can be written as (for the derivation, please refer to Appendix A)

$$\frac{\partial^2 u(x, t)}{\partial x^2} + \frac{1}{E(x)} \frac{dE(x)}{dx} \frac{\partial u(x, t)}{\partial x} = \frac{1}{c_L^2(x)} \frac{\partial^2 u(x, t)}{\partial t^2}, \tag{9}$$

where the longitudinal wave speed is

$$c_L(x) = \sqrt{\frac{E(x)(1 - \nu)}{\rho(x)(1 + \nu)(1 - 2\nu)}}. \tag{10}$$

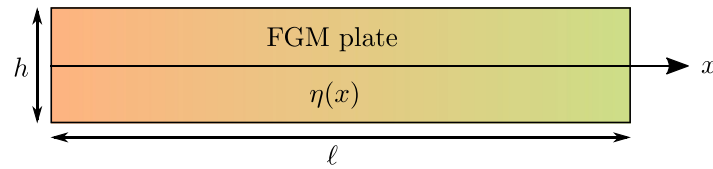


**Fig. 1.** One dimensional functionally graded plate. (For interpretation of the references to color in this figure legend, the reader is referred to the web version of this article.)

Please note that when referring to wave propagation in FGM plates, we use the term longitudinal waves. In this paper, we make the assumption of a high-frequency approximation. Based on the WKB solution (see [Appendix B](#)), it can be shown that the longitudinal wave speed (Eq. (10)) corresponds to the spatially dependent phase velocity of the longitudinal waves inside the plate. By combining Eqs. (6), (7), and (10), we can express the respective phase velocity as follows:

$$c_{ph}(x) = \sqrt{\frac{E_1[1 + aV(x)](1 - \nu)}{\rho_1[1 + bV(x)](1 + \nu)(1 - 2\nu)}} = c_{L0}\eta(x), \tag{11}$$

where

$$c_{L0} = \sqrt{\frac{E_1(1 - \nu)}{\rho_1(1 + \nu)(1 - 2\nu)}}, \quad \eta(x) = \sqrt{\frac{1 + aV(x)}{1 + bV(x)}}. \tag{12}$$

We denote the function  $\eta(x)$  as the material function. Using this function, which we take as a baseline, it is possible to express the corresponding volume fraction function as

$$V(a, b; x) = \frac{\eta^2(x) - 1}{a - b\eta^2(x)}. \tag{13}$$

By combining Eq. (12) with the condition on the volume fraction function Eq. (4) we can further express the necessary conditions on the material function  $\eta(x)$  as follows:

1. for  $a > b$ :

$$\eta(x) \in \left\langle 1, \sqrt{\frac{1+a}{1+b}} \right\rangle, \tag{14}$$

2. for  $b < a$ :

$$\eta(x) \in \left\langle \sqrt{\frac{1+a}{1+b}}, 1 \right\rangle. \tag{15}$$

For the sake of generality let us introduce new dimensionless quantities

$$X = \frac{x}{l}, \quad H = \frac{h}{\ell}. \tag{16}$$

According to Eq. (11) the phase velocity of the longitudinal waves inside of the plate can then be written as

$$c_{ph}(X) = c_{L0} \eta(X), \tag{17}$$

or in its dimensionless form

$$C_{ph}(X) = \frac{c_{ph}(X)}{c_{L0}} = \eta(X). \tag{18}$$

Our objective is to identify a material function profile that satisfies the following criteria:

1. The effective phase velocity, which we will define later in the text, depends solely on a single parameter  $q$ .
2. The material function profile equals one at the both ends of the plate ( $\eta(0) = \eta(1) = 1$ ) while also having zero derivatives at these points to achieve maximum impedance match.

While there are various analytic functions that satisfy the two aforementioned conditions, we have chosen a simple one for the sake of clarity and ease of interpretation. We made this choice because our objective is to demonstrate the validity of the presented concept rather than to explore the entire class of possible functions. The selected function  $\eta(X)$  is given by the following expression:

$$\eta(X) = 1 + q \sin^2(\pi X), \tag{19}$$



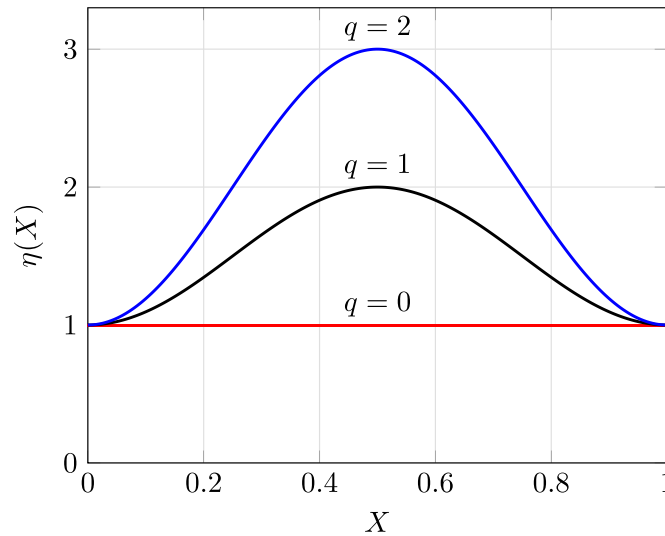


**Fig. 2.** Profiles of the material function  $\eta(s)$  for various values of the dimensionless parameter  $q$ . (For interpretation of the references to color in this figure legend, the reader is referred to the web version of this article.)

where  $q$  is the control parameter mentioned above. The advantage of this particular function is that it provides straightforward analytical expressions for the effective longitudinal velocity, as shown below. Example profiles for various values of the parameter  $q$  are plotted in Fig. 2.

Based on the conditions on the material function (14) and (15) and by noting that the local extreme of the material function happens at  $X = 1/2$  and is equal to  $\eta(1/2) = 1 + q$  we can express the necessary conditions on the parameter  $q$  as

1. for  $a > b$ :

$$q \in \left\langle 0, \sqrt{\frac{1+a}{1+b}} - 1 \right\rangle, \tag{20}$$

2. for  $b < a$ :

$$q \in \left\langle \sqrt{\frac{1+a}{1+b}} - 1, 0 \right\rangle. \tag{21}$$

The effective phase velocity, denoted by  $C_{\text{eff}}$ , represents the velocity necessary for a homogeneous plate with the same length as the FGM plate to maintain the same travel time for an edge-to-edge wave. Therefore, we can express it in its dimensionless form as

$$C_{\text{eff}} = \frac{1}{\int_0^1 \frac{dX}{c_{\text{ph}}(X)}}. \tag{22}$$

By combining Eqs. (18), (19) and (22) we obtain the following expression

$$C_{\text{eff}}(q) = \sqrt{1+q}. \tag{23}$$

The inverse formula of Eq. (23) then reads as

$$q = C_{\text{eff}}^2 - 1. \tag{24}$$

It is worth noting that the effective phase velocity is solely dependent on the parameter  $q$ .

Based on Eqs. (19), (20) and (21), we can observe that in the case of  $a > b$  the effective phase velocity in the FGM plate  $C_{\text{eff}} > 1$  and vice versa.

#### 4. Focusing and deflecting of elastic P-waves by a parallel plate FGM GRIN structure

In this section, we introduce a gradient refractive index (GRIN) structure that utilizes functionally graded materials to focus and deflect P-waves. The structure is composed of FGM plates, as described in Section 2, that are layered in parallel along the  $Y$  direction ( $Y = y/\ell$ ) and sandwiched between two homogeneous half-spaces. Both half-spaces have

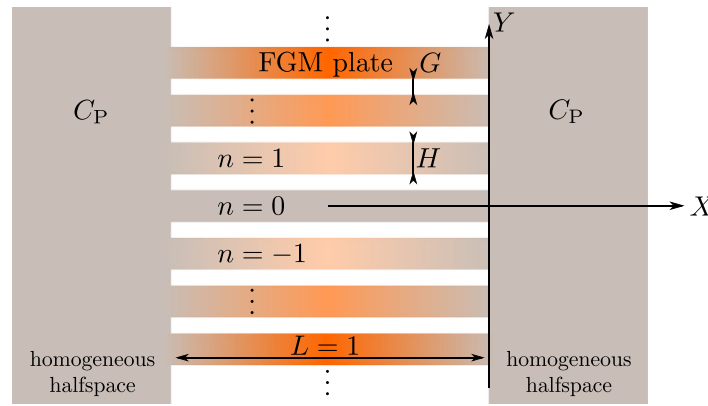


**Fig. 3.** Parallel plate FGM GRIN structure. (For interpretation of the references to color in this figure legend, the reader is referred to the web version of this article.)

the P-wave velocity  $c_P$  equal to a constant value (see e.g., [20]):

$$c_P = \sqrt{\frac{E_1(1 - \nu)}{\rho_1(1 + \nu)(1 - 2\nu)}} \equiv c_{L0}, \tag{25}$$

or in its dimensionless form  $C_P = c_P/c_{L0} = 1$ , see Fig. 3.

Here,  $L = 1$  represents the dimensionless length of the plate and  $H$  represents its thickness, both of which are explained in Section 2.  $G$  denotes the dimensionless width of the gap between two adjacent plates, while each individual plate is assigned an index  $n$ , with  $n = 0$  representing the middle plate that coincides with the  $X$  axis. The dimensionless effective longitudinal velocity in the  $n$ th plate is denoted as  $C_{\text{eff},n}$  and is determined by the choice of the parameter  $q$ , as given by Eq. (23).

In this paper, we consider a plane time-harmonic P-wave propagating in the  $X$  direction. As the wave encounters the structure, it splits into multiple partial longitudinal waves that travel through each plate. The difference in the effective longitudinal velocities of the corresponding plates causes the partial waves to reach the outlet at different times. This property can be leveraged to design the structure to e.g., focus waves onto a specific point or deflect the resulting beam (as discussed in the subsequent sections). It is worth noting that the material function at the edges of each plate, as discussed in Section 2, should have a unit value and zero derivatives to maximize impedance matching with the homogeneous half-spaces ( $C_L(X = 0) = C_L(X = 1) = C_P$ ) and thereby increase the transmission through the entire structure.

In the following sections, we will delve into the two specific cases of wave manipulation. It is noteworthy that the techniques employed in these cases are essentially the same as those used in GRIN optics (as seen in, for example, [31,32]), particularly when utilizing GRIN (flat) lens that enable us to manipulate the phase and direction of light.

#### 4.1. P-wave focusing

In this section, we illustrate the potential use of the previously described structure as a lens with a focal point located at a specific point on the  $X$  axis, at a distance  $X = F$  from the origin (refer to Fig. 4). To achieve this, we must ensure that the time required for each partial wave to travel to the focal point is constant, denoted by the dimensionless constant  $\tau$ . This can be achieved by the following distribution of the effective longitudinal velocities (see Fig. 4)

$$C_{\text{eff},n} = \frac{1}{\tau - \sqrt{Y_n^2 + F^2}}, \tag{26}$$

where

$$Y_n = n(H + G) \tag{27}$$

stands for the center position of the  $n$ th plate on the  $Y$  axis. The constant  $\tau$  must be chosen carefully in order to meet the constraints (20) and (21). In addition, it should be mentioned that the parameter  $\tau$  determines the properties of how FGM changes with spatial coordinate in individual plates. Based on Eq. (24) one can then compute the corresponding values of  $q$  for each plate.

#### 4.2. P-wave deflection

Another possibility of what we can realize using this type of structure is deflecting the wave-front of the incident P-wave by an angle  $\alpha$ , see Fig. 5. To reach this goal we use the following distribution of the effective longitudinal velocities

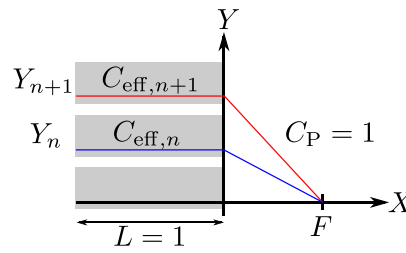


**Fig. 4.** Focusing parallel plate FGM GRIN structure. (For interpretation of the references to color in this figure legend, the reader is referred to the web version of this article.)

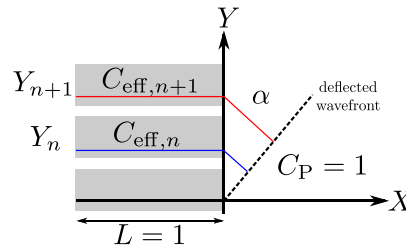


**Fig. 5.** Deflecting parallel plate FGM GRIN structure. (For interpretation of the references to color in this figure legend, the reader is referred to the web version of this article.)

corresponding to the individual plates

$$C_{\text{eff},n} = \frac{1}{\tau - Y_n \sin(\alpha)}, \tag{28}$$

where (by analogy with the preceding case)  $\tau$  denotes the dimensionless time needed for the wave to travel from the beginning of the FGM plate to the deflected waveform. Again, the condition expressed by Eqs. (20) and (21) must be fulfilled.

Numerical simulations exemplifying and verifying the two cases of P-waves manipulations are given in Section 5.

To conclude this section, there are two important points to note. Firstly, the wave manipulation scenarios that can be achieved using the structure we have proposed are not limited to the cases we have studied thus far. For example, it is possible to combine both approaches and focus the waves into a point off the symmetry axis. Secondly, our approach is applicable across a wide range of frequencies, provided that the high-frequency limit is met (as discussed in Appendix B). This is because the proposed wave manipulation is frequency independent. In the following section, we provide examples to demonstrate that this claim is justified.

### 5. Numerical results

For the sake of the following examples let us introduce a dimensionless frequency  $\mathcal{F}$  defined as

$$\mathcal{F} = \frac{\ell}{c_{l0}} f, \tag{29}$$

where  $f$  represents the frequency. The following examples use  $M_I$  - Aluminum (Al) and  $M_{II}$  - Alumina ( $\text{Al}_2\text{O}_3$ ) as the primary materials with the following material parameters

$$E_I = 70 \text{ GPa}, \quad \rho_I = 2700 \text{ kg m}^{-3}, \quad E_{II} = 393 \text{ GPa}, \quad \rho_{II} = 3960 \text{ kg m}^{-3}. \tag{30}$$

The corresponding values of  $a$  and  $b$  are

$$a = 4.61, \quad b = 0.47. \tag{31}$$

Based on Eq. (20) the parameter  $q$  can then take on the values

$$q \in (0, 0.95). \tag{32}$$

The length of the FGM plates is  $\ell = 0.21$  m. The corresponding dimensionless geometric parameters of the GRIN structure are  $H = 4.8 \cdot 10^{-2}$  (1 cm) and  $G = 2.4 \cdot 10^{-3}$  (0.5 mm). In order to verify the theory presented above, in this section we provide some of the results computed in COMSOL Multiphysics 5.5, employing the Elastic Waves (solid mechanics) interface in the frequency domain and two dimensions. Note, that with this setup the full Navier-Lamé equation is simulated (i.e. a possible influence by S-waves, the wave conversion etc. are present in the following results).

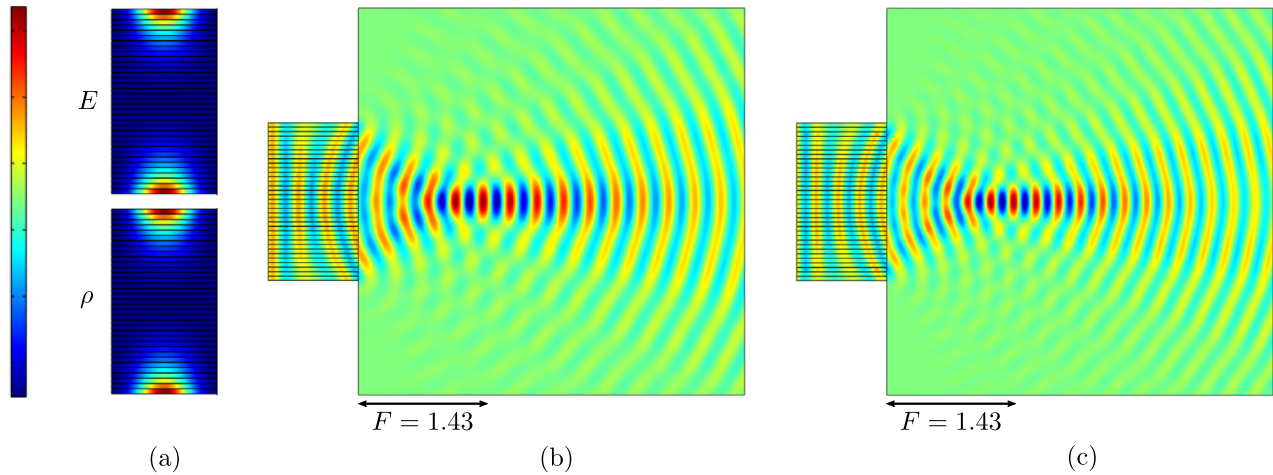


**Fig. 6.** Numerical simulation of the focusing parallel plate GRIN structure for P-waves. Distribution of the Young's modulus and the density (a), dimensionless volumetric strain at  $\mathcal{F} = 3.47$  (b) and  $\mathcal{F} = 4.18$  (c). Colorbar ranges (blue to red): (69, 258) GPa ( $E$ ); (2700, 3483)  $\text{kg m}^{-3}$  ( $\rho$ ); (-1, 1) (normalized volumetric strain). (For interpretation of the references to color in this figure legend, the reader is referred to the web version of this article.)

The uniform displacement was prescribed at the beginning of the FGM plates in the direction of their axes, thus emulating the impinging plane P-wave. On the lateral sides of the FGM plates we included the boundary conditions used in the derivation of the model Eq. (37), see Appendix A. The sides of the domain emulating the free half-space are supplied by the Comsol's Low reflecting boundary conditions. It was checked that the solution is mesh-independent (starting from 12 quadratic serendipity elements per shortest wavelength and an appropriate refinement around the corners). To account for the symmetry, all numerical calculations were performed in 2D.

Since we are interested in P-waves propagation, the natural variable to be evaluated is not the general displacement vector field  $\mathbf{u}$  but rather its divergence  $\nabla \cdot \mathbf{u}$ , i.e. the volumetric strain. As the wave propagation problem is linear, the plots are in arbitrary units without the loss of generality.

For the sake of generality, we give the results in dimensionless form. Reference dimensional values for aluminum are given for definiteness. First, we demonstrate results of the wave focusing lens based on the effective phase velocity  $C_{\text{eff}}$  distribution provided by Eq. (26), where the focal length  $F = 1.43$  (0.3 m). The structure is shown in Fig. 6(a), where the colors represent the Young's modulus and the density values. The volumetric strain of the wave traveling through this structure is presented in Figs. 6(b) (for  $\mathcal{F} = 3.47$ , 100 kHz in aluminum) and 6(c) (for  $\mathcal{F} = 4.18$ , 120 kHz in aluminum). In the theoretical high-frequency limit, the lens should behave independently on the choice of  $\mathcal{F}$ , which corresponds with the presented results, where the differences of the focal lengths are negligible.

Next, we present the wave deflecting structure subject to effective phase velocity distribution defined by Eq. (28) with the deflection angle of  $\pi/6$ . Similarly to the previous case, Fig. 7(a) represents the Young's modulus and the density distribution in the deflecting structure and Figs. 7(b), 7(c) display the volumetric strain corresponding to  $\mathcal{F} = 3.47$  (100 kHz in aluminum),  $\mathcal{F} = 4.18$  (120 kHz in aluminum), respectively. Once again, we observe very similar results as far as the deflect angle.

## 6. Discussion

To begin, we want to highlight that it is achievable to design a structure capable of controlling P-waves without relying on FGM techniques. This can be accomplished by employing uniform plates with constitutive material properties that match the desired effective velocity of longitudinal waves  $C_{\text{eff}}$ . Our initial numerical experiments indicate that this approach is effective. The overall energy losses, attributed to the discrepancy in wave velocity between the uniform plates and the free half-space, were roughly 15%–20% (measured at the focal point). However, while this homogeneous plate solution may appear straightforward compared to FGM, it is impractical. To achieve wave deflection or focusing, a wide range of materials with precisely tailored properties would be required. In contrast, FGM materials can be effectively composed of just two distinct materials.

The same scenario as depicted in Fig. 6 was calculated for a wide range of frequencies. To provide a clear demonstration of the dispersion effects, which are consistent with the outcomes obtained via the WKB method, we conducted the following numerical simulation. The volumetric strain on the centerline passing through the focal point was stacked for every frequency to form a normalized 2D plot (see Fig. 8). It is apparent that for lower frequencies the focal point is slightly shifted from the intended position (marked by the dashed line in Fig. 8). However, it quickly converges with increasing dimensionless frequency. Hence, the approximate expression for the longitudinal wave phase velocity (see Eq. (48)) for  $\mathcal{F} > 3$  is admissible.

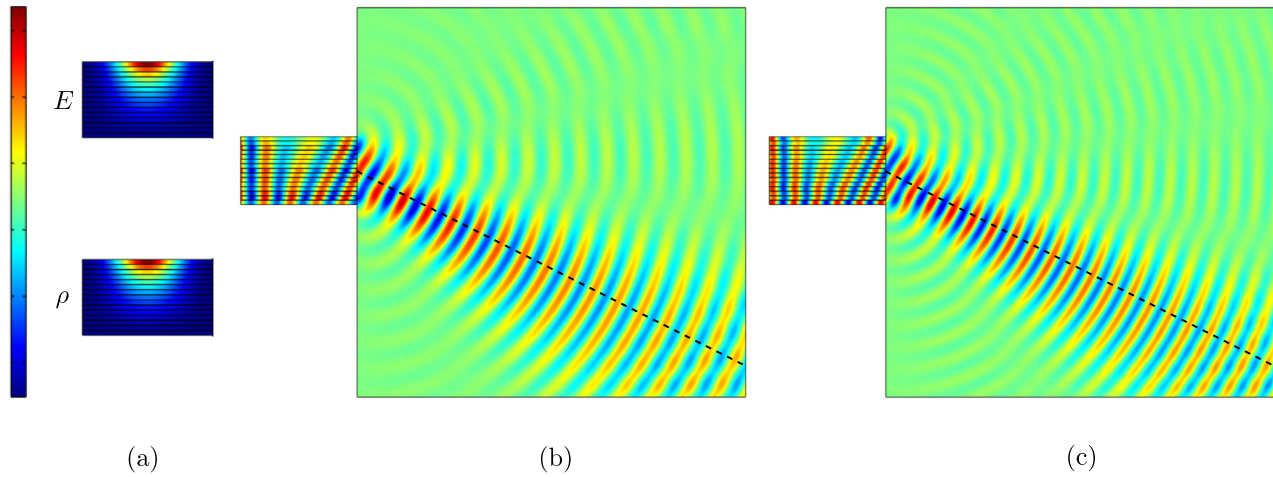


**Fig. 7.** Numerical simulation of the deflecting parallel plate GRIN structure for P-waves. Distribution of the Young's modulus and the density (a), dimensionless volumetric strain at  $\mathcal{F} = 3.47$  (b) and  $\mathcal{F} = 4.18$  (c). Colorbar ranges (blue to red):  $\langle 69, 353 \rangle$  GPa ( $E$ );  $\langle 2700, 3875 \rangle$   $\text{kg m}^{-3}$  ( $\rho$ );  $\langle -1, 1 \rangle$  (normalized volumetric strain). (For interpretation of the references to color in this figure legend, the reader is referred to the web version of this article.)

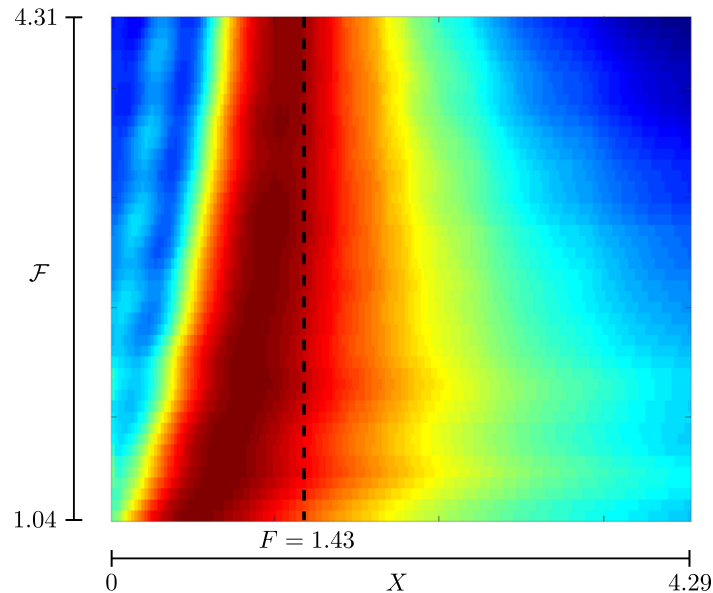


**Fig. 8.** Forming of the focal point at  $F = 1.43$  for various dimensionless frequencies  $\mathcal{F}$ . The depicted variable is the volumetric strain magnitude at the centerline  $Y = 0$  scaled by  $1/\mathcal{F}$  and normalized. The dashed line shows the intended focal point. (For interpretation of the references to color in this figure legend, the reader is referred to the web version of this article.)

Since our research was focused on manipulation of the elastic P-waves, only a  $\nabla \cdot \mathbf{u}$  was plotted in the previous figures. In reality, at the interface between the plates and the homogeneous half-space S-waves are also generated mainly due to impedance mismatch. In Fig. 9, one can see the comparison between the P-waves ( $\nabla \cdot \mathbf{u}$ ) and S-waves ( $\nabla \times \mathbf{u}$ ) for the focusing case (a) and the deflecting case (b) at  $\mathcal{F} = 4.18$ .

## 7. Conclusions

Our research demonstrates that functionally graded materials (FGMs), represented by an array of thin inhomogeneous plates, can be used to construct P-wave manipulating GRIN structures. By designing suitable profiles of longitudinal velocities within each plate, our proposed method is effective across a broad frequency range. We have presented several examples of wave manipulation, including focusing and deflection, and supported our theoretical reasoning through numerical simulations based on the full Navier–Lamé equation. We have also highlighted that the FGM approach is more practical than using homogeneous plates due to the extensive range of materials required by the latter. Furthermore, we have justified the neglect of dispersion effects based on the WKB method.

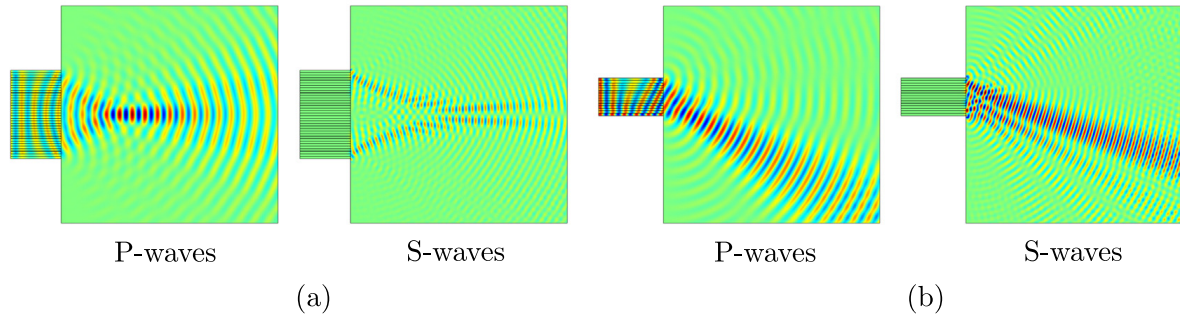


**Fig. 9.** Comparison of the P-waves and S-waves in the case of focusing (a) and deflecting (b) GRIN structure at  $\mathcal{F} = 4.18$ . (For interpretation of the references to color in this figure legend, the reader is referred to the web version of this article.)

In our paper, we initially made the assumption that the materials on both sides of the GRIN structure were the same ( $M_1$ ). Consequently, we proposed a straightforward material function profile that optimized the impedance match on both interfaces. However, it is crucial to highlight that our proposed method can also be applied when the two materials on either side of the structure differ. The only modification required in such cases is the adoption of a different material function profile, which (again) can be controlled by one or more suitable parameters and ensures impedance matching on both sides. The procedure to follow then remains identical.

Although our main intention was to present a method for manipulating P-waves using a flat GRIN structure in order to extend the existing methods used for this purpose, we believe that there will be interested parties among the scientific community who will build upon our work and utilize it for specific application purposes.

#### CRediT authorship contribution statement

**A. Krpensky:** Conceptualization, Methodology, Formal analysis, Investigation, Writing – original draft, Writing – review & editing, Resources. **V. Hruska:** Software, Validation, Visualization, Writing – original draft, Writing – review & editing. **M. Bednarik:** Conceptualization, Methodology, Formal analysis, Investigation, Writing – original draft, Writing – review & editing, Resources, Supervision.

#### Declaration of competing interest

The authors declare that they have no known competing financial interests or personal relationships that could have appeared to influence the work reported in this paper.

#### Data availability

Data will be made available on request.

#### Acknowledgments

This work was supported by the Grant Agency of the Czech Republic (GACR) grant No. 22-33896S and by the Grant Agency of the Czech Technical University in Prague No. SGS21/115/OHK3/2T/13.

#### Appendix A. Derivation of the model equation

In Fig. 10, we observe an isotropic thin plate positioned on the  $x$ - $y$  plane, with its thickness extending in the  $z$ -direction. To derive a model equation for the propagation of a longitudinal wave in the  $x$ -axis direction in a functionally graded material, we start with the generalized Hooke's law for isotropic materials that defines the strain tensor component  $\varepsilon_{ij}$  in terms of the stress tensor component  $\sigma_{ij}$  (see e.g., [33]):

$$\varepsilon_{ij} = \frac{1}{E(x)} [(1 + \nu)\sigma_{ij} - \nu\vartheta\delta_{ij}], \quad \varepsilon_{ij} = \frac{1}{2} \left( \frac{\partial u_i}{\partial x_j} + \frac{\partial u_j}{\partial x_i} \right), \quad \sigma_{ij} = \sigma_{ji}, \quad i, j, k = x, y, z, \quad (33)$$

where  $E(x)$  is called the modulus of elasticity or Young's modulus, which varies spatially,  $\nu$  is referred to as Poisson's ratio,  $\delta_{ij}$  is the Kronecker delta, and  $\vartheta = \sigma_{xx} + \sigma_{yy} + \sigma_{zz}$  is the trace of the stress tensor. Note that due to the relatively small magnitude of the Poisson ratio  $\nu$ , we neglect its spatial dependence and consider it to be constant.

In this study, we assume the plates to be thin. Further, we consider the propagation of longitudinal waves through a plate that is constrained from motion in the width direction. Under this condition, the plate material is allowed to displace in the wave propagation direction ( $x$ -direction) and the thickness direction ( $z$ -direction), but is arrested from motion in

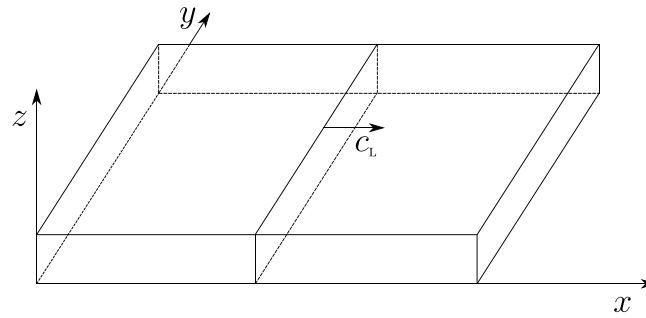


Fig. 10. Geometric specification of an isotropic thin plate.

the width direction ( $y$ -direction). As a result of the constraint on the plate's motion, every point on the plate is prevented from moving in the  $y$ -direction. Therefore, the displacement in the  $y$ -direction is assumed to be zero throughout the plate. This condition can be expressed mathematically as follows (see e.g., [34,35]):

$$\varepsilon_{xy} = \varepsilon_{yy} = \varepsilon_{zy} = 0 . \tag{34}$$

It should be noted that the constraint mentioned here is intrinsic to the scenario of an "infinite" plate, see e.g., [35]. In this case, the strain in the width direction becomes zero due to the plate's infinite width.

In general, the deformation field within a solid body can be represented by a vector  $\mathbf{u} = (u_x, u_y, u_z) = (u, v, w)$ , where  $u, v$ , and  $w$  represent the displacements in the  $x, y$ , and  $z$  directions, respectively. This vector describes the deformation of the considered thin plate in a reduced form:  $\mathbf{u} = (u(x, z, t), 0, w(x, z, t))$ .

If we use the condition for normal constraint, i.e.,  $\mathbf{u} \cdot \mathbf{n} = 0$ , where  $\mathbf{n}$  is the unit normal vector to the walls of the plate lying in the  $x$ - $y$  plane (the upper and lower surfaces), then we get that  $w = 0$ , which implies that  $\varepsilon_{zz} = 0$ , see e.g., [36–38]. Since the region is thin in the  $z$  direction it can be argued that the other nonzero stress components have little variation with  $z$  (see e.g., [39]), thus  $\varepsilon_{zx} = \varepsilon_{zy} = 0$  (now  $u(x, t)$ ).

By applying the above-mentioned conditions and using the relationship between strain and stress tensor components (33), we arrive at the following equations:

$$\sigma_{xx} = \frac{E(x)(1 - \nu)}{(1 + \nu)(1 - 2\nu)} \varepsilon_{xx} , \sigma_{yy} = \frac{E(x)\nu}{(1 + \nu)(1 - 2\nu)} \varepsilon_{xx} , \sigma_{zz} = \frac{E(x)\nu}{(1 + \nu)(1 - 2\nu)} \varepsilon_{xx} , \sigma_{yx} = \sigma_{zx} = \sigma_{zy} = 0 . \tag{35}$$

If we assume that body forces are negligible and take into account the relations given in Eq. (35), we can express the equation of motion for the  $u_x = u$  component of the displacement vector  $\mathbf{u}$  as follows:

$$\rho(x) \frac{\partial^2 u(x, t)}{\partial t^2} = \frac{\partial \sigma_{xx}}{\partial x} . \tag{36}$$

By substituting  $\sigma_{xx}$  from Eq. (35) into the equation of motion and considering that  $\varepsilon_{xx} = \partial u / \partial x$ , we obtain the following equation for longitudinal waves in an inhomogeneous thin plate after some manipulation:

$$\frac{\partial^2 u(x, t)}{\partial x^2} + \frac{1}{E(x)} \frac{dE(x)}{dx} \frac{\partial u(x, t)}{\partial x} = \frac{1}{c_L^2(x)} \frac{\partial^2 u(x, t)}{\partial t^2} , \tag{37}$$

where the longitudinal wave speed is (see, e.g. [40])

$$c_L(x) = \sqrt{\frac{E(x)(1 - \nu)}{\rho(x)(1 + \nu)(1 - 2\nu)}} . \tag{38}$$

### Appendix B. WKB solution of the model equation

In this section we derive an approximate analytical solution of the model Eq. (37) for the high frequency limit employing the WKB method, see e.g., [41].

Let us assume a time harmonic solution to the model Eq. (37) of the following form

$$u(x, t) = A \exp \left( i \int_0^x k(\tilde{x}) d\tilde{x} - i\omega t \right) , \tag{39}$$

where  $A$  is an integration constant,  $i = \sqrt{-1}$  is the imaginary unit,  $\omega$  the angular frequency and  $k(x)$  represents a spatially dependent wavenumber defined as

$$k(x) = \frac{\partial \varphi(x, t)}{\partial x} , \tag{40}$$

where  $\varphi(x, t) = \arg[u(x, t)]$ . By inserting the solution (39) into Eq. (37) we arrive at

$$ik'(x) - k^2(x) + i \frac{E'(x)}{E(x)} k(x) + \frac{\omega^2}{c_L^2(x)} = 0, \tag{41}$$

where the comma '  $\equiv d/dx$ . Based on the relations (6) and (7), the velocity for longitudinal waves (38) can be expressed as

$$c_L(x) = \sqrt{\frac{E(x)(1-\nu)}{\rho(x)(1+\nu)(1-2\nu)}} = \sqrt{\frac{E_1[1+aV(x)](1-\nu)}{\rho_1[1+bV(x)](1+\nu)(1-2\nu)}} = c_{L0}\eta(x), \tag{42}$$

where

$$c_{L0} = \sqrt{\frac{E_1(1-\nu)}{\rho_1(1+\nu)(1-2\nu)}}, \quad \eta(x) = \sqrt{\frac{1+aV(x)}{1+bV(x)}}. \tag{43}$$

By substituting this formula into Eq. (41) we arrive at

$$ik'(x) - k^2(x) + i \frac{E'(x)}{E(x)} k(x) + k_0^2 \zeta^2(x) = 0, \tag{44}$$

where  $\zeta(x) = 1/\eta(x)$  and  $k_0 = \omega/c_{L0}$ . Assuming the following series expansion of the wavenumber

$$k(x) = k_0 k_1(x) + k_2(x) + \frac{k_3(x)}{k_0} + \frac{k_4(x)}{k_0^2} + \dots \tag{45}$$

and substituting into Eq. (44) we arrive at the following system of equations (corresponding to the coefficients of the respective powers of  $k_0$ )

$$\begin{aligned} \zeta^2(x) - k_1^2(x) &= 0, \\ i \frac{E'(x)}{E(x)} k_1(x) + ik_1'(x) - 2k_1(x)k_2(x) &= 0, \\ &\vdots \end{aligned} \tag{46}$$

By solving this system of equations we arrive at

$$k_1(x) = \pm \zeta(x), \quad k_2(x) = \frac{i}{2} \left( \frac{E'(x)}{E(x)} + \frac{\zeta'(x)}{\zeta(x)} \right). \tag{47}$$

Assuming the high frequency limit we can then approximate the expression (45) as

$$k(x) \approx k_0 k_1(x) + k_2(x) = \pm k_0 \zeta(x) + \frac{i}{2} \left( \frac{E'(x)}{E(x)} + \frac{\zeta'(x)}{\zeta(x)} \right). \tag{48}$$

After substituting this expression for the wavenumber into Eq. (39) then after some algebra we obtain the following expression for the approximate analytical WKB solution of the model equation

$$u(x, t) = \frac{A}{\sqrt{E(x)\zeta(x)}} \exp \left( \pm i \int_0^x k_0 \zeta(\bar{x}) d\bar{x} - i\omega t \right), \tag{49}$$

where the signs + and - represent the two waves traveling in the positive  $x$  direction and the negative  $x$  direction, respectively. From the expression (49), we can calculate the spatially dependent phase speed of a wave traveling in the positive  $x$  direction (by choosing the sign + in the expression (49)) as

$$c_{ph}(x) = \omega \left( \frac{\partial \varphi(x, t)}{\partial x} \right)^{-1} = \frac{\omega}{k_0 \zeta(x)} \equiv \frac{\omega}{k(x)} = c_L(x) = \sqrt{\frac{E(x)(1-\nu)}{\rho(x)(1+\nu)(1-2\nu)}}. \tag{50}$$

Note that this result represents an approximation and is only valid for the high-frequency limit.

### References

[1] Shin Young Kim, Woorim Lee, Joong Seok Lee, Yoon Young Kim, Longitudinal wave steering using beam-type elastic metagratings, *Mech. Syst. Signal Process.* 156 (2021) 107688, <http://dx.doi.org/10.1016/j.ymssp.2021.107688>.  
 [2] R. Zhu, X.N. Liu, G.K. Hu, C.T. Sun, G.L. Huang, Negative refraction of elastic waves at the deep-subwavelength scale in a single-phase metamaterial, *Nature Commun.* 5 (1) (2014) <http://dx.doi.org/10.1038/ncomms6510>.  
 [3] Guangyuan Su, Yunhao Zhang, Yongquan Liu, Tiejun Wang, Steering flexural waves by amplitude-shift elastic metasurfaces, *J. Appl. Mech.* 88 (5) (2021) <http://dx.doi.org/10.1115/1.4050239>.



- [4] Si-Min Yuan, A-Li Chen, Liyun Cao, Hua-Wei Zhang, Shi-Wang Fan, Badreddine Assouar, Yue-Sheng Wang, Tunable multifunctional fish-bone elastic metasurface for the wavefront manipulation of the transmitted in-plane waves, *J. Appl. Phys.* 128 (22) (2020) 224502, <http://dx.doi.org/10.1063/5.0029045>.
- [5] Yangyang Chen, Jin Hu, Guoliang Huang, A design of active elastic metamaterials for control of flexural waves using the transformation method, *J. Intell. Mater. Syst. Struct.* 27 (10) (2015) 1337–1347, <http://dx.doi.org/10.1177/1045389x15590273>.
- [6] Jeonghoon Park, Dongwoo Lee, Junsuk Rho, Recent advances in non-traditional elastic wave manipulation by macroscopic artificial structures, *Appl. Sci.* 10 (2) (2020) 547, <http://dx.doi.org/10.3390/app10020547>.
- [7] Thomas Vasileiadis, Jeena Varghese, Visnja Babacic, Jordi Gomis-Bresco, Daniel Navarro Urrios, Bartłomiej Graczykowski, Progress and perspectives on phononic crystals, *J. Appl. Phys.* 129 (16) (2021) 160901, <http://dx.doi.org/10.1063/5.0042337>.
- [8] V. Laude, Principles and properties of phononic crystal waveguides, *APL Mater.* 9 (8) (2021) 080701, <http://dx.doi.org/10.1063/5.0059035>.
- [9] Islam M. El-Galy, Bassiouny I. Saleh, Mahmoud H. Ahmed, Functionally graded materials classifications and development trends from industrial point of view, *SN Appl. Sci.* 1 (11) (2019) <http://dx.doi.org/10.1007/s42452-019-1413-4>.
- [10] Azeem Pasha, Rajaprakash B.M, Functionally graded materials (FGM) fabrication and its potential challenges & applications, *Mater. Today Proc.* 52 (2022) 413–418, <http://dx.doi.org/10.1016/j.matpr.2021.09.077>.
- [11] J.N. Reddy, Analysis of functionally graded plates, *Internat. J. Numer. Methods Engrg.* 47 (1–3) (2000) 663–684, [http://dx.doi.org/10.1002/\(sici\)1097-0207\(200011030\)47:1/3<663::aid-nme787>3.0.co;2-8](http://dx.doi.org/10.1002/(sici)1097-0207(200011030)47:1/3<663::aid-nme787>3.0.co;2-8).
- [12] Victor Birman, Larry W. Byrd, Modeling and analysis of functionally graded materials and structures, *Appl. Mech. Rev.* 60 (5) (2007) 195–216, <http://dx.doi.org/10.1115/1.2777164>.
- [13] M. Bednarik, M. Cervenka, J.P. Groby, P. Lotton, One-dimensional propagation of longitudinal elastic waves through functionally graded materials, *Int. J. Solids Struct.* 146 (2018) 43–54, <http://dx.doi.org/10.1016/j.ijsolstr.2018.03.017>.
- [14] Mei-Ling Wu, Liang-Yu Wu, Wen-Pei Yang, Lien-Wen Chen, Elastic wave band gaps of one-dimensional phononic crystals with functionally graded materials, *Smart Mater. Struct.* 18 (11) (2009) 115013, <http://dx.doi.org/10.1088/0964-1726/18/11/115013>.
- [15] S.I. Fomenko, M.V. Golub, Ch. Zhang, T.Q. Bui, Y.-S. Wang, In-plane elastic wave propagation and band-gaps in layered functionally graded phononic crystals, *Int. J. Solids Struct.* 51 (13) (2014) 2491–2503, <http://dx.doi.org/10.1016/j.ijsolstr.2014.03.017>.
- [16] Xiaoliang Zhou, Yeli Sun, Shuai Yang, Zuguang Bian, Band gap manipulation on P-wave propagating in functionally graded phononic crystal by periodical thermal field, *Int. J. Mech. Sci.* 212 (2021) 106817, <http://dx.doi.org/10.1016/j.ijmecsci.2021.106817>.
- [17] Zuguang Bian, Shuai Yang, Xiaoliang Zhou, David Hui, Band gap manipulation of viscoelastic functionally graded phononic crystal, *Nanotechnol. Rev.* 9 (1) (2020) 515–523, <http://dx.doi.org/10.1515/ntrev-2020-0042>.
- [18] Xing-Liang Su, Yuan wen Gao, You he Zhou, The influence of material properties on the elastic band structures of one-dimensional functionally graded phononic crystals, *J. Appl. Phys.* 112 (12) (2012) 123503, <http://dx.doi.org/10.1063/1.4768934>.
- [19] Xiaoshi Su, Andrew N. Norris, Focusing, refraction, and asymmetric transmission of elastic waves in solid metamaterials with aligned parallel gaps, *J. Acoust. Soc. Am.* 139 (6) (2016) 3386–3394, <http://dx.doi.org/10.1121/1.4950770>.
- [20] Xiaoshi Su, Zhaocheng Lu, Andrew N. Norris, Elastic metasurfaces for splitting SV- and P-waves in elastic solids, *J. Appl. Phys.* 123 (9) (2018) 091701, <http://dx.doi.org/10.1063/1.5007731>.
- [21] Ruiju Huang, L. Scherrer, A. Sedov, Modeling the radiation of ultrasonic phased-array transducers with Gaussian beams, *IEEE Trans. Ultrason. Ferroelectr. Freq. Control* 55 (12) (2008) 2692–2702, <http://dx.doi.org/10.1109/tuffc.2008.984>.
- [22] Yu-Xiang Dai, Shou-Guo Yan, Bi-Xing Zhang, Ultrasonic beam steering behavior of linear phased arrays in solid, in: 2019 14th Symposium on Piezoelectricity, Acoustic Waves and Device Applications, SPAWDA, IEEE, 2019, <http://dx.doi.org/10.1109/spawda48812.2019.9019270>.
- [23] Yu-Xiang Dai, Shou-Guo Yan, Bi-Xing Zhang, An ultrasonic multi-wave focusing and imaging method for linear phased arrays, *Chin. Phys. B* 30 (7) (2021) 074301, <http://dx.doi.org/10.1088/1674-1056/abf91d>.
- [24] Borislav Vasic, Goran Isic, Rados Gajic, Kurt Hingerl, Controlling electromagnetic fields with graded photonic crystals in metamaterial regime, *Opt. Express* 18 (19) (2010) 20321, <http://dx.doi.org/10.1364/oe.18.020321>.
- [25] Yijun Feng, Yuwei Lin, Shuai Xiong, Xiaofei Xu, Electromagnetic wave lenses and reflectors designed with transformation electromagnetics, in: 2014 XXXIth URSI General Assembly and Scientific Symposium, URSI GASS, IEEE, 2014, <http://dx.doi.org/10.1109/ursigass.2014.6929145>.
- [26] Srijan Datta, Antonello Tamburrino, Lalita Udpa, Gradient index metasurface lens for microwave imaging, *Sensors* 22 (21) (2022) 8319, <http://dx.doi.org/10.3390/s22218319>.
- [27] G. Bao, L. Wang, Multiple cracking in functionally graded ceramic/metal coatings, *Int. J. Solids Struct.* 32 (19) (1995) 2853–2871, [http://dx.doi.org/10.1016/0020-7683\(94\)00267-z](http://dx.doi.org/10.1016/0020-7683(94)00267-z).
- [28] Hassan Mohamed Abdelalim Abdalla, Djaffar Boussaa, Roberta Sburlati, Daniele Casagrande, On the best volume fraction distributions for functionally graded cylinders, spheres and disks – A pseudospectral approach, *Compos. Struct.* 311 (2023) 116784, <http://dx.doi.org/10.1016/j.compstruct.2023.116784>.
- [29] S. Srividhya, K. Basant, R.K. Gupta, A. Rajagopal, J.N. Reddy, Influence of the homogenization scheme on the bending response of functionally graded plates, *Acta Mech.* 229 (10) (2018) 4071–4089, <http://dx.doi.org/10.1007/s00707-018-2223-2>.
- [30] Shyang-Ho Chi, Yen-Ling Chung, Mechanical behavior of functionally graded material plates under transverse load—part I: Analysis, *Int. J. Solids Struct.* 43 (13) (2006) 3657–3674, <http://dx.doi.org/10.1016/j.ijsolstr.2005.04.011>.
- [31] Xiaoshi Su, Andrew N. Norris, Colby W. Cushing, Michael R. Haberman, Preston S. Wilson, Broadband focusing of underwater sound using a transparent pentamode lens, *J. Acoust. Soc. Am.* 141 (6) (2017) 4408–4417, <http://dx.doi.org/10.1121/1.4985195>.
- [32] Shiyu Zhang, Ravi Kumar Arya, William G. Whittow, Darren Cadman, Raj Mittra, J.C. Vardaxoglou, Ultra-wideband flat metamaterial GRIN lenses assisted with additive manufacturing technique, *IEEE Trans. Antennas and Propagation* 69 (7) (2021) 3788–3799, <http://dx.doi.org/10.1109/tap.2020.3044586>.
- [33] Martin H. Sadd, *Elasticity, second ed.*, Academic Press, San Diego, CA, 2009.
- [34] Paweł Sobieszczyk, Marcin Majka, Dominika Kuźma, Teik-Cheng Lim, Piotr Zieliński, Effect of longitudinal stress on wave propagation in width-constrained elastic plates with arbitrary Poisson's ratio, *physica status solidi (b)* 252 (7) (2015) 1615–1619, <http://dx.doi.org/10.1002/pssb.201552256>.
- [35] Teik-Cheng Lim, Longitudinal wave motion in width-constrained auxetic plates, *Smart Mater. Struct.* 25 (5) (2016) 054008, <http://dx.doi.org/10.1088/0964-1726/25/5/054008>.
- [36] Zeng Cao, Xu Liang, Yu Deng, Xing Zha, Ronghua Zhu, Jianxing Leng, Novel semi-analytical solutions for the transient behaviors of functionally graded material plates in the thermal environment, *Materials* 12 (24) (2019) 4084, <http://dx.doi.org/10.3390/ma12244084>.
- [37] G. Scovazzi, T. Song, X. Zeng, A velocity/stress mixed stabilized nodal finite element for elastodynamics: Analysis and computations with strongly and weakly enforced boundary conditions, *Comput. Methods Appl. Mech. Engrg.* 325 (2017) 532–576, <http://dx.doi.org/10.1016/j.cma.2017.07.018>.
- [38] Kaizhou Lu, Charles E. Augarde, William M. Coombs, Zhendong Hu, Weak impositions of Dirichlet boundary conditions in solid mechanics: A critique of current approaches and extension to partially prescribed boundaries, *Comput. Methods Appl. Mech. Engrg.* 348 (2019) 632–659, <http://dx.doi.org/10.1016/j.cma.2019.01.035>.

- [39] Eugenio Oñate, *Structural Analysis with the Finite Element Method. Linear Statics*, 2009, in: *Lecture Notes on Numerical Methods in Engineering and Sciences*, Springer, Dordrecht, Netherlands, 2009.
- [40] Saeed Farahmand, Mohammad Hossein Soorgee, A numerical investigation on ultrasonic bulk wave propagation features in functionally graded plates, *J. Compos. Mater.* 54 (8) (2019) 1067–1077, <http://dx.doi.org/10.1177/0021998319874104>.
- [41] Zheng-Hua Qian, Feng Jin, Kikuo Kishimoto, Tianjian Lu, Propagation behavior of Love waves in a functionally graded half-space with initial stress, *Int. J. Solids Struct.* 46 (6) (2009) 1354–1361, <http://dx.doi.org/10.1016/j.ijsolstr.2008.11.003>.

## 3.5 Paper V

**Title:** *Exact analytical solution for shear horizontal wave propagation through locally periodic structures realized by viscoelastic functionally graded materials*

The fifth paper published in Composite Structures deals with the propagation of shear horizontal (SH) elastic waves in locally periodic inhomogeneous viscoelastic FGMs (see Sec. 2.5). The term shear refers to a type of bulk elastic waves whose particles oscillate perpendicular to the direction of propagation (in contrast to the P-waves defined in the previous section). The coordinate system is then oriented such that the corresponding wave vector (indicating the direction of propagation of the corresponding plane wave) lies in the (without the loss of generality)  $x - z$  plane and the designation horizontal in this context means that the particles oscillate along the  $y$  direction. Now we assume a locally periodic inhomogeneous FGM structure whose density and shear modulus (note that the shear modulus plays a similar role for the SH-waves as the Young modulus for the P-waves) vary continuously along the  $z$  axis (in this case oriented horizontally, whereas the  $x$  axis is oriented vertically) according to the locally periodic material function (see Eq. (2.80)) expressed by the square of the sine function (shifted vertically). The corresponding model equation of the Webster-type (see Sec. 2.2) is then derived describing the propagation of SH waves in such a media including the viscoelastic losses.

Please note that for the sake of readability, the further steps will now be stated in a slightly different order than is presented in the paper itself. The model equation in this case can be transformed to the canonical form of the Heun equation (see Sec. 2.1) and therefore the corresponding solution in the first period can be expressed by the local Heun functions. The so called continuation technique is also presented in order to deal with a singular point of the Heun equation lying in the respective interval. The solution is then extended to the whole FGM by employing the Floquet-Bloch theory (see Sec. 2.4), resulting in an exact analytical solution to the model equation for the whole locally periodic FGM structure. Based on the Floquet-Bloch theory the Bloch phase is defined determining the frequency bands in which the inhomogeneous structure acts like a band-stop filter (the incident plane wave is almost perfectly reflected). By assuming a homogeneous halfspace on both sides of the FGM structure, a plane SH-wave incident to the structure at a general angle of incidence from the left and further specifying the boundary conditions the transmission and reflection coefficients are defined. In order to better understand the behaviour of the derived analytical solution the wave splitting method is applied enabling us to split the solution into the two parts - one propagating to the right (in the positive sense of the  $z$  axis) and the other to the left. By this technique, we are also able to express the

reflection coefficient at any given point of the FGM structure and not only at the left side where the incoming plane SH-wave is incident. Lastly, the Riccati equation is derived for the reflection coefficient which has to be solved numerically and serves as tool to verify the correctness of the found exact analytical solutions.

In the next part of the paper, the reflection coefficient as a function of the frequency is first plotted for two specifically chosen materials of the FGM structure, two angles of incidence and including the viscoelastic losses. By comparison with the numerical solution of the corresponding Riccati equation the correctness of the found exact analytical solutions is verified. For the simplicity of further calculations, the losses are neglected hereinafter. Next, the right and the left going solutions obtained via the wave splitting method are plotted for two frequencies - one chosen inside of the stop band and the other lying outside, enabling us to better understand of how the waves behave inside of the locally periodic FGM structure. Lastly, the transmission coefficients are plotted for fixed first material and various second materials of the FGM, whereas the stop-bands corresponding to each one of the second materials are located at different frequencies with different bandwidths in the respective graph of the transmission coefficient. Therefore, the second material can be utilized as one of the control parameters of the FGM structure when using it as a filter. It should also be noted that we assumed the profile of the material function the same for each one of the specific calculations in this paper. But it itself contains two additional control parameters that can also be varied and therefore further studies can be conducted in order to assess the influence of those parameters on the behaviour of the transmission/reflection coefficient of the respective FGM structure.



# Exact analytical solution for shear horizontal wave propagation through locally periodic structures realized by viscoelastic functionally graded materials

Antonin Krpensky\*, Michal Bednarik

Czech Technical University in Prague, Faculty of Electrical Engineering, Technicka 2, Prague, 166 27, Czech Republic

## ARTICLE INFO

### Keywords:

Wave splitting method  
Riccati equation  
Heun's differential equation  
Heun functions  
Floquet–Bloch theory

## ABSTRACT

The paper presents a novel comprehensive exact analytical solution for modeling linear shear-horizontal (SH) wave propagation in an isotropic inhomogeneous layer made of functionally graded material, using local Heun functions. The layer is a composite of two materials with varying properties represented by spatial variations following the square of the sine function. The Voigt–Kelvin model is used to account for material losses. The study focuses on SH waves incident at a specific angle and employs the wave splitting technique to analyze forward and backward waves, facilitating the computation of reflection and transmission coefficients at any point in the inhomogeneous structure. The proposed solution utilizes the periodic nature of material functions and employs the Floquet–Bloch theory to derive an exact analytical solution. This approach is particularly suited for cases where SH waves encounter locally periodic functionally graded material. A Riccati equation-based verification is conducted to compare the frequency-dependent modulus of the reflection coefficient obtained from the analytical solution with numerically solved results. The presented work provides a comprehensive and versatile analytical solution for studying linear SH wave propagation in locally inhomogeneous isotropic layers, contributing to the theoretical understanding of elastic wave fields and practical applications.

## 1. Introduction

The SH waves have received considerable attention in the field of guided ultrasonic non-destructive testing and evaluation due to their unique characteristics, such as weak dispersion and the presence of only one directional displacement, see e.g., [1–3]. These properties make it an ideal candidate for various applications, including defect detection and characterization in structures. Guided SH wave devices have also gained significant interest for their potential use in high-sensitivity chemical and biochemical sensors in liquid environments, see e.g., [4,5]. These devices offer several advantages, such as high sensitivity, real-time monitoring capabilities, and the ability to detect low concentrations of analytes. Consequently, they have the potential to revolutionize fields such as environmental monitoring, biomedical research, and food safety testing. The propagation of SH waves in anisotropic laminated plates was studied e.g., in [6].

The propagation of plane elastic SH waves through an isotropic inhomogeneous layer is a crucial topic of both scientific and practical significance. To better understand the behavior of these waves in materials with varying properties, it is helpful to have access to analytical

solutions for the corresponding governing equations. The need for such solutions is evident in various scientific fields, including geophysics, where studying the propagation of waves through the Earth can provide insights into its internal structure. Additionally, these solutions can aid in exploring materials located beneath the Earth's surface [7]. There has been considerable attention given to the propagation of seismic waves through inhomogeneous half-spaces with varying elastic properties, as well as the scattering of these waves by different types of heterogeneities with scale lengths comparable to the wavelength [8]. In addition, material-property inhomogeneities can arise due to temperature gradients in various materials, and these scenarios have also been studied [9,10]. The issue of SH wave propagation through inhomogeneous media also plays an important role in new imaging techniques (see e.g. [11]).

The primary goal of FG composites is to combine the best mechanical properties of two or more materials into a single material with mechanical properties that surpass those of any constituent material alone. As a result of their exceptional properties, FG materials are increasingly being used in a variety of devices, as evidenced by recent

\* Corresponding author.

E-mail address: [antonin.krpensky@fel.cvut.cz](mailto:antonin.krpensky@fel.cvut.cz) (A. Krpensky).

research, see e.g., [12,13]. A comprehensive array of articles is available, delving into the analysis of FG plates, beams, and shells. Notable references include [14–18]. Certain studies delve deeper into the realm of nonlinear analysis for these FG plates, as demonstrated by [19,20]. Additionally, research endeavors extend to the domain of elastic wave propagation within FG plates and beams, as evident in [21,22].

SH waves can be used to detect defects, such as cracks or voids, in FG materials, enabling quality control and preventing catastrophic failure, see e.g. [23].

When the mechanical impedances of two media are mismatched, elastic waves are partly reflected at their interface. Research has investigated the use of FG materials to achieve this purpose, as exemplified in the study [24]. In various engineering and scientific applications, controlling or minimizing the reflected waves is frequently required, and FG materials are often utilized for this purpose. This is particularly crucial in sensor applications [25,26] and in cloaking thin plates [27, 28].

Elastic waves offer a promising means for material characterization of FG materials. However, for their effective use, it is crucial to have a good understanding of wave propagation in FG materials [29–31].

Elastic wave phenomena in composite materials and structures play a crucial role in designing new devices. Phononic crystals based on FG materials are among them, and designing an optimal phononic crystal is a complex task that requires a deeper understanding of elastic waves in such locally periodic structures [32–34].

As the material properties in inhomogeneous isotropic materials are functions of spatial coordinates, wave propagation represents a problem that is generally difficult to analyze without employing numerical methods. Such methods are discussed in detail in previous research [35,36]. However, to understand wave processes in inhomogeneous isotropic materials, it is desirable to know the exact analytical solutions of the corresponding model equations. Several approximate analytical methods are utilized, including the Wentzel–Kramers–Brillouin (WKB) method (see e.g., [37,38]), series expansion method [39], and Green’s function approach method [40,41]. Unfortunately, to the best of the authors’ knowledge, only a few publications present exact solutions for various material-property profiles [7,31,42–45].

The primary objective of this study is to introduce a comprehensive and exact analytical general solution for the linear elastodynamic governing equation of SH waves propagating through a locally inhomogeneous isotropic layer at a chosen angle of incidence. The material properties of the layer are described using a spatially-dependent periodic material function. Furthermore, to incorporate losses, it is possible to employ the Kelvin–Voigt model of the viscoelastic medium (see e.g., [45,46]).

Since the transmission properties of locally periodic structures (phononic crystals) are of interest from both theoretical and practical perspectives, our intention is to utilize this exact analytical solution for the considered inhomogeneous layer to find an exact analytical solution for the locally periodic structure using the Floquet–Bloch theory. To realize these objectives, our aim is to employ material functions expressed as periodic spatial functions.

As the obtained exact solutions describe only the overall elastic field, our further goal is to perform the separation of these solutions into forward and backward displacement traveling waves using the splitting method in the frequency domain. Forward and backward waves allow for straightforward computation of reflection and transmission coefficients for any point within the inhomogeneous structure and additionally enable the investigation of wave distribution within this structure.

To validate the found solutions, we plan to derive the Riccati equation for this purpose, which can be easily solved numerically. Based on this numerical solution, we will compute the reflection coefficient, which will subsequently be compared with the analytically computed reflection coefficient.

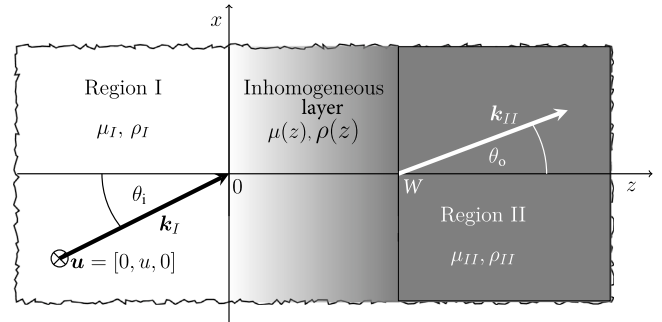


Fig. 1. Inhomogeneous isotropic layer sandwiched between two half-spaces I and II.

The paper is organized as follows. Firstly, in Section 2, the governing equation for the elastic SH wave in an inhomogeneous viscoelastic layer is introduced. Next, in Section 3, the wave splitting method is employed to obtain forward and backward traveling displacement waves. Then, in Section 4, the Riccati equation for numerical computation of the reflection coefficient is derived. Section 5 provides an exact analytical solution for the goniometric material function based on Heun functions. In Section 6, the analytic continuation of the general solution of Heun’s equation is discussed to obtain the general solution for Bloch waves. Section 7 focuses on the calculation of reflection coefficients for various case studies and the investigation of SH wave behavior in locally periodic structures. The analytical results are compared with numerical solutions based on the Riccati equation. Finally, in Section 8, the paper concludes with a summary of the findings. To make the paper more accessible, Appendix A outlines some features of the Heun’s differential equation and its solutions, while Appendix B provides an overview of the Floquet theory used in the analysis.

## 2. Model equation

In this section, a model equation describing the propagation of SH waves in an inhomogeneous layer represented by an FG material is presented. This layer has a width of  $W$  in the direction of propagation (direction of the  $z$  axis.), and it is unbounded in the remaining directions. The layer is sandwiched between two half-spaces, I and II, which are filled with homogeneous material, as shown in Fig. 1. Half-space I is filled with material characterized by parameters  $\mu_I$  and  $\rho_I$ , while half-space II is filled with material characterized by parameters  $\mu_{II}$  and  $\rho_{II}$ .

For the two-dimensional case of small-amplitude SH waves propagating in the  $x - z$  plane (see Fig. 1), displacement only occurs in the  $y$ -direction (anti-plane SH wave motion, i.e.  $\mathbf{u} = (0, u(x, z, t), 0)$ , where  $\mathbf{u}$  stands for the displacement vector and we can write the equation of motion for isotropic inhomogeneous medium without body forces as (see e.g., [32,33,37–39,44–46]):

$$\frac{\partial \tau_{yx}(x, z, t)}{\partial x} + \frac{\partial \tau_{yz}(x, z, t)}{\partial z} = \rho(z) \frac{\partial^2 u(x, z, t)}{\partial t^2}, \quad (1)$$

where  $\rho(z)$  is the density and the two shear stresses are

$$\tau_{yx}(x, z, t) = \hat{\mu} \frac{\partial u(x, z, t)}{\partial x}, \quad \tau_{yz}(x, z, t) = \hat{\mu} \frac{\partial u(x, z, t)}{\partial z}. \quad (2)$$

Here  $\hat{\mu}$  represents the operator of the position-dependent shear modulus including the viscoelastic losses for which the Kelvin–Voigt model is employed (see e.g., [45,46]):

$$\hat{\mu} = \mu_s(z) + \mu_v \frac{\partial}{\partial t}, \quad (3)$$

where  $\mu_s(z)$  is the storage shear modulus and  $\mu_v$  is the viscosity. Substituting the shear stresses into Eq. (1) we obtain

$$\frac{\partial}{\partial x} \left[ \hat{\mu} \frac{\partial u(x, z, t)}{\partial x} \right] + \frac{\partial}{\partial z} \left[ \hat{\mu} \frac{\partial u(x, z, t)}{\partial z} \right] = \rho(z) \frac{\partial^2 u(x, z, t)}{\partial t^2}. \quad (4)$$

By assuming a time harmonic wave of the form

$$u(x, z, t) = \tilde{u}(x, z) \exp(-j\omega t), \quad (5)$$

where  $j = \sqrt{-1}$  is the imaginary unit and  $\omega$  the angular frequency, the operator  $\hat{\mu}$  now becomes just

$$\mu(z) = \mu_s(z) - j\omega\mu_v. \quad (6)$$

Eq. (4) can then be expressed as

$$\frac{\partial^2 \tilde{u}(x, y)}{\partial x^2} + \frac{\partial^2 \tilde{u}(x, y)}{\partial z^2} + \frac{1}{\mu(z)} \frac{d\mu(z)}{dz} \frac{\partial \tilde{u}(x, z)}{\partial z} + \omega^2 \frac{\rho(z)}{\mu(z)} \tilde{u}(x, z) = 0. \quad (7)$$

It should be noted that at the boundaries between the inhomogeneous layer and the homogeneous media I and II, the continuity condition must be ensured for both the displacement vector and the stress tensor. Therefore, we can employ the separation (see Fig. 1)

$$\tilde{u}(x, z) = \tilde{u}(z) \exp\left(j \frac{k_I \sin \theta_i}{\sqrt{1-j\chi}} x\right), \quad (8)$$

where  $\theta_i$  is the angle of incidence, see Fig. 1,  $k_I = \omega/c_I$ ,  $c_I = \sqrt{\mu_I/\rho_I}$  and  $\chi = \omega\mu_v/\mu_I$ , where the subscript  $I$  means that the material properties are related to the region I, we can express Eq. (7) as

$$\frac{d^2 \tilde{u}(z)}{dz^2} + \frac{1}{\mu(z)} \frac{d\mu(z)}{dz} \frac{d\tilde{u}(z)}{dz} + \left[ \omega^2 \frac{\rho(z)}{\mu(z)} - \frac{k_I^2 \sin^2 \theta_i}{1-j\chi} \right] \tilde{u}(z) = 0. \quad (9)$$

For convenience, we rewrite Eq. (9) in its dimensionless form:

$$\frac{d^2 U(s)}{ds^2} + \frac{1}{\tilde{\eta}(s)} \frac{d\tilde{\eta}(s)}{ds} \frac{dU(s)}{ds} + \left[ K_I^2 \frac{\xi(s)}{\tilde{\eta}(s)} - x^2 \right] U(s) = 0. \quad (10)$$

Here

$$s = \frac{z}{\ell}, \quad U = \frac{\tilde{u}}{\ell}, \quad K_I = k_I \ell, \quad x^2 = \frac{K_I^2 \sin^2 \theta_i}{1-j\chi}, \quad \eta(s) = \frac{\mu_s(s)}{\mu_I}, \quad (11)$$

$$\xi(s) = \frac{\rho(s)}{\rho_I}, \quad \mu(s) = \mu_I(\eta(s) - j\chi) = \mu_I \tilde{\eta}(s),$$

where  $\ell$  is a characteristic length.

Eq. (10) represents the model equation for which an exact analytical solution will be sought for the chosen spatial dependence of the respective material parameters.

### 3. Wave splitting method

We will use the wave splitting method in the frequency domain (see e.g., [47]) to separate the overall displacement field  $U(s)$  (see Eq. (53)) into forward  $U_+(s)$  and backward  $U_-(s)$  traveling displacement waves. The wave splitting method is described in more detail e.g., in [48]. Therefore, here we just outline the use of this method.

Taking the derivative of Eq. (2) by time we obtain

$$\frac{\partial \tau_{yz}(x, z, t)}{\partial t} = \hat{\mu} \frac{\partial \dot{u}(x, z, t)}{\partial z}. \quad (12)$$

Using Eqs. (5) and (8) we can write

$$\tau_{yz}(x, z, t) = \tilde{\tau}(z) \exp\left(j \frac{k_I \sin \theta_i}{\sqrt{1-j\chi}} x - j\omega t\right), \quad (13)$$

$$\frac{\partial u(x, z, t)}{\partial t} \equiv \dot{u}(x, z, t) = -j\omega \tilde{u}(z) \exp\left(j \frac{k_I \sin \theta_i}{\sqrt{1-j\chi}} x - j\omega t\right) = \dot{\tilde{u}}(z) \exp\left(j \frac{k_I \sin \theta_i}{\sqrt{1-j\chi}} x - j\omega t\right). \quad (14)$$

Employing Eqs. (13) and (14) we can rewrite Eq. (12) as

$$-j\omega \tilde{\tau}(z) = \mu(z) \frac{d\dot{\tilde{u}}(z)}{dz} \quad (15)$$

that can be written in the following form using dimensionless quantities

$$\frac{d\dot{U}(s)}{ds} = -\frac{j\omega}{\tilde{\eta}(s)} T(s), \quad (16)$$

where  $\dot{U} = \dot{\tilde{u}}/\ell$  and  $T = \tilde{\tau}/\mu_I$ .

Based on Eq. (14) we can write that

$$\dot{U}(s) = -j\omega U(s). \quad (17)$$

Using Eq. (17) we can rewrite Eq. (10) as

$$\frac{dT(s)}{ds} = -j\omega \left[ \frac{\ell^2}{c_I^2} \left( \xi(s) - \frac{\tilde{\eta}(s) \sin^2 \theta_i}{1-j\chi} \right) \right] \dot{U}(s). \quad (18)$$

Recall that

$$T(s) = \tilde{\eta}(s) \frac{dU(s)}{ds}. \quad (19)$$

We can now express Eqs. (16) and (18) in the matrix form (representing the Cauchy formalism) as follows:

$$\frac{d}{ds} \begin{pmatrix} T(s) \\ \dot{U}(s) \end{pmatrix} = \begin{pmatrix} 0 & -j\omega \left[ \frac{\ell^2}{c_I^2} \left( \xi(s) - \frac{\tilde{\eta}(s) \sin^2 \theta_i}{1-j\chi} \right) \right] \\ -\frac{j\omega}{\tilde{\eta}(s)} T(s) & 0 \end{pmatrix} \begin{pmatrix} T(s) \\ \dot{U}(s) \end{pmatrix}. \quad (20)$$

The functions  $T(s)$  and  $\dot{U}(s)$  are independent and constitute a complete base of functions for the system of Eqs. (16) and (18).

The diagonalization can make the transition from the base of the functions  $T(s)$  and  $\dot{U}(s)$  to the base of the functions  $\dot{U}_+(s)$  and  $\dot{U}_-(s)$  (see e.g., [48]), between which the following relation holds after normalization

$$\begin{pmatrix} \dot{U}_+(s) \\ \dot{U}_-(s) \end{pmatrix} = \mathbb{M} \begin{pmatrix} \dot{U}(s) \\ T(s) \end{pmatrix}, \quad (21)$$

where

$$\mathbb{M} = \begin{pmatrix} 1 & -\frac{c_I}{\ell \sqrt{\tilde{\eta}(s) \left( \xi(s) - \frac{\tilde{\eta}(s) \sin^2 \theta_i}{1-j\chi} \right)}} \\ 1 & \frac{c_I}{\ell \sqrt{\tilde{\eta}(s) \left( \xi(s) - \frac{\tilde{\eta}(s) \sin^2 \theta_i}{1-j\chi} \right)}} \end{pmatrix}. \quad (22)$$

Based on Eq. (21) we get

$$\dot{U}_+(s) = \frac{1}{2} \left[ \dot{U}(s) - \frac{c_I}{\ell \sqrt{\tilde{\eta}(s) \left( \xi(s) - \frac{\tilde{\eta}(s) \sin^2 \theta_i}{1-j\chi} \right)}} T(s) \right], \quad (23)$$

$$\dot{U}_-(s) = \frac{1}{2} \left[ \dot{U}(s) + \frac{c_I}{\ell \sqrt{\tilde{\eta}(s) \left( \xi(s) - \frac{\tilde{\eta}(s) \sin^2 \theta_i}{1-j\chi} \right)}} T(s) \right], \quad (24)$$

Using this relation and Eq. (19) we can adjust the expressions (23) and (24) for the forward  $U_+(s)$  and backward  $U_-(s)$  displacements as

$$U_+(s) = \frac{1}{2} [U(s) + Q(s, \omega) T(s)] = \frac{1}{2} \left[ U(s) + \tilde{\eta}(s) Q(s, \omega) \frac{dU(s)}{ds} \right], \quad (25)$$

$$U_-(s) = \frac{1}{2} [U(s) - Q(s, \omega) T(s)] = \frac{1}{2} \left[ U(s) - \tilde{\eta}(s) Q(s, \omega) \frac{dU(s)}{ds} \right], \quad (26)$$

where

$$Q(s, \omega) = \frac{c_I}{j\omega \ell \sqrt{\tilde{\eta}(s) \left( \xi(s) - \frac{\tilde{\eta}(s) \sin^2 \theta_i}{1-j\chi} \right)}} = \frac{\mu_I}{j\omega \ell \sqrt{\mu(s) \rho(s) - \frac{\rho_I \mu(s) \tilde{\eta}(s) \sin^2 \theta_i}{1-j\chi}}}. \quad (27)$$

By summing Eqs. (25) and (26) we get the overall displacement field

$$U(s) = U_+(s) + U_-(s). \quad (28)$$

Furthermore, the following holds

$$T_+(s) = \frac{U_+(s)}{Q(s, \omega)}, \quad T_-(s) = -\frac{U_-(s)}{Q(s, \omega)}. \quad (29)$$

From here

$$T(s) = T_+(s) + T_-(s). \quad (30)$$

#### 4. The Riccati equation

The model Eq. (10) can be expressed using the relation (19) as

$$\frac{d}{ds} \left( \tilde{\eta}(s) \frac{dU(s)}{ds} \right) = (-K_I^2 \xi(s) + x^2 \tilde{\eta}(s)) U(s). \quad (31)$$

From Eq. (31) we can derive the Riccati equation with the help of which it is then relatively easy to numerically calculate the reflection coefficient

$$\mathcal{R}(s, \omega) = \frac{U_-(s)}{U_+(s)}. \quad (32)$$

Please note that in the notation of the functions  $U(s)$  and  $T(s)$ , we have omitted the explicit dependence on the parameter  $\omega$  for better readability hereinafter.

For this purpose, we introduce the impedance as

$$Z(s, \omega) = \frac{\mu_I T(s)}{\ell U(s)}. \quad (33)$$

Using the relations (17) and (19) we can express the impedance as follows

$$Z(s, \omega) = \frac{\mu_I \tilde{\eta}(s) \frac{dU(s)}{ds}}{-j\omega \ell U(s)}. \quad (34)$$

From here we get

$$\frac{dU(s)}{ds} = \frac{-j\omega \ell Z(s) U(s)}{\mu(s)}. \quad (35)$$

By using Eqs. (11) and (35) we get the following Riccati equation for the impedance from Eq. (31)

$$\frac{dZ(s, \omega)}{ds} = \frac{j\omega \ell}{\mu(s)} Z^2(s, \omega) - j\omega \ell \rho(s) + \frac{j\omega \ell \mu(s) \sin^2 \theta_i}{c_i^2 (1 - j\chi)}. \quad (36)$$

Based on the relations (27)–(30) we can express the impedance (33) using the reflection coefficients (32) as

$$\begin{aligned} Z(s, \omega) &= \frac{\mu_I}{-j\omega \ell Q(s)} \frac{U_+(s) - U_-(s)}{U_+(s) + U_-(s)} \\ &= \sqrt{\frac{\mu(s) \rho(s) - \frac{\rho_I \mu(s) \tilde{\eta}(s) \sin^2 \theta_i}{1 - j\chi}}{\mu(s) \rho(s) - \frac{\rho_I \mu(s) \tilde{\eta}(s) \sin^2 \theta_i}{1 - j\chi} + Z(s, \omega)}}. \end{aligned} \quad (37)$$

From this relation, we can then determine the necessary initial condition  $Z(s = s_0, \omega)$  for solving the Riccati equation (36).

Based on Eq. (37) we can express the reflection coefficient as

$$\mathcal{R}(s, \omega) = \frac{\sqrt{\mu(s) \rho(s) - \frac{\rho_I \mu(s) \tilde{\eta}(s) \sin^2 \theta_i}{1 - j\chi}} - Z(s, \omega)}{\sqrt{\mu(s) \rho(s) - \frac{\rho_I \mu(s) \tilde{\eta}(s) \sin^2 \theta_i}{1 - j\chi}} + Z(s, \omega)}. \quad (38)$$

into which we insert the solution of the Riccati equation (36).

#### 5. The exact analytical solution of the model equation

In this paper we assume a FG layer (plate) fabricated from the two materials  $M_I$  and  $M_{II}$  in which the given material property  $P$  is a function of the individual material properties and the volume fractions of the constituent materials (see e.g., [49]) expressed as

$$P = P_I V_I + P_{II} V_{II}, \quad (39)$$

where  $P_I$  and  $P_{II}$  denote the properties of the respective materials and  $V_I$  and  $V_{II}$  represent the volume fractions of the constituent materials that satisfy the following condition

$$V_I + V_{II} = 1. \quad (40)$$

The material composition in the FG layer varies continuously only along the thickness direction and denoting  $V_{II} = V(s)$ , based on

Eq. (40) we can write that  $V_I = 1 - V(s)$  and therefore Eq. (39) takes on the form

$$P(s) = P_{II} V(s) + P_I [1 - V(s)] = P_I \left[ 1 + \frac{P_{II} - P_I}{P_I} V(s) \right]. \quad (41)$$

By considering the volume function  $V(s) = \sin^2(ms + \phi)$ , where  $m \neq 0$ , we can use Eq. (41) to express the material functions  $\eta(s)$  and  $\xi(s)$  as

$$\eta(s) = 1 + \frac{\mu_{II} - \mu_I}{\mu_I} \sin^2(ms + \phi) = 1 + a \sin^2(ms + \phi), \quad (42)$$

$$\xi(s) = 1 + \frac{\rho_{II} - \rho_I}{\rho_I} \sin^2(ms + \phi) = 1 + b \sin^2(ms + \phi). \quad (43)$$

After substituting the material functions (42) and (43) into Eq. (10) we get

$$\begin{aligned} \frac{d^2 U(s)}{ds^2} + \frac{am \sin(2ms + \phi)}{1 - j\chi + a \sin^2(ms + \phi)} \frac{dU(s)}{ds} \\ + \left[ K_I^2 \frac{1 + b \sin^2(ms + \phi)}{1 - j\chi + a \sin^2(ms + \phi)} - x^2 \right] U(s) = 0, \end{aligned} \quad (44)$$

By introducing the following substitution

$$\sigma = \sin^2(ms - \phi) \quad (45)$$

it is possible to transform Eq. (44) into the Heun's differential equation

$$\begin{aligned} \frac{d^2 U}{d\sigma^2} + \left( \frac{1}{2\sigma} + \frac{1}{2(\sigma - 1)} + \frac{1}{\sigma + (1 - j\chi)/a} \right) \frac{dU}{d\sigma} \\ - \frac{(K_I^2 b - x^2 a)\sigma + K_I^2 - x^2(1 - j\chi)}{4am^2 \sigma(\sigma - 1)[\sigma + (1 - j\chi)/a]} U(\sigma) = 0, \end{aligned} \quad (46)$$

which corresponds to its canonical form given as

$$\frac{d^2 U}{d\sigma^2} + \left( \frac{\gamma}{\sigma} + \frac{\delta}{\sigma - 1} + \frac{\epsilon}{\sigma - q} \right) \frac{dU}{d\sigma} + \frac{\alpha\beta\sigma - g}{\sigma(\sigma - 1)(\sigma - q)} U(\sigma) = 0, \quad (47)$$

where  $\alpha, \beta, \gamma, \delta, \epsilon$  are generally complex exponent parameters that satisfy the (Fuchsian) condition (see e.g. [50])

$$1 + \alpha + \beta = \gamma + \delta + \epsilon. \quad (48)$$

The parameter  $g \in \mathbb{C}$  is an accessory parameter which does not influence the exponent parameters.

The general solution of Heun's equation in the vicinity of the regular singular point  $\sigma_0 = 0$  can be written as (see e.g. (A.14))

$$\begin{aligned} U(\sigma) &= A_1 H\ell(q, g; \alpha, \beta, \gamma, \delta; \sigma) + \\ &A_2 \sigma^{1-\gamma} H\ell(q, (q\delta + \epsilon)(1 - \gamma) + g; \alpha + 1 - \gamma, \beta + 1 - \gamma, \\ &2 - \gamma, \delta; \sigma) \equiv \\ &A_1 H\ell(q_1, g_1; \alpha_1, \beta_1, \gamma_1, \delta_1; \sigma) \\ &+ A_2 \sigma^{1-\gamma_1} H\ell(q_2, g_2; \alpha_2, \beta_2, \gamma_2, \delta_2; \sigma) \equiv \\ &A_1 H_{11}(\sigma) + A_2 \sigma^{1-\gamma_1} H_{12}(\sigma); \quad |\sigma| < 1, \end{aligned} \quad (49)$$

where  $A_1, A_2$  are integration constants and  $H\ell$  denotes the local Heun function, see (A.8).

By comparing Eq. (46) with its canonical form (47) and employing the condition (48) we get

$$\gamma = \frac{1}{2}, \quad \delta = \frac{1}{2}, \quad \epsilon = 1, \quad g = \frac{K_I^2 - x^2(1 - j\chi)}{4am^2}, \quad q = -\frac{1 - j\chi}{a}, \quad (50)$$

$$\alpha + \beta = 1, \quad \alpha\beta = -\frac{K_I^2 b - x^2 a}{4am^2}. \quad (51)$$

By solving the system of Eqs. (51) we can write

$$\alpha = \frac{1}{2} + \frac{1}{2} \sqrt{1 + \frac{K_I^2 b - x^2 a}{am^2}}, \quad \beta = \frac{1}{2} - \frac{1}{2} \sqrt{1 + \frac{K_I^2 b - x^2 a}{am^2}}. \quad (52)$$

By substituting from the relations (45), (50) and (52) into the solution (49) we obtain the general solution of Eq. (44):

$$U(s) = A_1 H\ell \left( -\frac{1 - j\chi}{a}, \frac{K_I^2 - x^2(1 - j\chi)}{4am^2}, \frac{1}{2} + \frac{1}{2} \sqrt{1 + \frac{K_I^2 b - x^2 a}{am^2}}, \right.$$



$$\frac{1}{2} - \frac{1}{2} \sqrt{1 + \frac{K_I^2 b - \kappa^2 a}{am^2}}, \frac{1}{2}, \frac{1}{2}; \sin^2(ms + \phi) \Bigg) + A_2 \sin(ms + \phi) H \ell \left( -\frac{1 - j\chi}{a}, \frac{m^2(2a - (1 - j\chi)) + K_I^2 - \kappa^2(1 - j\chi)}{4am^2}, 1 + \frac{1}{2} \sqrt{1 + \frac{K_I^2 b - \kappa^2 a}{am^2}}, 1 - \frac{1}{2} \sqrt{1 + \frac{K_I^2 b - \kappa^2 a}{am^2}}, \frac{3}{2}, \frac{1}{2}, \sin^2(ms + \phi) \right) \equiv A_1 H_{11}(s) + A_2 \sin(ms + \phi) H_{12}(s); \sin^2(ms + \phi) < 1. \tag{53}$$

As the local Heun functions are evaluable only for arguments lying in the interval [0, 1), the condition  $\sin^2(ms + \phi) < 1$  in Eq. (53) has to be satisfied.

Note that for zero values of the argument of local Heun functions and their derivatives, the following holds:

$$H_{11}(0) = H_{12}(0) = 1, \quad \left( \frac{dH_{11}(s)}{ds} \right)_{s=0} = m \sin(\phi) \frac{g_1}{\gamma_1 q_1}$$

and  $\left( \frac{dH_{12}(s)}{ds} \right)_{s=0} = m \sin(\phi) \frac{g_2}{\gamma_2 q_2}.$  (54)

Note, for example, that the mathematical software Maple (version 10 and higher) and Mathematica (version 12 and higher) can be used to evaluate the local Heun functions and their derivatives.

**6. Analytic continuation of the general solution of Heun’s equation and Bloch waves**

Given our objectives, it may be necessary to determine the solution of the Heun equation for the  $\sigma = 1$  case, which cannot be obtained using the local Heun functions. To do so, it will be necessary to extend the general solution and its derivatives to cover this scenario through analytic continuation.

To resolve the problem the following variable transformation

$$\bar{\sigma} = 1 - \sigma \tag{55}$$

is used. This means that the neighborhood of  $\sigma = 1$  is transformed into the neighborhood of  $\sigma = 0$ . Using the transformation (55) the Heun’s Eq. (47) with the parameters  $(q, g, \alpha, \beta, \gamma, \delta)$  can be rewritten into the following form:

$$\frac{d^2 U}{d\bar{\sigma}^2} + \left( \frac{\tilde{\gamma}}{\bar{\sigma}} + \frac{\tilde{\delta}}{\bar{\sigma} - 1} + \frac{\tilde{\epsilon}}{\bar{\sigma} - \tilde{q}} \right) \frac{dU}{d\bar{\sigma}} + \frac{\tilde{\alpha}\tilde{\beta}\tilde{\sigma} - \tilde{g}}{\bar{\sigma}(\bar{\sigma} - 1)(\bar{\sigma} - \tilde{q})} U(\bar{\sigma}) = 0, \tag{56}$$

where

$$\tilde{q} = 1 - q, \quad \tilde{g} = \alpha\beta - g, \quad \tilde{\alpha} = \alpha, \quad \tilde{\beta} = \beta, \quad \tilde{\delta} = \gamma, \quad \tilde{\gamma} = \delta. \tag{57}$$

The general solution of Eq. (56) is

$$U(\bar{\sigma}) = \tilde{A}_1 H \ell(\tilde{q}, \tilde{g}; \tilde{\alpha}, \tilde{\beta}, \tilde{\gamma}, \tilde{\delta}; \bar{\sigma}) + \tilde{A}_2 \bar{\sigma}^{1-\tilde{\gamma}} H \ell(\tilde{q}, (\tilde{q}\tilde{\delta} + \tilde{\epsilon})(1 - \tilde{\gamma}) + \tilde{g}; \tilde{\alpha} + 1 - \tilde{\gamma}, \tilde{\beta} + 1 - \tilde{\gamma}, 2 - \tilde{\gamma}, \tilde{\delta}; \bar{\sigma}),$$

$|\bar{\sigma}| < 1,$  (58)

where  $M$  and  $N$  are the integration constants. This solution also represents the solution of the model Eq. (47) around the singular point  $\sigma = 1$  (including this point).

Substituting from the relations (45) into the solution (58) we can write the general solution of Eq. (44) as

$$U(s) = \tilde{A}_1 H \ell(\tilde{q}, \tilde{g}; \tilde{\alpha}, \tilde{\beta}, \tilde{\gamma}, \tilde{\delta}; \cos^2(ms + \phi)) + \tilde{A}_2 \cos(ms + \phi) H \ell(\tilde{q}, (\tilde{q}\tilde{\delta} + \tilde{\epsilon})(1 - \tilde{\gamma}) + \tilde{g}; \tilde{\alpha} + 1 - \tilde{\gamma}, \tilde{\beta} + 1 - \tilde{\gamma}, 2 - \tilde{\gamma}, \tilde{\delta}; \cos^2(ms + \phi)) \equiv \tilde{A}_1 H_{21}(s) + \tilde{A}_2 \cos(ms + \phi) H_{22}(s), \quad \cos^2(ms + \phi) < 1, \tag{59}$$

In what follows, we shall make the assumption that the characteristic length is equivalent to the width of the inhomogeneous layer being studied, i.e.  $\ell = W$ .

In general, it is not possible to obtain a general solution to Eq. (44) over the entire interval  $s \in [0, 1]$  using only Eq. (53). This is because every point  $s_n = (\pi/2 - \phi + n\pi)/m$  ( $n \in \mathbb{Z}$ ) represents a singular point, where the solution based on local Heun functions does not converge. To address this issue, Eq. (58) must also be used in the vicinity of these singular points. Additionally, the integration constants must be calculated to ensure that the solution is continuous and smooth. This situation is illustrated in Fig. 2, assuming  $m = \pi$  and  $\phi = 0$  for the rest of this paper, where the singular point is at  $s = 1/2$ . Therefore, the solution must be divided into three parts for the respective intervals  $[0, s_1]$ ,  $[s_1, s_2]$ ,  $[s_2, 1]$ , where  $s_1 \in (0; 1/2)$  and  $s_2 \in (1/2; 1)$ . The two linearly independent solutions of Eq. (44) can then be expressed as

$$v(s) = \begin{cases} H_{11}(s); & 0 \leq s < s_1, \\ M_{11}H_{21}(s) + N_{11} \cos(\pi s)H_{22}(s) & s_1 \leq s < s_2, \\ M_{11}H_{12}(s) + N_{12} \sin(\pi s)H_{12}(s) & s_2 \leq s \leq 1. \end{cases} \tag{60}$$

$$w(s) = \begin{cases} \sin(\pi s)H_{12}(s)/\pi; & 0 \leq s < s_1, \\ M_{21}H_{21}(s) + N_{21} \cos(\pi s)H_{22}(s) & s_1 \leq s < s_2, \\ M_{22}H_{12}(s) + N_{22} \sin(\pi s)H_{12}(s) & s_2 \leq s \leq 1. \end{cases} \tag{61}$$

where the integration constants  $M_{ij}(K_I, a, b)$  and  $N_{ij}(K_I, a, b)$  are calculated such that both the functions  $v(s)$  and  $w(s)$  are continuous and smooth as mentioned above. Note that the integration constants  $M_{ij}$  and  $N_{ij}$  do not depend on  $s_1$  and  $s_2$ .

The functions  $v(s)$  and  $w(s)$  represent the normalized solution of Eq. (44) and it holds for them that

$$v(0) = 1, \quad v'(0) = 0, \quad w(0) = 0, \quad w'(0) = 1, \tag{62}$$

where the prime represents the derivative with respect to  $s$ .

The general solution of Eq. (44) can then be expressed as

$$U(s) = Av(s) + Bw(s), \quad s \in [0, 1], \tag{63}$$

where  $A$  and  $B$  are integration constants.

To gain insight into the behavior of elastic waves in locally periodic structures, such as a finite phononic crystal composed of  $N$  repetitions of a basic unit cell (see Fig. 3), the Floquet theory can be employed. This powerful approach allows us to express the general solution of Eq. (44) in terms of Bloch waves, as explained in Appendix B. Specifically, the Floquet multipliers can be expressed as follows:

$$\lambda_{1,2} = \frac{h \pm \sqrt{h^2 - 4}}{2}, \tag{64}$$

where  $h = v(1) + w'(1)$ . Then the following applies for the Bloch waves in the first cell (i.e. for  $s \in [0, 1]$ ):

$$F_{1,2}(s) = v(s) + \frac{\lambda_{1,2} - v(1)}{w(1)} w(s), \tag{65}$$

see Eq. (B.11). According to the basic property of the Bloch waves (see Eq. (B.5)) the Bloch waves in the whole crystal (i.e.  $s \in [0, N]$ ) can then be expressed as

$$F_{1,2}(s) = \lambda_{1,2}^{\lfloor s \rfloor} F_{1,2}(s - \lfloor s \rfloor), \tag{66}$$

where  $\lfloor s \rfloor$  represents the greatest integer less than or equal to  $s$ . Hence, the general solution of Eq. (44) for the whole crystal can be written as a linear combination of the two Bloch waves:

$$U(s) = CF_1(s) + DF_2(s), \quad s \in [0, N], \tag{67}$$

where  $C$  and  $D$  are the integration constants.

To describe the propagation of waves in both the forward and backward directions, we can use the functions  $U_+(s)$  and  $U_-(s)$ , respectively. These functions can be expressed using the relations (25) and (26) as

$$U_{\pm}(s) = \frac{1}{2} [CF_1(s) + DF_2(s) \pm \eta(s)Q(s)(CF_1'(s) + DF_2'(s))], \quad s \in [0, N]. \tag{68}$$

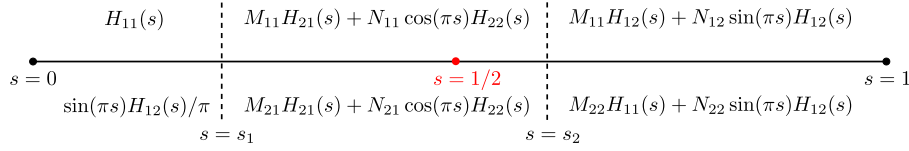


Fig. 2. Mutual coupling of solutions at points  $s_1$  and  $s_2$ .

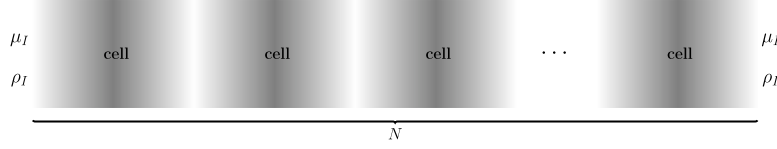


Fig. 3. Phononic crystal composed of  $N$  FG material cells.

### 7. Computation of selected quantities and verification of found analytical solutions

To calculate the reflection and transmission coefficients, we must determine the integration constants  $C$  and  $D$  in Eq. (68). We can assume a plane wave of unit amplitude approaching the crystal from the left in the following form:

$$U_i = \exp \left[ jK_I \sqrt{\frac{1 - \sin^2(\theta_i)}{1 - j\chi}} s \right], \quad (69)$$

where  $\theta_i$  is the angle of incidence, see Fig. 1.

The integration constants  $C$  and  $D$  can be determined by solving the following system of equations (representing the boundary conditions, see Section 2):

$$1 + \mathcal{R}_0 = U(s = 0), \quad (70)$$

$$jK_I \sqrt{\frac{1 - \sin^2(\theta_i)}{1 - j\chi}} (1 - \mathcal{R}_0) = U'(s = 0), \quad (71)$$

$$U_-(s = N) = 0, \quad (72)$$

where  $\mathcal{R}_0$  is the reflection coefficient at  $s = 0$ . The first two equations, (70) and (71), represent the continuity conditions for the wave solution at  $s = 0$ . The third equation, (72), must also hold since the reflection coefficient at  $s = N$  must be equal to 0, as both the density and the shear modulus are continuous and have zero derivative at this point. Solving this system of equations gives us the integration constants  $C$  and  $D$ , and completes the wave solution for the entire problem. The general spatially and frequency dependent reflection  $\mathcal{R}(s, \omega)$  and transmission  $\mathcal{T}(s, \omega)$  coefficients can now be expressed as

$$\mathcal{R}(s, \omega) = \frac{U_-(s)}{U_+(s)}, \quad \mathcal{T}(s, \omega) = \frac{U_+(s)}{U_+(0)}, \quad s \in [0, N], \quad (73)$$

whereas  $\mathcal{R}(0, \omega) \equiv \mathcal{R}_0$  from Eqs. (70) and (71).

The reflection coefficient  $\mathcal{R}(s_0, \omega)$ , where  $s_0 \in [0, 1]$ , is calculated based on the relation (73) and represents the reflection coefficient inside the FG layer at  $s_0$  (for more information, refer to e.g., [51]).

To demonstrate the correctness of the found exact analytical solution, the frequency dependencies of the reflection coefficient moduli at the point  $s = 0$  for FG material ( $M_I = \text{Al}$ ,  $M_{II} = \text{Al}_2\text{O}_3$ ) are compared in Figure Fig. 4. Both normal incidence (Fig. 4(a)) and oblique incidence (Fig. 4(b)) are considered. These dependencies are calculated analytically based on Eq. (73) and also numerically based on the Riccati equation (36) substituted into Eq. (38). The numerical solution of the Riccati equation has been obtained using the standard Runge–Kutta–Fehlberg method (RKF45).

From this comparison, it is evident that both the analytical and numerical results are identical.

Table 1

Material properties of considered constituents.

	Al	Ni	Al <sub>2</sub> O <sub>3</sub>	ZrO <sub>2</sub>
	Aluminium	Nickel	Alumina	Zirconia
$\mu_I$ (GPa)	30	75	150	70
$\rho_I$ (kg m <sup>-3</sup> )	2700	8880	3960	5700
$c_I = \sqrt{\mu_I/\rho_I}$ (m s <sup>-1</sup> )	3333	2906	6155	3504

In order to clearly observe the formation of forbidden bands and the consequences arising from the Floquet–Bloch theory, we will not consider losses in the following part of the text, i.e.,  $\chi = 0$ .

In Fig. 5, the frequency dependencies of both the reflection coefficient and transmission coefficients are plotted for two different angles of incidence, namely  $\theta_i = 0^\circ$  and  $\theta_i = 45^\circ$ . The figures are complemented by the absolute values of the cosine of the Bloch phase (B.3). The regions where  $|\cos(\zeta)| > 1$  represent the forbidden bands (band gaps). These bands are highlighted in gray color in the figures.

Based on the comparison of Figs. 4 and 5, it can be observed that the inclusion of losses leads to a decrease in the values reached by the reflection coefficient module for individual frequencies. Additionally, in the regions corresponding to the forbidden bands, the dependence of the reflection coefficient module on frequency is asymmetric when considering losses.

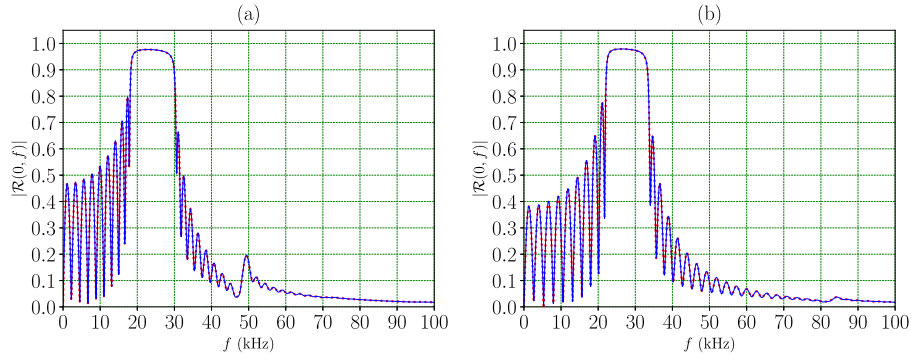
In Fig. 6, spatial dependencies of the absolute, real, and imaginary values of the forward  $U_+(s)$  and backward  $U_-(s)$  displacement waves in the phononic crystal are captured for a frequency  $f = 25$  kHz located within the bandgap. From the figure, it can be observed that for this case,  $\text{Re}[U_+(s)] = -\text{Im}[U_-(s)]$  and  $\text{Im}[U_+(s)] = -\text{Re}[U_-(s)]$ . This implies that  $|\mathcal{R}(s)| = 1$  for  $s \in [0, 10]$ . Once the frequency is chosen outside of the bandgap, the aforementioned equality between the real and imaginary components no longer holds, as shown in Fig. 7.

Fig. 8 shows the spatial dependencies of the absolute, real, and imaginary values of the shear stress  $T(s)$  within the phononic crystal for two frequencies. One frequency (25 kHz) is situated within the band gap, while the other is located outside this band (40 kHz), see Fig. 5. The shear stress is analytically computed using Eq. (19).

In Fig. 9, it is shown how the frequency dependence of the transmission coefficient module of a phononic crystal can be influenced by the choice of material  $M_{II}$  used to fabricate the FG material, while keeping the same geometric parameters (length of the crystal and number of considered units). It is evident that the choice of FG materials not only affects the position of the bandgaps but also their width. The material parameters of the used materials are given in Table 1.

### 8. Conclusion

Our paper aimed to find an exact analytical solution of the model equation that is expressed using the local Heun functions and describes



**Fig. 4.** Comparison of the frequency dependencies of the reflection coefficient moduli at the point  $s = 0$  for FG material ( $M_I = \text{Al}$ ,  $M_{II} = \text{Al}_2\text{O}_3$ , see Table 1) calculated via the numerical solution of the Riccati equation (36) (dotted red line) with the analytical solution based on the relation (73) (solid blue line);  $N = 10$ ,  $W = 0.1 \text{ m}$ ,  $\mu_v = 5 \cdot 10^4 \text{ Pa s}^{-1}$ . (a)  $\theta_i = 0^\circ$ , (b)  $\theta_i = 20^\circ$ .

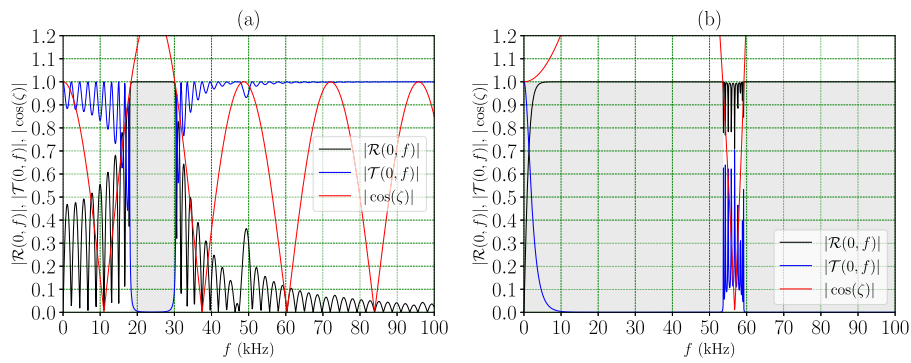


**Fig. 5.** Frequency dependencies of the reflection (solid black line) and transmission (solid blue line) coefficient moduli at the point  $s = 0$  for FG material ( $M_I = \text{Al}$ ,  $M_{II} = \text{Al}_2\text{O}_3$ , see Table 1) calculated based on the relations (73) and corresponding cosines of Bloch phases (B.3) (red line);  $N = 10$ ,  $W = 0.1 \text{ m}$ ,  $\chi = 0$ . (a)  $\theta_i = 0^\circ$ , (b)  $\theta_i = 45^\circ$ .

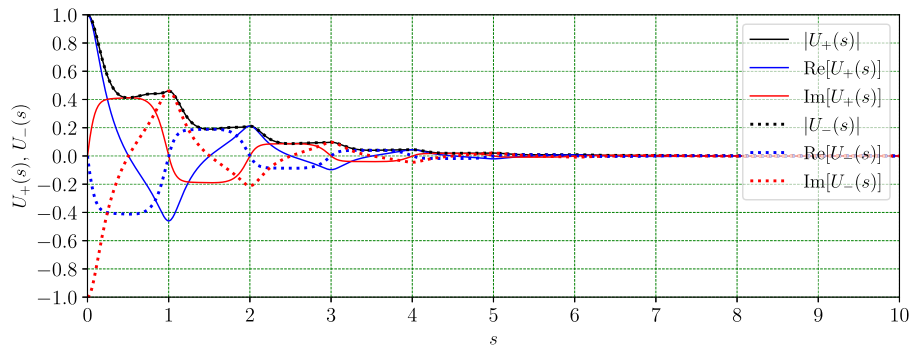


**Fig. 6.** Spatial dependencies of absolute, real, and imaginary values of the forward  $U_+(s)$  and backward  $U_-(s)$  displacement waves within a phononic crystal ( $M_I = \text{Al}$ ,  $M_{II} = \text{Al}_2\text{O}_3$ ) for a frequency located within the forbidden band;  $f = 25 \text{ kHz}$ ,  $N = 10$ ,  $W = 0.1 \text{ m}$ ,  $\chi = 0$ ,  $\theta_i = 0^\circ$ .

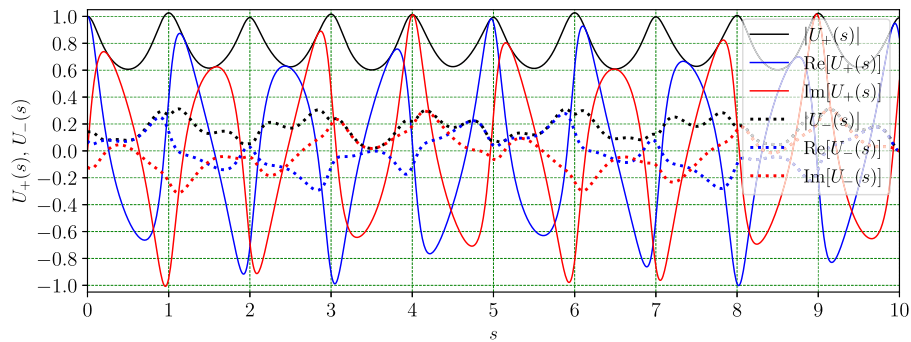


**Fig. 7.** Spatial dependencies of absolute, real, and imaginary values of the forward  $U_+(s)$  and backward  $U_-(s)$  displacement waves within a phononic crystal ( $M_I = \text{Al}$ ,  $M_{II} = \text{Al}_2\text{O}_3$ ) for a frequency outside the forbidden band;  $f = 40 \text{ kHz}$ ,  $N = 10$ ,  $W = 0.1 \text{ m}$ ,  $\chi = 0$ ,  $\theta_i = 0^\circ$ .

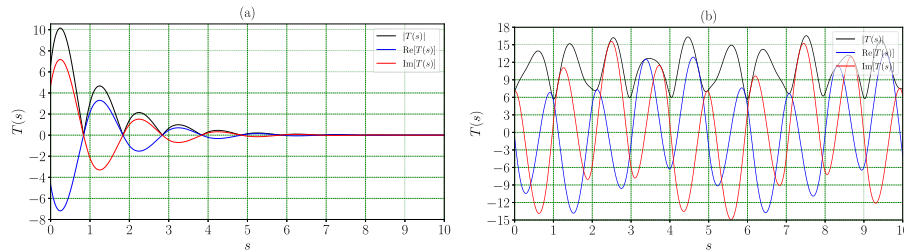


Fig. 8. Spatial dependencies of absolute, real, and imaginary values of the shear stress  $T(s)$  within a phononic crystal ( $M_I = \text{Al}$ ,  $M_{II} = \text{Al}_2\text{O}_3$ ) for two frequencies outside the forbidden band;  $N = 10$ ,  $W = 0.1 \text{ m}$ ,  $\chi = 0$ ,  $\theta_i = 0^\circ$ . (a)  $f = 25 \text{ kHz}$  (inside the forbidden band) (b)  $f = 40 \text{ kHz}$  (outside the forbidden band).

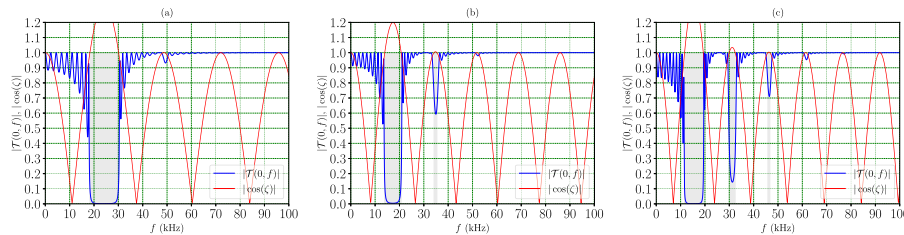


Fig. 9. Frequency dependencies of the transmission (blue line) coefficient moduli at the point  $s = 0$  for three FG materials calculated based on the relation (73) and corresponding cosines of Bloch phases (B.3) (red line);  $N = 10$ ,  $W = 0.1 \text{ m}$ ,  $\chi = 0$ ,  $\theta_i = 0^\circ$ . (a)  $\text{Al} \rightarrow \text{Al}_2\text{O}_3$ , (b)  $\text{Al} \rightarrow \text{Ni}$  (c)  $\text{Al} \rightarrow \text{ZrO}_2$  (see Table 1).

the propagation of linear shear horizontal (SH) waves through an isotropic inhomogeneous layer realized with functionally graded (FG) material, which is a composite of two chosen materials. We considered the scenario where SH waves impinge on the inhomogeneous layer at a specified angle of incidence. The Kelvin–Voigt model was employed to express the losses in the material. The spatial dependence of the material parameters in the propagation direction was formulated using material functions corresponding to the square of the sine function. We selected the trigonometric form of these material functions not only for solvability purposes but also because their periodic nature enables modeling of locally periodic structures, such as phononic crystals.

To obtain the solution for the inhomogeneous layer, we employed a transformation technique to convert the model equation into Heun’s differential equation. This allowed us to express the solution as a linear combination of local Heun functions, with their arguments confined to the open interval  $(-1, 1)$ . However, to achieve a solution that covers the entire spatial period of the material functions (i.e., arguments within the closed interval  $[-1, 1]$ ), we employed an analytic continuation technique through translational transformation. This approach yielded a modified solution providing an exact analytical solution across the entire interval.

Moreover, we employed the wave splitting method in this article to separate the overall displacement field  $U(s)$  into forward  $U_+(s)$  and backward  $U_-(s)$  traveling displacement waves. This enabled us to describe the behavior of SH waves within the inhomogeneous layer (FG material) and calculate both the reflection and transmission coefficients at any point within the inhomogeneous medium.

The periodic nature of the material functions was relatively straightforwardly utilized to find an exact general analytical solution using the Floquet–Bloch theory for the case where an SH wave is incident on a locally periodic FG material at a chosen angle.

To facilitate the verification of the obtained exact analytical solution for the locally periodic structure, we derived the Riccati equation for the introduced impedance from the given model equation. By numerically solving this equation, we were able to readily compute the reflection coefficient at the desired point and frequency. The verification process involved comparing the frequency dependency of the modulus of the reflection coefficient obtained from the numerical solution with the result obtained using the exact analytical solution for the considered locally periodic structure. It should be noted that the derived Riccati equation can also be used for other material functions.

Subsequently, we demonstrated the utilization of the obtained exact analytical solution and the approach based on the wave splitting method in selected computations to analyze the behavior of SH waves in a locally periodic structure. To facilitate comprehension of the text, we provided notes in the Appendix of our article concerning the solution of the Heun’s differential equation and the utilized Floquet–Bloch theory.

In contrast to a number of previously published exact analytical solutions that consider different material functions, the presented solution is not limited to the very specific case where the material functions for shear modulus and mass density are equal, which results in a constant propagation velocity. The found general analytical solution can be used not only for calculating the transmission properties of locally periodic structures but can also be applied with various boundary conditions as needed for the solved problems, for example, for Love surface waves. The solution presented by us can be used not only for studying the behavior of SH waves in locally periodic structures but can also serve as a benchmark for various numerical solutions. In our work, we demonstrated that through a suitable transformation, the solved problem can be reduced to solving the Heun’s differential equation, which progressively finds broader application in various areas of physics. Building upon our work, it is possible to further reduce the problem to solving the Heun’s differential equation for other material functions, for example, expressed using hyper-geometric functions.

The fundamental outcomes of our work can be summarized as follows. We presented a new comprehensive general solution of the model equation describing the propagation of linear harmonic SH waves in a locally inhomogeneous isotropic layer. Using the Floquet–Bloch theory, we have applied this solution to the case where the inhomogeneous medium is represented by a locally periodic structure. We have demonstrated how, in the frequency domain, this solution can be separated into forward and backward displacement traveling waves using the wave splitting method. This method can be straightforwardly employed not only for computing reflection and transmission coefficients at any point within the considered inhomogeneous structure but also for studying elastic fields within this structure.

Furthermore, we derived the Riccati equation, which can be relatively easily solved numerically. Consequently, this equation allows us to calculate the transmission properties of the considered inhomogeneous structure not only for the chosen material functions but also for various other cases. Although our work is of a purely theoretical nature,

our results and presented approaches can serve as a foundation not only for further theoretical research but also for modeling various practical needs, such as in geophysics or sensor design.

We expect that these presented results and the chosen approaches will appeal to a broader professional public interested in the utilization of FG materials for particularly influencing the transmission properties of locally periodic structures.

**CRedit authorship contribution statement**

**Antonin Krpensky:** Conceptualization, Methodology, Formal analysis, Investigation, Writing – original draft, Writing – review & editing, Visualization, Validation, Resources. **Michal Bednarik:** Conceptualization, Methodology, Formal analysis, Investigation, Writing – original draft, Writing – review & editing, Visualization, Validation, Resources, Supervision.

**Declaration of competing interest**

The authors declare that they have no known competing financial interests or personal relationships that could have appeared to influence the work reported in this paper.

**Data availability**

No data was used for the research described in the article.

**Acknowledgment**

This work was supported by the Grant Agency of the Czech Republic 22-33896S.

**Appendix A. Heun’s equation and its solution**

To ensure that this paper is self-contained, we provide an overview of Heun’s equation and its degenerate forms in the Appendices.

Heun’s differential equation is the most general second-order differential equation with four regular singular points located at  $z = 0, 1, a, \infty$  (where  $a \neq 0, 1, \infty$ ). The canonical form of the general second-order Heun’s differential equation is:

$$\frac{d^2U}{dz^2} + \left(\frac{\gamma}{z} + \frac{\delta}{z-1} + \frac{\epsilon}{z-a}\right) \frac{dU}{dz} + \frac{\alpha\beta z - h}{z(z-1)(z-a)}U(z) = 0, \tag{A.1}$$

where  $\{\alpha, \beta, \gamma, \delta, \epsilon, h\}$  are parameters, generally complex and arbitrary, linked by the Fuchsian constraint (see e.g. [50])

$$1 + \alpha + \beta = \gamma + \delta + \epsilon. \tag{A.2}$$

The parameter  $h$  is referred to as an accessory (or auxiliary) parameter since it falls outside the domain of the usual Riemann classification scheme. In numerous applications,  $h$  acts as an eigen-parameter and does not influence the exponent parameters  $\alpha, \beta, \gamma, \delta, \epsilon$ . It is worth noting that Heun’s equation is invariant under an interchange of parameters  $\alpha$  and  $\beta$ .

We can write Eq. (A.1) in the following form:

$$\frac{d^2U}{dz^2} + u(z) \frac{dU}{dz} + w(z)U(z) = 0, \tag{A.3}$$

which enables us to introduce the constants

$$u_0 = \lim_{z \rightarrow z_0} (z - z_0)u(z), \tag{A.4}$$

$$w_0 = \lim_{z \rightarrow z_0} (z - z_0)^2w(z). \tag{A.5}$$

For the second order linear differential Eq. (A.3) we can write the characteristic (indicial) equation (see e.g. [50]):

$$\lambda^2 + (u_0 - 1)\lambda + w_0 = 0. \tag{A.6}$$

**Table A.2**

The roots of the indicial equation of Heun’s differential equation.

Regular singular point	Roots
0	$0, 1 - \gamma$
1	$0, 1 - \delta$
$a$	$0, 1 - \epsilon$
$\infty$	$\alpha, \beta$

The roots of characteristic Eq. (A.6) are the exponents which correspond to the regular singular points. We can construct two linearly independent solutions of Eq. (A.1) in the vicinity of the regular singular point  $z_0$  if the roots  $\lambda_1, \lambda_2$  of the characteristic Eq. (A.6) do not differ by a positive integer<sup>1</sup>  $s = \lambda_1 - \lambda_2$  if  $Re(\lambda_1) \geq Re(\lambda_2)$  (see e.g. [50,52]). The two linearly independent solutions have different analytic properties at  $z = z_0$ . The two linearly independent solutions  $U_1$  and  $U_2$  of Eq. (A.3) can be written in the form of the Frobenius series (see e.g. [50,52])

$$U_k(\lambda_k; z) = \sum_{n=0}^{\infty} c_n^{(\lambda_k)} (z - z_0)^{n+\lambda_k}, \quad k = 1, 2, \tag{A.7}$$

where the coefficients  $c_n^{(\lambda_k)}$  are calculated by means the three-term recursion (A.11) and  $\lambda_{1,2}$  are the roots of the indicial Eq. (A.6).

The solution for the regular singular point  $z_0 = 0$  is considered fundamental because if it is not, a transformation of the independent variable  $z \rightarrow z - z_0$  can be applied to make it so.

To find a solution of Heun’s differential equation in the vicinity of the regular singular point  $z_0 = 0$ , we evaluate the limits (A.4) and (A.5), which yield  $u_0 = \gamma$  and  $w_0 = 0$ . This solution is analytic for  $|z| < 1$ , and the corresponding characteristic Eq. (A.6) yields the roots  $\lambda_1 = 0$  and  $\lambda_2 = 1 - \gamma$ .

The roots of the characteristic equations for all regular singular points are summarized in Table A.2 (see e.g., [50,52]).

The solution of Heun’s equation for  $\lambda_1 = 0$  about the singular point  $z_0 = 0$ , normalized to unity, is called the local Heun function and it is usually denoted by  $H\ell(a, h; \alpha, \beta, \gamma, \delta; z)$ , i.e.

$$H\ell(a, h; \alpha, \beta, \gamma, \delta; z) \equiv U_1(\lambda_1; z) = \sum_{n=0}^{\infty} c_n^{(\lambda_1)} z^n, \quad |z| < 1 \tag{A.8}$$

and its derivative (the prime local Heun function) is given as

$$\frac{d}{dz} H\ell(a, h; \alpha, \beta, \gamma, \delta; z) \equiv H\ell'(a, h; \alpha, \beta, \gamma, \delta; z) = \sum_{n=1}^{\infty} n c_n^{(\lambda_1)} z^{n-1}, \quad |z| < 1. \tag{A.9}$$

After substitution of the series (A.7) into Heun’s equation (A.3) we obtain the following three-term recursion (see e.g. [52,53])

$$c_{-1}^{(\lambda_k)} = 0, \quad c_0^{(\lambda_k)} = 1, \tag{A.10}$$

$$c_{n+1}^{(\lambda_k)} = A_n c_n^{(\lambda_k)} + B_n c_{n-1}^{(\lambda_k)} = 0, \quad n \geq 0, \tag{A.11}$$

where

$$A_n = \frac{(n + \lambda_k)[(n + \lambda_k - 1 + \gamma)(1 + a) + a\delta + \epsilon] + h}{a(n + \lambda_k + 1)(n + \lambda_k + \gamma)},$$

$$B_n = -\frac{(n + \lambda_k - 1 + \alpha)(n + \lambda_k - 1 + \beta)}{a(n + \lambda_k + 1)(n + \lambda_k + \gamma)}, \quad k = 1, 2; \quad \lambda_1 = 0,$$

$$\lambda_2 = 1 - \gamma. \tag{A.12}$$

Using relations (A.10) and (A.11), we can compute the coefficients of the local Heun function that corresponds to the first solution of Heun’s equation when  $k = 1$ . Similarly, we can use the recursive relation for  $k = 2$  to obtain the second solution of Heun’s equation.

<sup>1</sup> If both roots are identical,  $\lambda_1 = \lambda_2$ , only one solution is obtained.

However, to simplify the process and use the recursion (A.11) for the local Heun function, we can apply an  $F$ -homotopic transformation (elementary power transformation), as described in [52,53]. This transformation leads to the following equality:

$$U_2(\lambda_2; z) = z^{1-\gamma} H\ell(a, (a\delta + \epsilon)(1 - \gamma) + h; \alpha + 1 - \gamma, \beta + 1 - \gamma, 2 - \gamma, \delta; z) = z^{1-\gamma} \sum_{n=0}^{\infty} c_n^{(\lambda_2)} z^n, \quad |z| < 1, \quad (A.13)$$

where it is assumed that  $\gamma$  is not an integer.

Accounting for the above mentioned facts, we can write the general solution of Heun's equation (A.1) as

$$U(z) = C_1 H\ell(a, h; \alpha, \beta, \gamma, \delta; z) + C_2 z^{1-\gamma} H\ell(a, (a\delta + \epsilon)(1 - \gamma) + h; \alpha + 1 - \gamma, \beta + 1 - \gamma, 2 - \gamma, \delta; z), \quad (A.14)$$

where  $C_1$  and  $C_2$  are integration constants.

### Appendix B. Bloch waves within one-dimensional phononic crystal

Because Eq. (10) is transitionally invariant, i.e., it is invariant under a translation with  $d = 1$  along  $s$ , we can express  $U(s)$  within a periodic phononic crystal based on the Floquet theory (see, e.g., [54–56]). Before, we must define the notions of the characteristic equation and characteristic exponent associated with Eq. (44). The characteristic equation is:

$$\lambda^2 - [v(d) + w'(d)]\lambda + 1 = 0, \quad (B.1)$$

and the characteristic exponent (the Bloch wave number)  $\kappa$  is a number that satisfies equations:

$$\exp(\pm j\kappa d) = \lambda_{1,2} \Rightarrow \lambda_1 \lambda_2 = 1, \quad (B.2)$$

where  $\lambda_{1,2}$  are the roots of characteristic Eq. (B.1).

It is clear that  $\kappa d$  is defined up to an integer multiple of  $2\pi$ , and based on the relation (B.2), we can write the Bloch phase  $\zeta$  as:

$$2 \cos(\zeta) = 2 \cos[\kappa(k)d] = v(d) + w'(d), \quad (B.3)$$

which determines the band structure of the photonic crystal.

According to the Floquet theory, if roots  $\lambda_1$  and  $\lambda_2$  of characteristic Eq. (B.1) differ from each other, then Eq. (44) has two linearly independent solutions (see, e.g., [56]):

$$F_{1,2}(s) = P_{1,2}(s) \exp(\pm j\kappa s), \quad (B.4)$$

where  $F_{1,2}(s)$  are the Bloch waves and  $P_{1,2}(s)$  are periodic functions with the periodicity of the structure, i.e.,

$$P_{1,2}(s + d) = P_{1,2}(s). \quad (B.5)$$

According to Eqs. (B.4) and (B.5), the Bloch waves satisfy the translational property:

$$F_{1,2}(s + d) = \lambda_{1,2} F_{1,2}(s). \quad (B.6)$$

The periodic functions  $P_{1,2}(s)$  represent the wave function behavior inside a single cell. The Bloch waves  $F_{1,2}(s)$  are one-dimensional traveling waves of spatial frequency  $\kappa$  that are modulated in amplitude and phase in a periodic manner by functions  $P_{1,2}(s)$ . The complex exponential components ( $\exp(\pm j\kappa s)$ ) of the Bloch waves alone determine the net changes in phase and amplitude from a position in one cell to the corresponding position in a neighboring cell. The phase change is given by  $\text{Re}(\kappa)$  and the amplitude change by  $\text{Im}(\kappa)$ . Whereas  $P_{1,2}(s)$  are periodic,  $F_{1,2}(s)$  are generally aperiodic. Only some degenerate cases exist in which the Bloch waves are periodic.

Thus, for  $\lambda_1 \neq \lambda_2$ , the general solution of Eq. (44) can be expressed with the Bloch functions as:

$$U(s) = C F_1(s) + D F_2(s). \quad (B.7)$$

If  $\lambda_1 \neq \lambda_2$ , the Bloch phase can be either real, i.e.,  $|\cos(\zeta)| < 1$ , or complex, i.e.,  $|\cos(\zeta)| > 1$ . The Bloch phase is real in allowed bands and complex in bandgaps (see, e.g., [55]).

If characteristic Eq. (B.1) has a double root  $\lambda_1 = \lambda_2 \equiv \lambda = \pm 1$  (identical Bloch waves), then Eq. (44) has the following linearly independent solutions:

$$F(s) = P_1(s) \exp(j\kappa s), \quad (B.8)$$

and

$$G(s) = [s P_1(s) + P_2(s)] \exp(j\kappa s). \quad (B.9)$$

It is not difficult to ensure that solution  $G(s)$  (the hybrid Floquet mode) has the following translational property (see, e.g., [56]):

$$G(s + d) = \lambda G(s) + \lambda d F(s). \quad (B.10)$$

The double root corresponds to bandedges, i.e., boundaries between allowed bands and bandgaps and in this case  $|\cos(\zeta)| = 1$ .

For the considered photonic crystal,  $v'(d)$  and  $v(d)$  are never simultaneously zero in the investigated frequency range, which allows us to express the Bloch waves as (see, e.g., [55,56]):

$$F_{1,2}(s) = v(s) + \frac{\lambda_{1,2} - v(d)}{w(d)} w(s), \quad \text{if } v(d) \neq 0, \quad (B.11)$$

$$F_{1,2}(s) = w(s) + \frac{\lambda_{1,2} - w'(d)}{v'(d)} v(s), \quad \text{if } v'(d) \neq 0. \quad (B.12)$$

For  $\lambda_1 = \lambda_2 \equiv \lambda = \pm 1$ , the Bloch waves are identical,  $F_1(s) = F_2(s) \equiv F(s)$ , and the second linearly independent solution is:

$$G(s) = \frac{\lambda d}{w(d)} w(s), \quad \text{if } w(d) \neq 0, \quad (B.13)$$

$$G(s) = \frac{\lambda d}{v'(d)} v(s), \quad \text{if } v'(d) \neq 0. \quad (B.14)$$

In addition, in the investigated frequency range, apart from the bandedges,  $v'(d) \neq 0$  and  $w(d) \neq 0$  are valid and enable us to employ only Bloch waves (B.11).

In our case, it is easy to see that  $v(d) = w'(d)$ . Thus, we can write the cosine of the Bloch phase  $\zeta$  as  $\cos(\zeta) = v(d)$ .

### References

- [1] Kubrusly AC, Freitas MA, von der Weid JP, Dixon S. Interaction of SH guided waves with wall thinning. *NDT E Int* 2019;101:94–103. <http://dx.doi.org/10.1016/j.ndteint.2018.10.007>.
- [2] Huan Q, Chen M, Li F. A high-sensitivity and long-distance structural health monitoring system based on bidirectional SH wave phased array. *Ultrasonics* 2020;108:106190. <http://dx.doi.org/10.1016/j.ultras.2020.106190>.
- [3] Miao H, Li F. Shear horizontal wave transducers for structural health monitoring and nondestructive testing: A review. *Ultrasonics* 2021;114:106355. <http://dx.doi.org/10.1016/j.ultras.2021.106355>.
- [4] Josse F, Bender F, Cernosek RW. Guided shear horizontal surface acoustic wave sensors for chemical and biochemical detection in liquids. *Anal Chem* 2001;73(24):5937–44. <http://dx.doi.org/10.1021/ac010859e>.
- [5] Ramshani Z, Reddy AS, Narakathu BB, Wabeke JT, Obare SO, Atashbar MZ. SH-SAW sensor based microfluidic system for the detection of heavy metal compounds in liquid environments. *Sensors Actuators B* 2015;217:72–7. <http://dx.doi.org/10.1016/j.snb.2014.12.026>.
- [6] Djeran-Maigre I, Kuznetsov SV. Velocities, dispersion, and energy of SH-waves in anisotropic laminated plates. *Acoust Phys* 2014;60(2):200–7. <http://dx.doi.org/10.1134/s106377101402002x>.
- [7] Kowalczyk S, Matysiak S, Perkowski DM. On some problems of SH wave propagation in inhomogeneous elastic bodies. *J Theoret Appl Mech* 2016;1125. <http://dx.doi.org/10.15632/jtam-pl.54.4.1125>.
- [8] Wuttke F, Fontara IK, Dineva P, Rangelov T. SH-wave propagation in a continuously inhomogeneous half-plane with free-surface relief by BIEM. *ZAMM - J Appl Math Mech / Z Angew Math Mech* 2014;95(7):714–29. <http://dx.doi.org/10.1002/zamm.201300198>.

- [9] Bednarik M, Cervenka M. Description of waves in inhomogeneous domains using Heun's equation. *Waves Random Complex Media* 2017;28(2):236–52. <http://dx.doi.org/10.1080/17455030.2017.1338788>.
- [10] Bian Z, Zhang S, Zhou X. Band gap manipulation of functionally graded phononic crystal by periodical thermal field. *Mech Adv Mater Struct* 2019;28(12):1288–92. <http://dx.doi.org/10.1080/15376494.2019.1663321>.
- [11] Taljanovic MS, Gimber LH, Becker GW, Latt LD, Klausner AS, Melville DM, Gao L, Witte RS. Shear-wave elastography: Basic physics and musculoskeletal applications. *RadioGraphics* 2017;37(3):855–70. <http://dx.doi.org/10.1148/rg.2017160116>.
- [12] Himasekhar Sai B. A review on functionally gradient materials (FGMs) and their applications. *Int J Curr Eng Technol* 2018;8(01). <http://dx.doi.org/10.14741/ijcet.v8i01.10894>.
- [13] Mohammadi M, Rajabi M, Ghadiri M. Functionally graded materials (FGMs): A review of classifications, fabrication methods and their applications. *Process Appl Ceram* 2021;15(4):319–43. <http://dx.doi.org/10.2298/pac2104319m>.
- [14] Garg A, Belarbi M-O, Chalak H, Chakrabarti A. A review of the analysis of sandwich FGM structures. *Compos Struct* 2021;258:113427. <http://dx.doi.org/10.1016/j.compstruct.2020.113427>.
- [15] Hirane H, Belarbi M-O, Houari MSA, Tounsi A. On the layerwise finite element formulation for static and free vibration analysis of functionally graded sandwich plates. *Eng Comput* 2021;38(S5):3871–99. <http://dx.doi.org/10.1007/s00366-020-01250-1>.
- [16] Garg A, Belarbi M-O, Tounsi A, Li L, Singh A, Mukhopadhyay T. Predicting elemental stiffness matrix of FG nanoplates using Gaussian Process Regression based surrogate model in framework of layerwise model. *Eng Anal Bound Elem* 2022;143:779–95. <http://dx.doi.org/10.1016/j.enganabound.2022.08.001>.
- [17] Vinh PV, Tounsi A, Belarbi M-O. On the nonlocal free vibration analysis of functionally graded porous doubly curved shallow nanoshells with variable nonlocal parameters. *Eng Comput* 2022;39(1):835–55. <http://dx.doi.org/10.1007/s00366-022-01687-6>.
- [18] Garg A, Chalak HD, Li L, Belarbi M-O, Sahoo R, Mukhopadhyay T. Vibration and buckling analyses of sandwich plates containing functionally graded metal foam core. *Acta Mech Solida Sin* 2022;35(4):1–16. <http://dx.doi.org/10.1007/s10338-021-00295-z>.
- [19] Ding H-X, Eltaher M, She G-L. Nonlinear low-velocity impact of graphene platelets reinforced metal foams cylindrical shell: Effect of spinning motion and initial geometric imperfections. *Aerosp Sci Technol* 2023;140:108435. <http://dx.doi.org/10.1016/j.ast.2023.108435>.
- [20] Zhang Y-W, She G-L, Ding H-X. Nonlinear resonance of graphene platelets reinforced metal foams plates under axial motion with geometric imperfections. *Eur J Mech A Solids* 2023;98:104887. <http://dx.doi.org/10.1016/j.euromechsol.2022.104887>.
- [21] She G-L, Wu F. Wave propagation in double nano-beams in thermal environments using the reddy's high-order shear deformation theory. *Adv Nano Res* 2022.
- [22] Vinh PV, Belarbi M-O, Tounsi A. Wave propagation analysis of functionally graded nanoplates using nonlocal higher-order shear deformation theory with spatial variation of the nonlocal parameters. *Waves Random Complex Media* 2022;1–21. <http://dx.doi.org/10.1080/17455030.2022.2036387>.
- [23] Qu Z, Shen X, Cao X. Nondestructive evaluation of functionally graded subsurface damage on cylinders in nuclear installations based on circumferential SH waves. *Sci Technol Nucl Install* 2016;2016:1–7. <http://dx.doi.org/10.1155/2016/3035180>.
- [24] Chen S, Zhang Y, Hao C, Lin S, Fu Z. Functionally graded materials for impedance matching in elastic media. *Phys Lett A* 2014;378(1–2):77–81. <http://dx.doi.org/10.1016/j.physleta.2013.10.040>.
- [25] Müller E, Drašar Č, Schilz J, Kaysser W. Functionally graded materials for sensor and energy applications. *Mater Sci Eng A* 2003;362(1–2):17–39. [http://dx.doi.org/10.1016/s0921-5093\(03\)00581-1](http://dx.doi.org/10.1016/s0921-5093(03)00581-1).
- [26] Liew KM, Sivashanker S, He XQ, Ng TY. The modelling and design of smart structures using functionally graded materials and piezoelectrical sensor/actuator patches. *Smart Mater Struct* 2003;12(4):647–55. <http://dx.doi.org/10.1088/0964-1726/12/4/316>.
- [27] Farhat M, Guenneau S, Enoch S. Ultrabroadband elastic cloaking in thin plates. *Phys Rev Lett* 2009;103(2). <http://dx.doi.org/10.1103/physrevlett.103.024301>.
- [28] Farhat M, Guenneau S, Enoch S, Movchan AB. Cloaking bending waves propagating in thin elastic plates. *Phys Rev B* 2009;79(3). <http://dx.doi.org/10.1103/physrevb.79.033102>.
- [29] Liu G, Han X, Lam K. Stress waves in functionally gradient materials and its use for material characterization. *Composites B* 1999;30(4):383–94. [http://dx.doi.org/10.1016/s1359-8368\(99\)00010-4](http://dx.doi.org/10.1016/s1359-8368(99)00010-4).
- [30] Samadhiya R, Mukherjee A, Schmauder S. Characterization of discretely graded materials using acoustic wave propagation. *Comput Mater Sci* 2006;37(1–2):20–8. <http://dx.doi.org/10.1016/j.commatsci.2005.12.036>.
- [31] Moghaddam AM, Ahmadian M, Kheradpisheh A. Acoustic wave propagation through a functionally graded material plate with arbitrary material properties. *Proc Inst Mech Eng, L* 2013;227:100–10. <http://dx.doi.org/10.1177/1464420712472632>.
- [32] Golub MV, Fomenko S, Bui T, Zhang C, Wang Y-S. Transmission and band gaps of elastic SH waves in functionally graded periodic laminates. *Int J Solids Struct* 2012;49(2):344–54. <http://dx.doi.org/10.1016/j.ijsolstr.2011.10.013>.
- [33] Golub MV, Boström A, Folkow PD. Wave propagation of functionally graded layers treated by recursion relations and effective boundary conditions. *Int J Solids Struct* 2013;50(5):766–72. <http://dx.doi.org/10.1016/j.ijsolstr.2012.11.003>.
- [34] Bian Z, Yang S, Zhou X, Hui D. Band gap manipulation of viscoelastic functionally graded phononic crystal. *Nanotechnol Rev* 2020;9(1):515–23. <http://dx.doi.org/10.1515/ntrev-2020-0042>.
- [35] Jha D, Kant T, Singh R. A critical review of recent research on functionally graded plates. *Compos Struct* 2013;96:833–49. <http://dx.doi.org/10.1016/j.compstruct.2012.09.001>.
- [36] Fomenko S, Golub M, Zhang C, Bui T, Wang Y-S. In-plane elastic wave propagation and band-gaps in layered functionally graded phononic crystals. *Int J Solids Struct* 2014;51(13):2491–503. <http://dx.doi.org/10.1016/j.ijsolstr.2014.03.017>.
- [37] Qian Z-H, Jin F, Kishimoto K, Lu T. Propagation behavior of Love waves in a functionally graded half-space with initial stress. *Int J Solids Struct* 2009;46(6):1354–61. <http://dx.doi.org/10.1016/j.ijsolstr.2008.11.003>.
- [38] Zhang LG, Zhu H, Xie HB, Wang J. Love wave in an isotropic half-space with a graded layer. *Appl Mech Mater* 2013;325–326:252–5. <http://dx.doi.org/10.4028/www.scientific.net/amm.325-326.252>.
- [39] Zhu H, Zhang L, Han J, Zhang Y. Love wave in an isotropic homogeneous elastic half-space with a functionally graded cap layer. *Appl Math Comput* 2014;231:93–9. <http://dx.doi.org/10.1016/j.amc.2013.12.167>.
- [40] Kumar P, Mahanty M, Chattopadhyay A, Singh AK. Green's function technique to study the influence of heterogeneity on horizontally polarised shear-wave propagation due to a line source in composite layered structure. *J Vib Control* 2020;26(9–10):701–12. <http://dx.doi.org/10.1177/1077546319889861>.
- [41] Kumhar R, Kundu S, Pandit DK, Gupta S. Green's function and surface waves in a viscoelastic orthotropic FGM enforced by an impulsive point source. *Appl Math Comput* 2020;382:125325. <http://dx.doi.org/10.1016/j.amc.2020.125325>.
- [42] Chiu T-C, Erdogan F. One-dimensional wave propagation in a functionally graded elastic medium. *J Sound Vib* 1999;222(3):453–87. <http://dx.doi.org/10.1006/j.svi.1998.2065>.
- [43] Han X, Liu G, Lam K, Ohyoshi T. A quadratic layer element for analyzing stress waves in fgms and its application in material characterization. *J Sound Vib* 2000;236. <http://dx.doi.org/10.1006/j.svi.2000.2966>.
- [44] Bednarik M, Cervenka M, Lotton P, Simon L. Analytical solutions for elastic SH-waves propagating through an isotropic inhomogeneous layer. *Compos Struct* 2019;220:875–87. <http://dx.doi.org/10.1016/j.compstruct.2019.04.053>.
- [45] Krpensky A, Bednarik M. Surface Love-type waves propagating through viscoelastic functionally graded media. *J Acoust Soc Am* 2021;150(5):3302–13. <http://dx.doi.org/10.1121/1.50006964>.
- [46] Sahu SA, Saroj PK, Dewangan N. SH-waves in viscoelastic heterogeneous layer over half-space with self-weight. *Arch Appl Mech* 2013;84(2):235–45. <http://dx.doi.org/10.1007/s00419-013-0796-8>.
- [47] De Ryck L, Lauriks W, Fella ZEA, Wirgin A, Groby JP, Leclaire P, Depollier C. Acoustic wave propagation and internal fields in rigid frame macroscopically inhomogeneous porous media. *J Appl Phys* 2007;102:024910. <http://dx.doi.org/10.1063/1.2752135>.
- [48] de Ryck L. Acoustical characterisation of macroscopically inhomogeneous porous materials (Ph.D. thesis), Faculteit Wetenschappen, Katholieke Universiteit Leuven; 2008.
- [49] Bednarik M, Cervenka M, Groby J, Lotton P. One-dimensional propagation of longitudinal elastic waves through functionally graded materials. *Int J Solids Struct* 2018;146:43–54. <http://dx.doi.org/10.1016/j.ijsolstr.2018.03.017>, URL <https://www.sciencedirect.com/science/article/pii/S0020768318301252>.
- [50] Kristensson G. Second order differential equations: Special functions and their classification. Springer New York; 2010. <http://dx.doi.org/10.1007/978-1-4419-7020-6>.
- [51] Walther K. Reflection factor of gradual-transition absorbers for electromagnetic and acoustic waves. *IRE Trans Antennas Propag* 1960;8:608–21. <http://dx.doi.org/10.1109/tap.1960.1144901>.
- [52] Olver FWJ, Lozier DW, Boisvert RF, Clark CW. NIST handbook of mathematical functions paperback and CD-ROM. Cambridge, England: Cambridge University Press; 2010.
- [53] Ronveaux A, editor. Heun's differential equations. Oxford Science Publications; 1995.
- [54] Nusinsky I, Hardy AA. Band-gap analysis of one-dimensional photonic crystals and conditions for gap closing. *Phys Rev B* 2006;73(12). <http://dx.doi.org/10.1103/physrevb.73.125104>.
- [55] Caffrey S, Morozov GV, Sprung DWL, Martorell J. Floquet–Bloch solutions in a sawtooth photonic crystal. *Opt Quantum Electron* 2017;49(3). <http://dx.doi.org/10.1007/s11082-017-0939-1>.
- [56] Bednarik M, Cervenka M. Propagation of electromagnetic waves through non-uniform dielectric layers. *J Opt Soc Amer B* 2018;35(10):2541. <http://dx.doi.org/10.1364/josab.35.002541>.

### ■ 3.6 Paper VI:

**Title:** *Willis couplings in continuously varying cross-sectional area duct*

The sixth paper (and also the last one of the presented collection) published in The Journal of the Acoustical Society of America returns back from the topic of elastic waves to the acoustical ones. The main subject of this research is an inhomogeneous axially symmetric acoustic waveguide (duct) section of a finite length and a continuously varying cross-sectional area given by the respective functional dependence of the corresponding radius of the waveguide represented by the function  $\eta$  (see Sec. 2.1). Since in this paper we also include the viscothermal losses then both the density and the compressibility of the air inside of the waveguide are also spatially dependent on the respective coordinate.




The first step is (once again) to formulate the model equation, or in this case the two first order model differential equations (but when those two are combined they, again, reproduce the Webster-type equation as always). The reason for why in this case we are using the two first order equations instead of one second order equation is that the problem can now be formulated in the space-state representation, whereas the state vector represents the pressure and the volume velocity at the specified point and the state matrix describes the spatial evolution of the state vector along the respective coordinate. The key point is to express a linear relationship of the state vector at the left side of the waveguide to the one at the right side, or in other words to find the corresponding transfer matrix of the waveguide section. This is done by a second order homogenization of the waveguide section realized by a Peano-Baker expansion of the state matrix up to the second order, which is a low frequency limit approximation in contrast to e.g., the WKB method (see Sec. 2.3). Then by some further manipulation, we were able to derive the effective propagation matrix of the waveguide containing three parameters: the effective density and compressibility which correspond to the first order of the approximation and the so called Willis coupling coefficients, which are additional terms present due to the second order of the approximation. For all of those parameters, the analytical expressions are given, but it should be noted that they contain integral formulas which generally cannot be solved analytically and therefore some numerical integration method needs to be employed. The effective transfer matrix is then obtained from the propagation matrix. It is noteworthy that if we were to assume a locally periodic structure consisting of  $N$  such waveguide sections connected in series then the total transfer matrix can be obtained simply by exponentiation of the effective transfer matrix to the  $N$ -th power (this is not presented in the paper).



Now the second part of the paper follows where the obtained results are compared to the numerical results provided by the standardly used transfer matrix method (TMM). First, the frequency limits of the approximation are discussed. Next, the comprehensive comparison is made between the first and the second order of the approximation (and the numerical results) for various parameters of the waveguide, namely the reflection and transmission coefficients and the impedances as seen from the left and the right side. Then, the effective parameters given by the analytical expressions are compared to the ones obtained via the TMM, whereas we can see a very good agreement between the individual results in for the low frequencies (well below the discussed limits). In the appendix, we also show that in the case of a symmetrical profile of the radius function the Willis coupling coefficients vanish.

SEPTEMBER 13 2023

## Willis couplings in continuously varying cross-sectional area duct

A. Krpenský  ; M. Bednařík  ; J-P. Groby 



*J. Acoust. Soc. Am.* 154, 1660–1666 (2023)

<https://doi.org/10.1121/10.0020849>



CrossMark



LEARN MORE

Advance your science and career as a member of the  
**Acoustical Society of America**

# Willis couplings in continuously varying cross-sectional area duct

A. Krpenský,<sup>1</sup> M. Bednařík,<sup>1</sup> and J.-P. Groby<sup>2,a)</sup>

<sup>1</sup>Faculty of Electrical Engineering, Department of Physics, Czech Technical University in Prague, Technická 2, 166 27 Prague 6, Czech Republic

<sup>2</sup>Laboratoire d'Acoustique de l'Université du Mans, Unité Mixte de Recherche 6613, Institut d'Acoustique - Graduate School, Centre National de la Recherche Scientifique, Le Mans Université, France

## ABSTRACT:

Acoustic wave propagation in a one-dimensional periodic and asymmetric duct is studied theoretically and numerically to derive the effective properties. Closed form expressions for these effective properties, including the asymmetric Willis coupling, are derived through truncation of the Peano–Baker series expansion of the matricant (which links the state vectors at the two sides of the unit-cell) and Padé's approximation of the matrix exponential. The results of the first-order and second-order homogenization (with Willis coupling) procedures are compared with the numerical results. The second-order homogenization procedure provides scattering coefficients that are valid over a much larger frequency range than the usual first-order procedure. The frequency well below which the effective description is valid is compared with the lower bound of the first Bragg bandgap when the profile is approximated by a two-step function of identical indicator function, i.e., two different cross-sectional areas over the same length. This validity limit is then questioned, particularly with a focus on impedance modeling. This article attempts to facilitate the engineering use of Willis materials. © 2023 Acoustical Society of America. <https://doi.org/10.1121/10.0020849>

(Received 3 April 2023; revised 4 August 2023; accepted 20 August 2023; published online 13 September 2023)

[Editor: Yong Li]

Pages: 1660–1666

## I. INTRODUCTION

Since the seminal work of Willis in the 1980s,<sup>1</sup> the eponymous materials have received an increasing attention. This increasing attention has even been exponential since their experimental evidence or demonstration.<sup>2–4</sup> The Willis coupling parameters couple the potential and kinetic energy in the acoustic conservation relations; therefore, enhancing the ability to control waves in metamaterials compared to other materials that do not exhibit such coupling. These parameters have thus been employed to design and analyze  $\mathcal{PT}$  symmetric,<sup>5</sup> wave front shaping,<sup>6</sup> or non-reciprocal<sup>7–9</sup> systems. Most of the works to date have focused on the physical origins,<sup>10</sup> calculation,<sup>11–13</sup> and enhancement<sup>14</sup> of Willis coupling, but only a few have focused on deriving a closed form of these parameters<sup>15</sup> to ease Willis material engineering use. Effectively, various systems are asymmetric and can thus be modeled as Willis materials. In this article, we will focus on a one-dimensional (1D) periodic system, the properties of which vary continuously in a periodic manner.

This system simply consists of a duct, the radius of which varies continuously and periodically, leading to an asymmetric profile. The acoustic wave propagation of such a system has been extensively studied in the past, mostly for two purposes: the acoustic wave propagation in horns<sup>16,17</sup> and in corrugated ducts in the absence<sup>18</sup> or in the presence<sup>19</sup> of flow. The propagation of plane acoustic waves in ducts,

the cross-sectional area of which varies in space, is generally based on the Webster equation. This equation is commonly used to analyze and design mufflers, resonators, and other types of acoustic filters for noise control applications,<sup>20,21</sup> but also in the analysis of musical instruments, such as flutes and organ pipes, where the geometry of the instrument affects the resonance frequencies and the sound quality.<sup>22</sup> An accurate, or at least a reasonably close, analytical solution for the Webster equation is thus crucial to study the behavior of sound waves in such systems. Several papers have been dedicated to solving this equation.<sup>23–26</sup> Although an approximate analytical solution accounting for viscothermal losses has been proposed,<sup>27</sup> these losses that occur at the duct boundaries are often neglected. To our knowledge, any of the former articles were focused on deriving the effective properties in such problems in the presence of viscothermal losses and when the corrugation profile is asymmetric.

Inspired by Refs. 9, 15, and 28, the closed form expressions of the effective properties, including the asymmetric Willis coupling, describing the acoustic wave propagation in a duct (the radius of which varies periodically and continuously) are derived and analyzed. A related article was published on elasticity,<sup>12</sup> in which the procedure was different and validated on a two-layer laminate under SH polarization.

The article is organized as follows. In Sec. II, the equations describing the acoustic wave propagation in the duct of continuously varying radius are reminded. The procedure to derive the effective properties, based on the first-order Padé's approximation of the matrix exponential and

<sup>a)</sup>Email: Jean-Philippe.Groby@univ-lemans.fr

Peano–Baker series expansion of the matricant, is described and applied to our problem in Sec. III. Results in two specific cases, i.e., one where the profile leads to narrow duct portion of short period and the other where the profile leads to wider duct of longer period, are discussed in Sec. IV. In particular, the dispersion introduced by the radius profile is analyzed in view of homogenization limit.

**II. GENERAL STATEMENT**

We consider the 1D acoustic wave propagation in a  $d$ -periodic duct of a continuously varying circular cross-sectional area  $S(x) = \pi r(x)^2$  as depicted in Fig. 1. Assuming an implicit time dependence  $e^{-i\omega t}$ , pressure  $p(x)$ , and flow  $\mathcal{V}(x) = S(x)V(x)$ , where  $V(x)$  is the particle velocity, satisfy the following first-order equations

$$\begin{cases} i\omega \tilde{\rho}(x)\mathcal{V} = \frac{\partial p}{\partial x}, \\ i\omega \tilde{C}(x)p = \frac{\partial \mathcal{V}}{\partial x}, \end{cases} \quad (1)$$

where  $\tilde{\rho}(x) = \rho(x)/S(x)$  and  $\tilde{C}(x) = C(x)S(x)$  are, respectively, the reduced density and compressibility (inverse of

the bulk modulus,  $\tilde{C} = 1/\tilde{K}$ ). This system is usually cast in the matrix form

$$\frac{\partial}{\partial x} \mathbf{W} = \begin{bmatrix} 0 & i\omega \tilde{\rho}(x) \\ i\omega \tilde{C}(x) & 0 \end{bmatrix} \mathbf{W} = \mathbf{A}(x)\mathbf{W}, \quad (2)$$

where  $\mathbf{W} = \langle p, \mathcal{V} \rangle^T$  is the state vector and  $\mathbf{A}(x)$  is the propagation matrix. The latter matrix  $\mathbf{A}$  depends on  $x$  and does not commute with itself for different values of  $x$ , i.e.,  $\mathbf{A}(x)\mathbf{A}(x') - \mathbf{A}(x')\mathbf{A}(x) \neq 0$  when  $x' \neq x$ . The solution of the system represented by Eq. (2), which relates the state vectors at both sides of the unit-cell via  $\mathbf{W}(d) = \mathbf{M}_d \mathbf{W}(0)$ , also involves a matricant  $\mathbf{M}_d$  that takes the form of a Peano–Baker series expansion

$$\mathbf{M}_d = \mathbf{Id} + \int_0^d \mathbf{A}(x)dx + \int_0^d \mathbf{A}(x) \left( \int_0^x \mathbf{A}(\zeta)d\zeta \right) dx + \dots, \quad (3)$$

which is usually evaluated iteratively. Each iteration corresponds to an increase in the order of the Taylor expansion. Of particular interest is the second-order iteration that reads as

$$\mathbf{M}_d^{(2)} = \begin{bmatrix} 1 - \omega^2 \int_0^d \tilde{\rho}(x) \int_0^x \tilde{C}(\zeta) d\zeta dx & i\omega \bar{\rho}d \\ i\omega \bar{C}d & 1 - \omega^2 \int_0^d \tilde{C}(x) \int_0^x \tilde{\rho}(\zeta) d\zeta dx \end{bmatrix} + \mathcal{O}(\bar{k}d)^3, \quad (4)$$

where  $\bar{\rho} = \int_0^d \tilde{\rho}(x) dx/d$  and  $\bar{C} = \int_0^d \tilde{C}(x) dx/d$  are the mean values of  $\tilde{\rho}$  and  $\tilde{C}$ , and  $\bar{k} = \omega \sqrt{\bar{\rho}\bar{C}}$ .

**III. DERIVATION OF THE EFFECTIVE PROPERTIES**

We assume a  $d$ -periodic 1D reciprocal system of respective propagation matrix  $\mathbf{A}_e$ . The state vectors at both sides of the unit-cell are related via  $\mathbf{W}(d) = \exp(\mathbf{A}_e d)\mathbf{W}(0) = \mathbf{T}\mathbf{W}(0)$ , with  $\mathbf{T}$  the transfer matrix of respective elements  $t_{ij}$ ,  $(i, j) \in (1, 2)$ . Following Ref. 15, the propagation matrix is correctly approximated by the inversion of the first-order Padé’s approximation of the transfer matrix (i.e., the matrix exponential)

$$\begin{aligned} \mathbf{A}_e &\approx \frac{2}{d}(\mathbf{T} + \mathbf{Id})^{-1}(\mathbf{T} - \mathbf{Id}) \\ &\approx \frac{2}{d} \frac{1}{2 + t_{11} + t_{22}} \begin{bmatrix} t_{11} - t_{22} & 2t_{12} \\ 2t_{21} & t_{22} - t_{11} \end{bmatrix}, \end{aligned} \quad (5)$$

which directly provides the elements of a reciprocal Willis material

$$\mathbf{A}_e = i\omega \begin{bmatrix} \chi_e^a & \rho_e \\ C_e & -\chi_e^a \end{bmatrix}, \quad (6)$$

where  $\rho_e$  is the effective density,  $C_e$  is the effective compressibility, and  $\chi_e^a$  is the even Willis coupling related to the

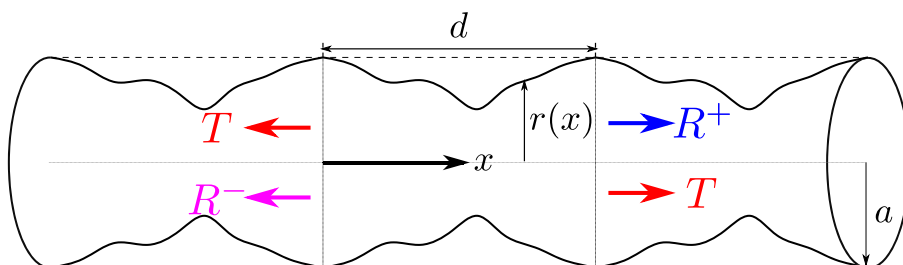


FIG. 1. (Color online) Sketch of the configuration and representation of the scattering problem.

possible asymmetry of the unit-cell. Note that the reciprocal feature of the system, i.e.,  $\det(\mathbf{T}) = 1$  has been accounted for in Eq. (5). Checking this property can be employed as a validation step (see Appendix A).

Introducing the matricant elements in Eq. (5) leads to

$$\rho_e = \bar{\rho}, \quad C_e = \bar{C},$$

and

$$\chi_e^a = \frac{i\omega}{2d} \left( \int_0^d \bar{\rho}(x) \int_0^x \bar{C}(\zeta) d\zeta dx - \int_0^d \bar{C}(x) \int_0^x \bar{\rho}(\zeta) d\zeta dx \right). \quad (7)$$

The effective density and compressibility are  $\mathcal{O}(\omega)$ , while  $\chi_e^a$  is exhibited at the next order and is thus  $\mathcal{O}(\omega)^2$ . The effective density and compressibility are classical results from the first-order homogenization. Quantities evaluated according to the first-order homogenization are hereafter referred to as sub-index  $H$ . When the profile is symmetric, i.e.,  $r(x) = r(d-x)$ ,  $\forall x \in [0, d/2]$ ,  $\chi_e^a$  vanishes (see the Appendix B) and thus, the effective density and compressibility become valid at the second order. In other words, the first-order homogenization results become valid at the second order when the profile is symmetric. When the profile is piecewise constant, the effective properties,

including the Willis coupling, fall back on the formulas derived in Ref. 28. In addition, the Willis coupling vanishes at low frequency because an asymmetric structure falls back to symmetric at low frequency. The asymmetric Willis coupling is effectively a linear function of the frequency (in the absence of losses) because it appears at the second order. In the absence of losses,  $\chi_e^a$  is purely imaginary.

#### IV. RESULTS AND DISCUSSION

We consider a duct, the maximum radius of which is  $a = 1.5$  cm, such that the profile  $r(x)$  consists of a reduction of this radius. Only plane waves are also propagating below the cut-on frequency of the first mode in a duct of radius  $a$ , which is frequencies below  $\approx 6100$  Hz. Viscothermal losses are accounted for via the Stinson's formula,<sup>29</sup> which are addressed in Appendix C. The structuration of the duct geometry introduced by the periodic radial profile  $r(x)$  induces dispersion of the waves traveling in the duct. To get a grip on it, the dispersion relation of the acoustic waves in a periodic duct composed of two different cross-sectional areas,  $S_{max}$  associated with a radius  $a$  and  $\tilde{S}$  corresponding to a radius  $\tilde{r}$ , of the same length, i.e.,  $d/2$ , is considered. This dispersion relation turns out to be that of a periodic 1D Su-Schrieffer-Heeger model,<sup>30</sup> where the coupling coefficients are simply given by the ratios of the two different cross-sectional areas.<sup>31</sup> This relation reads as

$$\cos(kd/2) = \pm \sqrt{\left( \left( \frac{S_{max}}{S_{max} + \tilde{S}} \right)^2 + \left( \frac{\tilde{S}}{S_{max} + \tilde{S}} \right)^2 + \frac{2S_{max}\tilde{S}}{(S_{max} + \tilde{S})^2} \cos(k_e d) \right)}, \quad (8)$$

where  $k_e$  is the effective wavenumber in the presence of the periodic structuration and  $k$  is the wave number in the straight duct. When  $k_e d = \pi$ , the frequency of the lower bound of the first Bragg bandgap can be calculated in the absence of losses. This frequency,  $f_{\tilde{r}}^B$ , is supposed to provide a good approximation of the quantity well below which the effective models are valid. The question that naturally arises becomes: which value of  $\tilde{r}$  (or  $\tilde{S}$ ) should be considered? We thus consider two limit cases: the first one where  $kd$  is small but  $r(x)$  leads to a narrow duct portion and the second one where  $kd$  is larger and  $r(x)$  leads to a wider duct cross-sectional area on average.

Figures 2(a) and 2(b) depict the two continuous profiles considered, the equations of which are provided in Appendix D. In the first case,  $d = 2$  cm and the profile has a maximum reduction of the duct radius of 90%. In the second case,  $d = 6$  cm and the profile has a maximum reduction of the duct radius of 50% and much less on average. These two profiles are discretized in 301 segments which are used to

evaluate the integrals (trapezoidal rule) in the effective parameter closed form expressions [Eq. (7)]. Instead of iteratively evaluating Eq. (3) to calculate the matricant, we evaluate the total transfer matrix that links the state vectors at both sides of the unit-cell, by multiplying the transfer matrices of each segment  $T_j$ , i.e.,  $T_{tot} = \prod_{j=1}^{301} T_j$ . This solution is then considered as the reference solution, from which the effective properties can be numerically evaluated<sup>12,15</sup> via  $A_n = \log(T_{tot})/d$  (see also Appendix E). The corresponding effective properties are referred to as the sub-index  $n$ . Figures 2(c)–2(f) depict the dispersion relation (real and imaginary parts of the wavenumber) of the acoustic waves for both profiles. The lower bound of the Bragg bandgap is numerically evaluated around 2300 Hz in both cases. Either  $\tilde{r} = \min(r(x))$  (the minimum radius over a period) or  $\tilde{r} = 2\bar{r} - a$  (the radius that produces the same area reduction as that produced by the profile) are considered to evaluate  $f_{\tilde{r}}^B$ . In the first case,  $f_{\min(r(x))}^B \approx 1100$  Hz and  $f_{2\bar{r}-a}^B \approx 4500$  Hz, while in the second case,

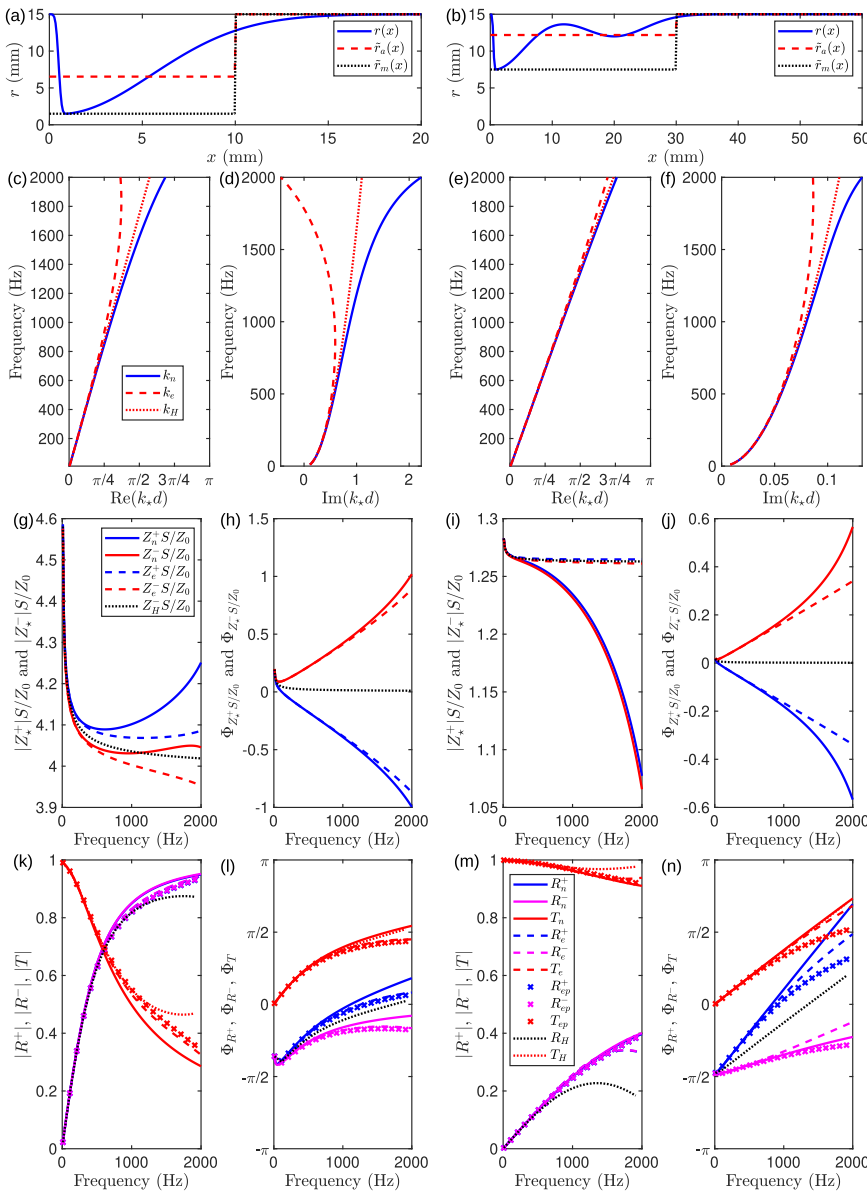


FIG. 2. (Color online) Continuous profiles in the (a) first and (b) second cases (blue curve) as well as the two approximations in two equal portions of different sectional areas with  $\tilde{r}_a$  (dashed red curve) and with  $\tilde{r}_m$  (dotted black curve). (c) and (e) Real and (d) and (f) imaginary parts of the wavenumber–dispersion relation—in the first and second cases, respectively. (g) and (i) Modulus and (h) and (j) phase of the normalized impedances  $Z^\pm S/Z_0$ . (k) and (m) Modulus and (l) and (n) phase of the scattering coefficients, i.e.,  $R^+$ ,  $R^-$ , and  $T$ . (c)–(f) Results as calculated numerically (continuous curves), with the first-order homogenization (dotted curves), and with the second-order homogenization (dashed curves). (k)–(n) The markers refer to the scattering coefficients as calculated with the first-order Padé’s approximation of  $\text{expm}(A_e d)$ .

$f_{\min(r(x))}^B \approx 1700$  Hz and  $f_{2\bar{r}-a}^B \approx 2500$  Hz. Although this frequency is better approximated in the second case than in the first case,  $f_{\min(r(x))}^B \approx 1100$  Hz and  $f_{2\bar{r}-a}^B \approx 2500$  Hz seem to be appropriate for the first and second cases, respectively, in view of the homogenization limit. In terms of rule, if  $2\bar{r} - a > a/2$ ,  $f_{2\bar{r}-a}^B$  is appropriate and if  $2\bar{r} - a < a/2$ ,  $f_{\min(r(x))}^B$  is appropriate. Nevertheless, speaking in terms of percentage of  $k_{ed}$  does not seem to be representative when asymmetric structures are considered because the main difference between first and second homogenization is not in  $k_H = \omega\sqrt{\rho_e C_e}$  instead of  $k_e = \omega\sqrt{\rho_e C_e + \chi_e^2}$  but rather in  $Z_H = \sqrt{\rho_e/C_e}$  instead of  $Z_e^\pm = \rho_e/(\sqrt{\rho_e C_e + \chi_e^2 \mp \chi})$ . The wavenumber  $k_n$  is even better approximated by  $k_H$  than it is by  $k_e$  over the considered frequency range, as can be seen in Figs. 2(c)–2(f). Please note that the range of  $\text{Re}(k_e d)$  over which the dispersion relationships are represented is large

and far exceeds the range of validity of the usual homogenization procedures. The two impedances  $Z_n^\pm$  are better approximated by  $Z_e^\pm$  than they are by  $Z_H$  and in particular, their phases [see Figs. 2(g)–2(j)]. Please note that the dynamics of the impedance modulus in the second case [Fig. 2(i)] is different from that in the first case [Fig. 2(g)]. The ratio between the wavelength and the period is thus not the only limit in terms of homogenization, because it only relies on the effective wavenumber and the impedance has also to be accounted for. This is clearly visible on the scattering coefficients by a single unit-cell depicted in Figs. 2(k)–2(n). In both cases, the scattering coefficients calculated via the second-order homogenization, that is, when the Willis coupling is accounted for, is accurate over a wider range of frequencies than those calculated via the first-order homogenization. Although this is an obvious result, it is worth noting. The asymmetry of the radius profiles are more

visible on the phases of the reflection coefficients than on their moduli. These phase differences are clearly exhibited when Willis coupling is accounted for via  $Z_e^\pm$  [see Figs. 2(h) and 2(j)]. The phase of the reflection coefficient as calculated with the first-order homogenization stands between those as calculated with the Willis coupling. At low frequencies, the phases are equal because an asymmetric structure falls back to symmetric. When the frequency increases, the phases start to differentiate. The results of the first-order homogenization results fail when the phase difference between the two reflection coefficients become too large, while the results of the second-order homogenization are still satisfactory. The second-order homogenization fails for both transmission and reflection coefficients when the phase of the reflection coefficients are not correctly modeled anymore. Please note that the scattering coefficients of a single unit-cell as calculated with the first-order Padé's approximation of the function  $\expm(A_e d)$  is in good agreement with the numerically calculated scattering coefficients. This means that the main source of error in the derivation of the effective properties yields in the truncation of the Peano–Baker series to evaluate the matricant at the second

iteration (second-order Taylor expansion). Please also note that for longer structures, i.e., more than a single unit-cell, the matrix exponential is mandatory to evaluate the scattering coefficients. Finally, the impact of the error on  $k_e$  and  $Z_e^\pm$  can be tempered in the case of longer structures. Indeed, the error on  $k_e$  can have a greater impact in this case, as the wave propagates over a greater distance in the material.

Figures 3(a)–3(l) depict the normalized effective properties as evaluated numerically (blue continuous curves) and from their closed form expressions (red dashed curves) given in Eq. (7) for both profiles. Closed form expressions are in excellent agreement with the numerical results, although they deviate when the frequency increases. As pointed out in the previous paragraph, these effective properties are valid over a shorter frequency range in the first case, which is when the profile leads to a narrow duct portion, than in the second case, which is when the period is longer, and the duct is wider. Whatever the case, the Willis coupling cannot be neglected in relation to the other effective parameters at high frequency. The Willis coupling is almost purely imaginary which is in accordance with Eq. (7). Compared to the other normalized effective properties, the Willis coupling clearly

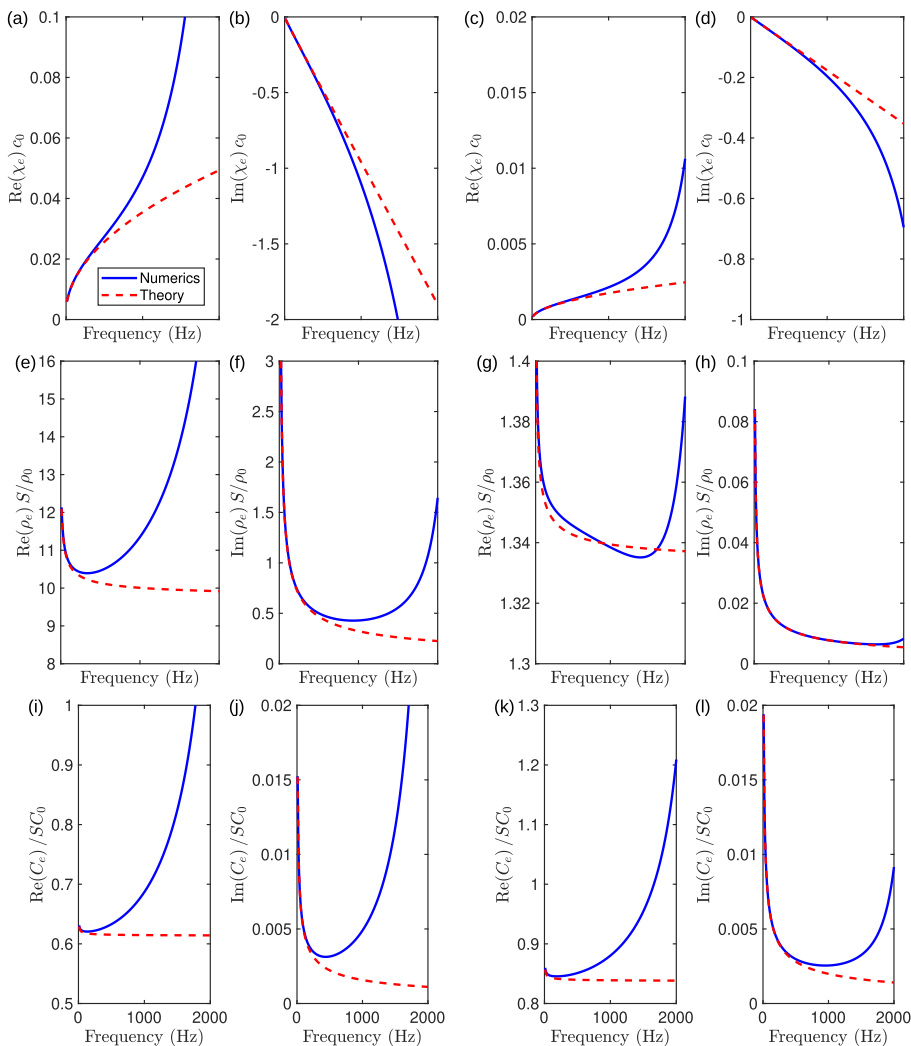


FIG. 3. (Color online) (a) and (c) Real and (b) and (d) imaginary parts of the normalized asymmetric Willis coupling. (e) and (g) Real and (f) and (h) imaginary parts of the normalized effective density. (i) and (k) Real and (j) and (l) imaginary parts of the normalized effective compressibility. Numerical results are depicted in blue continuous curves and closed form expressions of the coefficients are depicted in red dashed curves.

cannot be neglected, which emphasizes the need to use a second-order homogenization procedure.

**V. CONCLUSION**

The effective properties describing the acoustic wave propagation in a duct, the radius of which varies continuously and periodically and leads to an asymmetric over the period, are derived with the help of the first-order Padé’s approximation of the matrix exponential function and truncation of the Peano–Baker series. Each iteration corresponds to an increase in the order of the Taylor expansion. The first-order (classical) homogenization results are recovered using the first iteration to evaluate the matricant, while the second-order homogenization, derived using the second iteration to evaluate the matricant, features the Willis coupling as an additional parameter. The lowest bound of the first Bragg bandgap, when the unit-cell radius profile is approximated by a two-step function of identical indicator function, is considered to assess the frequency well below which the effective models are valid. The radial structuration actually induces wave dispersion. It turns out that the validity of the effective Willis material derived to model this asymmetric periodic duct not only relies on a percentage of  $k_{ed}$ , but also on the impedance modeling. Effectively, the asymmetric Willis coupling that is exhibited at the second order impacts the effective wavenumber but also makes the impedance of the wave propagating in the positive or in the negative directions different as the unit-cell is asymmetric. The modeling of these two impedances has also to be accounted for to derive the real and practical validity limit of the scattering coefficients calculated with the effective properties. Wavenumbers, impedances, effective properties, and scattering coefficients, as calculated with the second-order homogenization procedure, are found in good agreement with the numerical results calculated with the standard transfer matrix method, thus validating the proposed method. This article paves the way for the modeling of more complicated ducts with periodic asymmetric radial structuration, like acoustic black holes, possibly in the presence of flow. It also questions the validity limits of the effective properties.

**ACKNOWLEDGMENTS**

This work was supported by the Grant Agency of the Czech Republic Grant No. 22-33896S. J.-P.G. is thankful for the financial support of the Metaroom Project No. ANR-18-CE08-0021 which is co-funded by A.N.R. and R.C.G.

**APPENDIX A: VERIFYING THAT THE MATRICANT IS UNITARY AT THE SECOND ORDER**

The determinant of the matrix Eq. (4) reads as

$$\begin{aligned} \det(\mathbf{M}_d^{(2)}) &= 1 + \omega^2 \left( \bar{C}\bar{\rho} - \int_0^d \tilde{C}(x) \int_0^x \tilde{\rho}(\zeta) d\zeta dx \right. \\ &\quad \left. - \int_0^d \tilde{\rho}(x) \int_0^x \tilde{C}(\zeta) d\zeta dx \right) + \mathcal{O}(\bar{k}d)^3 \\ &= 1 + \mathcal{O}(\bar{k}d)^3. \end{aligned} \tag{A1}$$

Note that Eq. (A1) vanishes because both functions  $\tilde{\rho}(x)$  and  $\tilde{C}(x)$  are zero for  $x < 0$  and integration by part formula.

**APPENDIX B: CANCELLATION OF THE WILLIS COUPLING IN THE CASE OF A SYMMETRIC PROFILE**

Equation (7) can be further expanded as follows:

$$\begin{aligned} \chi_e^a &= \frac{i\omega}{2d} \left( \bar{\rho} \int_0^{d/2} \tilde{C}(x) dx - \bar{C} \int_0^{d/2} \tilde{\rho}(x) dx \right. \\ &\quad \left. + \int_0^d \tilde{C}(x) \int_{d/2}^x \tilde{\rho}(\zeta) d\zeta dx \right. \\ &\quad \left. - \int_0^d \tilde{\rho}(x) \int_{d/2}^x \tilde{C}(\zeta) d\zeta dx \right). \end{aligned} \tag{B1}$$

When the profile is symmetric, i.e.,  $r(x)$  is symmetric with respect to  $d/2$ , the first two terms in Eq. (B1) cancel (since  $\int_0^{d/2} \tilde{\rho}(x) dx = \bar{\rho}d/2$  and  $\int_0^{d/2} \tilde{C}(x) dx = \bar{C}d/2$ ) and the last two terms vanish since they represent an integration over  $[0; d/2]$  of a multiple of a symmetric and an antisymmetric function with respect to  $d/2$ .

**APPENDIX C: ACCOUNTING FOR THE VISCO-THERMAL LOSSES**

Circular cross-sectional ducts are considered throughout this article. The boundaries give rise to visco-thermal losses from viscous and thermal skin depths. Assuming that only plane waves propagate in a circular cross-sectional duct of radius  $r$ , the effective complex and frequency dependent density and compressibility read as<sup>29</sup>

$$\begin{aligned} \rho &= \rho_0 \left( 1 - \frac{2}{r\sqrt{i\omega\rho_0/\eta}} \frac{J_1\left(r\sqrt{i\omega\rho_0/\eta}\right)}{J_0\left(r\sqrt{i\omega\rho_0/\eta}\right)} \right)^{-1}, \\ C &= \left( 1 + \frac{2(\gamma - 1)}{r\sqrt{iPr\omega\rho_0/\eta}} \frac{J_1\left(r\sqrt{iPr\omega\rho_0/\eta}\right)}{J_0\left(r\sqrt{iPr\omega\rho_0/\eta}\right)} \right) / \gamma P_0, \end{aligned} \tag{C1}$$

where  $\rho_0$ ,  $\gamma$ ,  $\eta$ , and  $Pr$  are, respectively, the density, specific heat ratio, dynamic density, and Prandtl number of the saturating fluid, and  $P_0$  is the atmospheric pressure. The reduced density and bulk modulus can then be evaluated by  $\tilde{\rho}(x) = \rho(x)/S(x)$  and  $\tilde{C}(x) = C(x)S(x)$ , with  $S(x) = \pi r(x)^2$  for each value of  $r(x)$ .

**APPENDIX D: EQUATIONS OF THE TWO PROFILES**

The equations of the two profiles considered are provided below. Both are generated via asymmetric Gaussian functions

$$\mathcal{G}(x) = \frac{1}{\sqrt{2\pi}} \exp\left(-\frac{(x/\sigma - \zeta)^2}{2}\right) \left(1 + \operatorname{erf}\left(\alpha \frac{x/\sigma - \zeta}{\sqrt{2}}\right)\right), \tag{D1}$$

with  $\operatorname{erf}(x)$  being the error function and  $\sigma$ ,  $\zeta$ , and  $\alpha$  being the constant values.



The period  $d$  is 2 cm in the first case and the profile is

$$r(x) = a - 0.9a \frac{\mathcal{G}(x)}{\max(\mathcal{G}(x))}, \quad (\text{D2})$$

with  $\alpha = 40$ ,  $\zeta = 0.1$ , and  $\sigma = 5 \times 10^{-3}$ , and  $\max(f(x))$  is the maximum value of  $f(x)$ ,  $x \in [0, d]$ . The period  $d$  is 6 cm in the second case and the profile is

$$r(x) = a - 0.5a \frac{\mathcal{G}(x)}{\max(\mathcal{G}(x))} - 0.2a \frac{\mathcal{G}^\dagger(x)}{\max(\mathcal{G}^\dagger(x))}, \quad (\text{D3})$$

with  $\alpha = \alpha^\dagger = 40$ ,  $\zeta = 0.1$ , and  $\sigma = 5 \times 10^{-3}$ , and  $\zeta^\dagger = 0.2$ , and  $\sigma^\dagger = 5 \times 10^{-2}$ .

## APPENDIX E: NUMERICAL EVALUATION OF THE EFFECTIVE PROPERTIES

Let us assume that the state vectors at both sides of the unit-cell of length  $d$  are linked by the total transfer matrix  $\mathbf{T}_{\text{tot}}$ . The effective properties can be numerically evaluated via

$$\begin{aligned} \mathbf{A}_n &= \log_m(\mathbf{T}_{\text{tot}})/d \\ &= i\omega \begin{bmatrix} \chi_n^a & \rho_n \\ C_n & -\chi_n^a \end{bmatrix} \\ &= \frac{1}{\sqrt{2}} \begin{bmatrix} Z_n^+ & -Z_n^- \\ 1 & 1 \end{bmatrix} \begin{bmatrix} ik_n & 0 \\ 0 & -ik_n \end{bmatrix} \frac{1}{\sqrt{2}} \begin{bmatrix} 1/Z_n^+ & -1 \\ 1/Z_n^- & 1 \end{bmatrix}. \end{aligned} \quad (\text{E1})$$

The impedances  $Z_n^\pm$  and wavenumber  $k_n$  can simply be calculated from the diagonalization of  $\mathbf{A}_e$ . This procedure turns out to be a numerical version of the procedure derived in Ref. 12.

- <sup>1</sup>J. Willis, "Variational principles for dynamic problems for inhomogeneous elastic media," *Wave Motion* **3**, 1–11 (1981).
- <sup>2</sup>S. Koo, C. Cho, J. Jeong, and N. Park, "Acoustic omni meta-atom for decoupled access to all octants of a wave parameter space," *Nat. Commun.* **7**, 13012 (2016).
- <sup>3</sup>M. B. Muhlestein, C. F. Sieck, P. S. Wilson, and M. R. Haberman, "Experimental evidence of Willis coupling in a one-dimensional effective material element," *Nat. Commun.* **8**, 15625 (2017).
- <sup>4</sup>Y. Liu, Z. Liang, J. Zhu, L. Xia, O. Mondain-Monval, T. Brunet, A. Alù, and J. Li, "Willis metamaterial on a structured beam," *Phys. Rev. X* **9**, 011040 (2019).
- <sup>5</sup>A. Merkel, V. Romero-García, J.-P. Groby, J. Li, and J. Christensen, "Unidirectional zero sonic reflection in passive  $\mathcal{PT}$ -symmetric Willis media," *Phys. Rev. B* **98**, 201102 (2018).
- <sup>6</sup>J. Li, C. Shen, A. Díaz-Rubio, S. Tretyakov, and S. Cummer, "Systematic design and experimental demonstration of bianisotropic metasurfaces for scattering-free manipulation of acoustic wavefronts," *Nat. Commun.* **9**, 1342 (2018).
- <sup>7</sup>L. Quan, D. L. Sounas, and A. Alù, "Nonreciprocal Willis coupling in zero-index moving media," *Phys. Rev. Lett.* **123**, 064301 (2019).

- <sup>8</sup>Y. Zhai, H.-S. Kwon, and B.-I. Popa, "Active Willis metamaterials for ultracompact nonreciprocal linear acoustic devices," *Phys. Rev. B* **99**, 220301 (2019).
- <sup>9</sup>C. Olivier, G. Poignand, M. Malléjac, V. Romero-García, G. Penelet, A. Merkel, D. Torrent, J. Li, J. Christensen, and J.-P. Groby, "Nonreciprocal and even Willis couplings in periodic thermoacoustic amplifiers," *Phys. Rev. B* **104**, 184109 (2021).
- <sup>10</sup>C. F. Sieck, A. Alù, and M. R. Haberman, "Origins of Willis coupling and acoustic bianisotropy in acoustic metamaterials through source-driven homogenization," *Phys. Rev. B* **96**, 104303 (2017).
- <sup>11</sup>M.-F. Ponge and P. O. D. Torrent, "Dynamic homogenization theory for nonlocal acoustic metamaterials," *Extreme Mech. Lett.* **12**, 71–76 (2017).
- <sup>12</sup>A. L. Shuvalov, A. A. Kutsenko, A. N. Norris, and O. Poncelet, "Effective Willis constitutive equations for periodically stratified anisotropic elastic media," *Proc. R. Soc. A* **467**, 1749–1769 (2011).
- <sup>13</sup>S. Nemat-Nasser, J. R. Willis, A. Srivastava, and A. V. Amirkhizi, "Homogenization of periodic elastic composites and locally resonant sonic materials," *Phys. Rev. B* **83**, 104103 (2011).
- <sup>14</sup>A. Melnikov, Y. K. Chiang, Q. Li, S. Oberst, A. Alù, S. Marburg, and D. Powell, "Acoustic meta-atom with experimentally verified maximum Willis coupling," *Nat. Commun.* **10**, 3148 (2019).
- <sup>15</sup>J.-P. Groby, M. Malléjac, A. Merkel, V. Romero-García, V. Tournat, D. Torrent, and J. Li, "Analytical modeling of one-dimensional resonant asymmetric and reciprocal acoustic structures as Willis materials," *New J. Phys.* **23**, 053020 (2021).
- <sup>16</sup>L. Campos, "Some general properties of the exact acoustic fields in horns and baffles," *J. Sound Vib.* **95**, 177–201 (1984).
- <sup>17</sup>V. Pagneux, N. Amir, and J. Kergomard, "A study of wave propagation in varying cross-section waveguides by modal decomposition. Part I. Theory and validation," *J. Acoust. Soc. Am.* **100**, 2034–2048 (1996).
- <sup>18</sup>J. C. Samuels, "On propagation of waves in slightly rough ducts," *J. Acoust. Soc. Am.* **31**, 319–325 (1959).
- <sup>19</sup>J. Golliard, Y. Aurégan, and T. Humbert, "Experimental study of plane wave propagation in a corrugated pipe: Linear regime of acoustic-flow interaction," *J. Sound Vib.* **472**, 115158 (2020).
- <sup>20</sup>L. Beranek and T. Mellow, *Acoustics: Sound Fields, Transducers and Vibration*, 2nd ed. (Academic Press, San Diego, CA, 2019).
- <sup>21</sup>M. Červenka and M. Bednařík, "Acoustic bandpass filters employing shaped resonators," *J. Sound Vib.* **383**, 76–88 (2016).
- <sup>22</sup>A. Chaigne and J. Kergomard, *Acoustics of Musical Instruments, Modern Acoustics and Signal Processing*, 1st ed. (Springer, New York, 2016).
- <sup>23</sup>E. Eisner, "Complete solutions of the 'Webster' horn equation," *J. Acoust. Soc. Am.* **41**, 1126–1146 (1967).
- <sup>24</sup>S. W. Rienstra, "Webster's horn equation revisited," *SIAM J. Appl. Math.* **65**, 1981–2004 (2005).
- <sup>25</sup>O. V. Rudenko and A. B. Shvartsburg, "Nonlinear and linear wave phenomena in narrow pipes," *Acoust. Phys.* **56**, 429–434 (2010).
- <sup>26</sup>M. Bednařík and M. Červenka, "A wide class of analytical solutions of the webster equation," *J. Sound Vib.* **469**, 115169 (2020).
- <sup>27</sup>P. Honzík, S. Durand, N. Joly, and M. Bruneau, "On the acoustic transfer function of slowly tapered small horns filled with thermo-viscous fluid," *Acta Acust. united Acust.* **99**, 694–702 (2013).
- <sup>28</sup>M. Malléjac, T. Cavalieri, V. Romero-García, A. Merkel, D. Torrent, J. Christensen, J. Li, and J.-P. Groby, "Non-locality of the Willis coupling in fluid laminates," *Wave Motion* **110**, 102892 (2022).
- <sup>29</sup>M. R. Stinson, "The propagation of plane sound waves in narrow and wide circular tubes, and generalization to uniform tubes of arbitrary cross-sectional shape," *J. Acoust. Soc. Am.* **89**, 550–558 (1991).
- <sup>30</sup>W. P. Su, J. R. Schrieffer, and A. J. Heeger, "Solitons in polyacetylene," *Phys. Rev. Lett.* **42**, 1698–1701 (1979).
- <sup>31</sup>A. Coutant, A. Sivadon, L. Zheng, V. Achilleos, O. Richoux, G. Theocharis, and V. Pagneux, "Acoustic Su-Schrieffer-Heeger lattice: Direct mapping of acoustic waveguides to the Su-Schrieffer-Heeger model," *Phys. Rev. B* **103**, 224309 (2021).





## Chapter 4

### Conclusions and future work

In the thesis the control and analysis of the acoustic and elastic wave fields was demonstrated by the six selected inhomogeneous structures corresponding to the six publications included in Chapt. 3, whereas in the preceding Chapt. 2 an overview of the mathematical methods commonly used in the papers was provided.

The first publication deals with the propagation of elastic Love-type waves inside of a FGM viscoelastic inhomogeneous isotropic elastic surface layer (laid over a homogeneous substrate) whose density and shear modulus vary according to the respective material function. The exact analytical solution to the model equation was derived in a form of a combination of the triconfluent Heun functions for a completely new class of profiles of the material function. Furthermore, the derivation of the corresponding dispersion equation was performed followed by several case studies with the observation that the dispersion relation can be controlled by a variable height of the corresponding gaussian-like profile of the material function.

The second publication is a direct continuation to the first one, whereas in this case the surface layer is repeated several times, resulting in a locally periodic inhomogeneous layer represented by the corresponding locally periodic material function laid over a homogeneous substrate. The solutions from the first publication were extended to the whole structure by employing the Floquet-Bloch theory and the case study was performed again with the Gaussian-like profile of the first period of the material function. The results were presented by me at the The 29th International Congress on Sound and Vibration.

In the third publication we focused on a two-dimensional acoustical waveguide with nonuniform (inhomogeneous) mean flow profile given by a symmetric polynomial, for which an approximate analytical solution was formulated based on the triconfluent Heun functions and the case study followed in order to assess the approximation validity for several powers of the profile, whereas in principle this type of approximate analytical solution is generally applicable to other types of the mean flow profiles as long as the approximation is still valid. The comparison of this approach with the WKB method was discussed further highlighting advantages of the solution provided by us.

In the fourth paper, we proposed a novelty type of a GRIN structure utilised for manipulation of the elastic P-wave field, specifically focusing and deflecting. The proposed structure consists of inhomogeneous FGM plates layered in parallel to each other and separated by thin gaps. By the WKB method applied to the corresponding model equation an approximate analytical expression for the effective phase velocity of each one of the plates was formulated and based on the geometrical approach the focusing and the deflecting structures were proposed and further validated by a numerical simulations.

The fifth paper presents an exact analytical solution to the model equation describing the propagation of elastic SH waves in a FGM viscoelastic locally periodic inhomogeneous structure for a general angle of incidence of the incoming plane wave by the Heun functions and further extended to the whole domain by employing the Floquet-Bloch theory. Based on that the expressions for the transmission and reflection coefficients are derived followed by a few case studies followed by the observation that this type of structure behaves as a selective band-stop filter, whereas the positions and the widths of the respective frequency bands can be controlled by a suitable choice of the second materials of the FGM structure.

In the sixth paper, the second order low frequency limit homogenization was performed on an inhomogeneous acoustical waveguide whose cross-sectional are varies continuously along the direction of the wave propagation with the first order model differential equations formulated in the state-space representation by employing the Peano-Baker expansion of the state matrix, resulting in analytical expressions for the effective density, compressibility and the Willis coupling coefficients. The frequency limit of this approximation is further discussed together with the numerical verification. This approach presents a low frequency alternative to the standardly used TMM with several advantages.

At this point there are many possibilities for the future continuation of the research. The main focus is currently devoted to the study of an

acoustic black hole (ABH) which (in theory) should act as a non-reflective termination for flexural waves propagating inside of a homogeneous elastic beam. The ABH is realized by adding a relatively short part to the edge of the beam with continuously varying (diminishing) thickness and either including the viscoelastic losses or assuming the ABH itself to be terminated with a dissipation element modifying the overall impedance of the ABH. A model differential equation of a fourth order (Euler-Bernoulli equation, see e.g., [14]) can be derived and by using a factorization method separated into the two second order equations of the Webster type. For a general cubic polynomial profile of the ABH we are then able to express the exact analytical solution by a combination of the Heun functions or (in some specific cases) hypergeometric functions. Based on varying the coefficients of the polynomial (which play the role of the parameters of the respective inhomogeneous structure here) we can then assess the possibility of controlling the reflection coefficient by the shape of the ABH.

Another possibility for the future work is to return back to the problematics of propagation of the Love-type waves inside of a FGM viscoelastic inhomogeneous layer, but in this case to express the material function in the same way as in the fifth paper, therefore enabling us to express the general solution as a combination of the Heun functions (in contrast to the previously used triconfluent Heun functions in the first two papers). The same extension can then be made to the locally periodic layer by employing the Floquet-Bloch theory. A study then can be made assessing the possibilities of controlling the corresponding dispersion relation by the suitable choice of the second material of the respective FGM.

Next, the approach presented for SH waves in the fifth paper can also be applied to derive an exact analytical solution to the model equation describing the propagation of the longitudinal waves through a locally periodic elastic structure. The results can then serve as a basis for utilizing the Su-Schrieffer-Heeger (SSH, see e.g., [15]) model which is an effective method for determining the dispersion relation of the corresponding locally periodic structures.

As another potential future work can be mentioned a direct continuation to the sixth presented paper. Since the demonstrated second order homogenisation procedure works only in the low frequency limit, it can be further accompanied by the WKB approximation method which on the contrary works in the high frequency limit. By combination of those two approaches an approximate expressions for the transmission and reflection coefficients can be made for both the low frequencies and the high frequencies together, providing (possibly) a good approximation in the whole frequency range. It should also be mentioned that this type of technique can be potentially utilised for a any area of acoustics and elastoacoustics where the respective

model equation (including a continuously varying material function) can be transformed into the state space model.



## Bibliography

- [1] K. F. Riley, M. P. Hobson, and S. J. Bence. *Mathematical Methods for Physics and Engineering*. Cambridge University Press, third edition, 2006. ISBN 978-0-521-67971-8.
- [2] G. Kristensson. *Second Order Differential Equations*. Springer, 2010. ISBN 978-1-4419-7019-0.
- [3] A. Ronveaux. *Heun's differential equations*. Oxford University Press, 1995. ISBN 978-0-19-859695-0.
- [4] T. Birkandan and M. Hortaçsu. Quantum field theory applications of heun type functions. *Reports on Mathematical Physics*, 79(1):81–87, February 2017. doi: 10.1016/s0034-4877(17)30022-8.
- [5] M. Hortaçsu. Heun Functions and Some of Their Applications in Physics. *Advances in High Energy Physics*, 2018:1–14, July 2018. doi: 10.1155/2018/8621573.
- [6] F. W. J. Olver, D. W. Lozier, R. F. Boisvert, and C. W. Clark. *NIST Handbook of Mathematical Functions*. Cambridge University Press, 2010. ISBN 978-0-521-14063-8.
- [7] D. T. Blackstock. *Fundamentals of Physical Acoustics*. John Wiley & Sons, 2000. ISBN 978-0-471-31979-5.
- [8] A. Ishimaru. *Electromagnetic Wave Propagation, Radiation, and Scattering*. IEEE Press Series on Electromagnetic Wave Theory. John Wiley & Sons, 2017. ISBN 978-1-118-09881-3.
- [9] M. S. P. Eastham. *The Spectral Theory of Periodic Differential Equations*. Scottish Academic Press, 1973. ISBN 0701119365.

- [10] N. Jiménez, J.-P. Groby, and V. Romero-García. The transfer matrix method in acoustics: Modelling one-dimensional acoustic systems, phononic crystals and acoustic metamaterials. In N. Jiménez, O. Umnova, and J.-P. Groby, editors, *Acoustic Waves in Periodic Structures, Metamaterials, and Porous Media*, page 103–164. Springer, 2021. ISBN 978-3-030-84300-7. doi: 10.1007/978-3-030-84300-7\_4.
- [11] G. Bao and L. Wang. Multiple cracking in functionally graded ceramic/metal coatings. *International Journal of Solids and Structures*, 32(19):2853–2871, October 1995. doi: 10.1016/0020-7683(94)00267-z.
- [12] M. Naebe and K. Shirvanimoghaddam. Functionally graded materials: A review of fabrication and properties. *Applied Materials Today*, 5:223–245, December 2016. doi: 10.1016/j.apmt.2016.10.001.
- [13] D. T. Sarathchandra, S. Kanmani Subbu, and N. Venkaiah. Functionally graded materials and processing techniques: An art of review. *Materials Today: Proceedings*, 5(10):21328–21334, 2018. doi: 10.1016/j.matpr.2018.06.536.
- [14] J. Y. Lee and W. Jeon. Exact solution of Euler-Bernoulli equation for acoustic black holes via generalized hypergeometric differential equation. *Journal of Sound and Vibration*, 452:191–204, July 2019. doi: 10.1016/j.jsv.2019.02.016.
- [15] A. Coutant, A. Sivadon, L. Zheng, V. Achilleos, O. Richoux, G. Theocharis, and V. Pagneux. Acoustic Su-Schrieffer-Heeger lattice: Direct mapping of acoustic waveguides to the Su-Schrieffer-Heeger model. *Physical Review B*, 103(22), June 2021. doi: 10.1103/physrevb.103.224309.



## Appendix A

### List of author's publications

#### A.1 Related to the thesis

##### A.1.1 Publications indexed in Web of Science

- KRPENSKÝ, A. and M. BEDNAŘÍK. Surface Love-type waves propagating through viscoelastic functionally graded media. *Journal of the Acoustical Society of America*. 2021, 150(5), 3302-3313. ISSN 0001-4966. DOI 10.1121/10.0006964.
- KRPENSKÝ, A., V. HRUŠKA and M. BEDNAŘÍK. A new class of approximate analytical solutions of the Pridmore-Brown equation. *Journal of Mathematical Physics*. 2022, 63(8), ISSN 0022-2488. DOI 10.1063/5.0098473.
- KRPENSKÝ, A., V. HRUŠKA and M. BEDNAŘÍK. Elastic P-wave manipulation utilizing functionally graded parallel plate gradient refractive index structures. *Wave Motion*. 2023, 122 ISSN 1878-433X. DOI 10.1016/j.wavemoti.2023.103208.
- KRPENSKÝ, A. and M. BEDNAŘÍK. Exact analytical solution for shear horizontal wave propagation through locally periodic structures realized by viscoelastic functionally graded materials. *Composite Structures*. 2023, 324 ISSN 1879-1085. DOI 10.1016/j.compstruct.2023.117539.

- KRPEŇSKÝ, A., M. BEDNAŘÍK and J.-P. GROBY. Willis couplings in continuously varying cross-sectional area duct. *Journal of the Acoustical Society of America*. 2023, 154 1660-1666. ISSN 0001-4966. DOI 10.1121/10.0020849.

## ■ A.1.2 Publications indexed in Scopus

- KRPEŇSKÝ, A. and M. BEDNAŘÍK. Surface love-type waves propagating through locally periodic inhomogeneous media. In: *Proceedings of the 29th International Congress on Sound and Vibration*. Prague, 2023-7-9/2023-7-13. IIAV CZECH s.r.o., 2023. ISSN 2329-3675. ISBN 978-80-11-03423-8.

## ■ A.2 Not related to the thesis

### ■ A.2.1 Publications indexed in Web of Science

- HRUŠKA, V., A. KRPEŇSKÝ, M. BEDNAŘÍK and F. CZWIELONG. Novel design for acoustic silencers for ducts with flow based on the bound states in the continuum. *Archive of Applied Mechanics*. 2023, 93(12), 4517-4526. ISSN 0939-1533. DOI 10.1007/s00419-023-02508-y.

### ■ A.2.2 Other

- HRUŠKA, V., A. KRPEŇSKÝ, M. BEDNAŘÍK and F. CZWIELONG. Design of low drag reactive silencers based on the bound states in the continuum. In: *Forum Acusticum 2023*. Torino, 2023-09-11/2023-09-15. Madrid: European Acoustics Association, 2023. p. 3233-3237. ISSN 2221-3767. ISBN 978-88-88942-67-4. DOI 10.61782/fa.2023.0834.